GROWTH AND CHARACTERIZATION OF CARBON NANOTUBES FOR IMPROVED FIELD EMISSION

A thesis submitted to the
Faculty of Technology, University of Delhi
for the award of the degree of

DOCTOR OF PHILOSOPHY
in
APPLIED PHYSICS

by

Srividya Sridhar

Under the guidance of

(PROF. R. K. SINHA)
Department of Applied Physics
Delhi College of Engineering
(Now Delhi Technological University)
Delhi

Dr. HARSH
Scientist G (Retd.)
Solid State Physics Laboratory
New Delhi

Delhi College of Engineering
(Now, Delhi Technological University)
Faculty of Technology
University of Delhi
Delhi-110042, India

CERTIFICATE

This is to certify that the thesis entitled, *"Growth and Characterization of Carbon Nanotubes for Improved Field Emission"* which is being submitted by Ms. Srividya Sridhar for the award of degree of Doctor of Philosophy to the Faculty of Technology, University of Delhi, India, is entirely based on the work carried out by her under our supervision. The work reported in this thesis embodies the work of the candidate herself and is original one and has not been submitted to any other University or Institution for the award of any degree or diploma.

(Prof. R. K. Sinha)

Supervisor

Department of Applied Physics

Delhi College of Engineering

Now Delhi Technological University)

(Faculty of Technology, University of Delhi)

Bawana Road, Delhi – 110042, India

(Dr. Harsh)

Co Supervisor

Scientist G (Retd.)

Solid State Physics Laboratory

Lucknow Road, Timarpur

New Delhi -110054 , India

CERTIFICATE

This is to certify that the thesis entitled, *"Growth and Characterization of Carbon Nanotubes for Improved Field Emission"* which is being submitted by Ms. Srividya Sridhar for the award of degree of Doctor of Philosophy to the Faculty of Technology, University of Delhi, India, is entirely based on the work carried out by her under our supervision. The work reported in this thesis embodies the work of the candidate herself and is original one and has not been submitted to any other University or Institution for the award of any degree or diploma.

Place: Delhi **Srividya Sridhar**

Date: **(Candidate)**

(Prof. R. K. Sinha)
Supervisor
Department of Applied Physics
Delhi College of Engineering
Now Delhi Technological University
(Faculty of Technology, University of Delhi)
Bawana Road, Delhi – 110042, India

(Dr. Harsh)
Co Supervisor
Scientist G (Retd.)
Solid State Physics Laboratory
Lucknow Road, Timarpur
New Delhi – 110054, India

Head, Department of Applied Science and Humanities & Dean
(Faculty of Technology, University of Delhi)
Delhi – 110042, India

In memory of my father

Late Shri. Sivakumar

ACKNOWLEDGEMENTS

I am greatly indebted to **Dr. R. K. Sinha, Professor, Department of Applied Physics, Delhi Technological University** (Formerly Delhi College of Engineering, University of Delhi), Delhi, for aptly suggesting the problem and for his valuable suggestions, discussions, intuitive guidance and active encouragement throughout the progress of this work.

It is my privilege to acknowledge the active support of **Dr. Harsh, Visiting Professor Centre for Nanoscience and Nanotechnology, Jamia Millia Islamia,** Delhi, for his valuable guidance and ideas at various stages of my work.

I would like to take this opportunity to thank the **Director, Delhi Technological University**, Delhi and **the Dean, Faculty of Technology (University of Delhi)** for the encouragement and interest in the work.

Extensive laboratory work was carried out at **Solid States Physical Laboratory (SSPL), Timarpur, Delhi.** I am greatly indebted to the Director and other authorities there for allowing me to use their facility for various experimental works.

My sincere thanks are due to **all my collaborators for my publications** specifically **Dr. P. M. Ajayan, Rice University, Dr. R Vajtai, Rice University and Dr. K. Kordás, University of Oulu,** for useful discussion on the research problem and developing innovative ideas for research work.

I gratefully acknowledge **C.S. Tiwary, Liehui Ge** and all other co-workers, for their timely support, guidance and inculcating enthusiasm at various stages of this work.

I take the pleasure for thanking the technical staff of Department of Applied Physics, for their full cooperation during the course of this work.

I proudly record my deep sense of gratitude to my mother, my husband, my parents-in-laws, my daughters and all other family members for their constant encouragement and moral support.

Place: Delhi **(Srividya Sridhar)**

Date: **Candidate**

ABSTRACT

Carbon nanotube (CNT) based cold cathodes are considered to be the most promising material for fabrication of next generation high-performance flat panel displays and vacuum microelectronic devices. Various improvisations in the synthesizing techniques in order to improve the field emission properties of the CNTs like use of buffer layer, effect of thickness of the buffer layer used, control of the density of the CNTs produced by chemical vapor deposition (CVD) technique, growing CNTs on Inconel super alloy to increase the current density, decoration of the grown CNTs with aluminium (Al) and copper (Cu) to reduce the turn on and threshold field of emission and a simple, novel method for infiltrating iron (Fe) nanoparticle into the CNT forest with the help of a magnet have been presented. A detailed report on increase in the current density from 10 mA/cm^2 to 30 mA/cm^2 with the help of titanium (Ti) buffer layer have been presented. Moreover, improved adhesion of CNTs with the substrate due to the incorporation of Ti buffer layer have also been studied. Secondly, the effect of varying the thickness of the Ti buffer layer on the field emission properties of CNTs are discussed. This was followed by the investigation of a simple density control technique during the CNT synthesis with the help of Ti capping layer. This method not only improved the density of the CNTs grown by CVD but also increased the adhesion of the CNTs with the substrate and reduced the screening effect to a larger extent. The result of increasing the current density to around 100 mA/cm^2 by growing CNTs on Inconel super alloy is discussed in detail. Further, the limitations of the CNTs grown on silicon (Si) like early arcing, rapid failure of the device is also discussed. This is followed by the development

of new technique of decorating the CNTs with Al and Cu for enhanced field emission characteristics. The technique is shown to yield ultra low turn on and threshold voltages of 0.13 V/μm and 0.14 V/μm respectively for the Al decorated CNTs grown on Al coated Si. The excellent field emission properties of the metal decorated CNTs is shown to be due to the edge effect, reduced screening effect, lower contact resistance. A thorough investigation of the development of one step process of infiltrating Fe_3O_4 nanoparticles into the CNT forest by a novel and simple technique with the help of a magnet has been reported. The results presented here may be adopted for CNT based cold cathodes suitable for high power microwave vacuum devices and also for long-life low-power applications.

CONTENTS

List of Figures

Figure 6.9: (a) and (b) are the SEM images taken after field emission experiment on the CNTs grown on Si and Inconel respectively with Al decoration on them.

List of Tables

CHAPTER I

Introduction to CNTs and Field Emission

1.1 Introduction to Carbon Nanotubes

Because of their unique combination of properties, carbon nanotubes are expected to play a significant role in many applications. As a result, researches all over the globe have developed immense interest in its remarkable physical, chemical and electronic properties. Over the years, research has occurred in investigating different methods of carbon nanotube growth, examining properties of nanotubes and also exploring new potential applications for CNTs. It is certain that these allotropes of carbon have generated immense interest in the scientific community.

Many articles credit the discovery of carbon nanotubes to Ijima for his seminal article published in *Nature* in 1991 [1]**.** However, it is important to note that one can trace the discovery of carbon nanotubes to 1952 when two Soviet scientists, Radushkevich and Luk‟yanovich who were investigating thermal decomposition of carbon at 600 °C stated the formation of carbon particles in ‘elongated wormlike structures [2], thus marking the discovery of CNTs. Few articles credit the Russian scientists this discovery since high resolutions images were not obtained back then. Further, the 1952 article can be thought of as the only published

example that pre-dates Ijima's discovery. Other research work has been conducted that refer to tubular carbon structures [3-5].

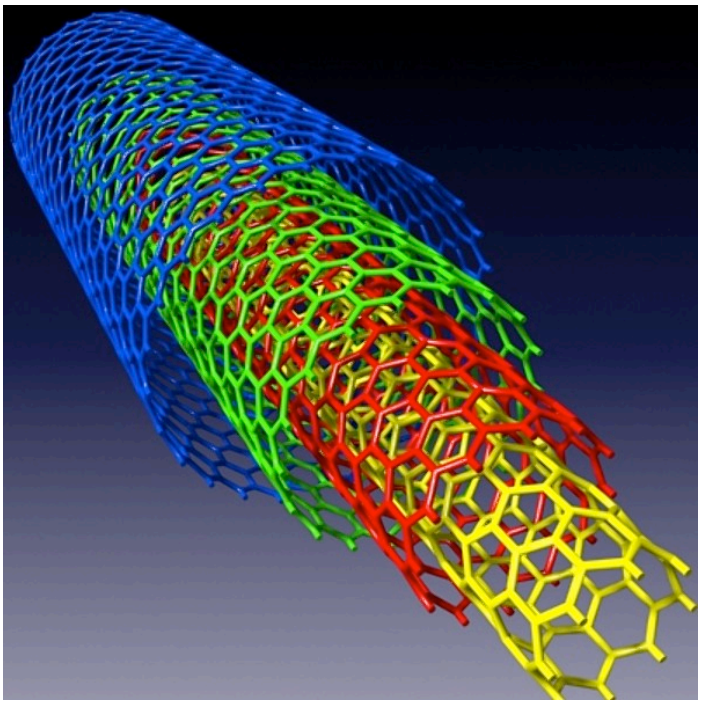

Figure 1.1 Simple structure of a multi walled CNT

Perhaps the most important point in the history of CNTs is the discovery of carbon allotrope – fullerenes in the year 1985 by Smalley, Curt and Kroto [6]. It was very interesting for the researchers to note from the laser vaporization of a graphite target, a family of carbon clusters especially in C_{60}. This cluster resembled a football in shape and was further named after American architect, R. Buckminster Fuller as fullerenes. For their discovery, Smalley, Curl and Kroto were awarded the Nobel Prize in Chemistry in 1996 [6]. This discovery changed the perspective of many scientists on carbon and generated immense interest in the potential applications of this newly found allotrope.

In terms of structure, fullerenes are closely related to the nanotubes discovered by Ijima [1]. While earlier reports of CNTs were published in highly specialized journal with limited access to only certain parts of the scientific community, Ijima's article was published in the highly reputed *Nature* with an 2012 Impact factor of 38.597 and was read by people in a wide range of scientific disciplines. Thus, the timely publication of the article is a well known journal gave carbon nanotubes, the required limelight. It is of no surprise that the topic still remains as a frequently researched and published topic, well after 20 years from its publicity.

1.2 Structure of Carbon Nanotubes

In order to understand the structure of CNTs, it is important to first examine the structure of two related forms of carbon – graphene and buckminsterfullerene.

Graphene is a planar sheet composed of trivalent, sp^2-bonded carbon atoms that form a perfect two - dimensional hexagonal array. The sp^2-bonded nature of the carbon atoms allows delocalization of π-electrons throughout the sheet, thereby providing the structure the property of aromaticity. When these graphene sheets are stacked, it constitutes graphite.

On the other hand, the structure of fullerenes is quite different. C_{60} is the most stable of this family of fullerenes and can be imagined as the result of folding an imperfect graphene sheet to form a truncated icosahedron. It is interesting to realize that the introduction of defects in graphene greatly disturbs its structure. For example, if heptagonal rings were included in the structure of graphene, the layer would fold itself into a saddle shape while the inclusion of pentagonal rings would cause the graphene sheet to completely fold around itself to form a cage, as for the fullerenes. What makes the structure of C_{60} fullerene exceptional is the fact that its

structure consists of hexagonal rings and 12 pentagonal rings and is the smallest fullerene wherein no two pentagons share an edge. More importantly, this structure has been proved to be exceptionally stable over time.

Fundamentally, carbon nanotube structures can be grouped into two broad categories: single-walled carbon nanotubes (SWCNTs) and multi-walled carbon nanotubes (MWCNTs). Before dwelling into the different forms of CNT structure, it is best to understand the structure of an ideal CNT. Generally, an idealized carbon nanotube is shaped like a cylinder with a convex hemispherical cap at both ends. In simple terms, one can imagine constructing this shape by cutting a molecule of C_{60} in half, then forming a cylinder by rolling up a single graphene sheet and implanting it between the two hemispherical caps. The resulting closed tube is a single-walled nanotube.

Multi-walled nanotubes are a variation of this structure where several tubes are found within one another, in a Russian doll-like arrangement. The number of walls can greatly vary from few walls to hundreds of them. At the same time, the diameters of MWCNTs also have a wide range – in some cases 100 nm. Generally, MWCNTs posses metallic character and are produced in catalytic process.

Carbon nanotubes can also be classified as zigzag, chiral or armchair. If the plane of graphene is rolled-up perpendicular to the tube axis, then the line revolving the tube has an armchair-like shape. Under an angle of 30° the configuration of the structure formed is zigzag while the tubes with an angle in between are called chiral. Any single-wall nanotube

configuration can be generated by superimposing the hexagon at the original point O to a hexagon indicated by (a, b) defined by a chiral vector:

$$R = ax + by$$

where x and y are the primitive vectors whose length are both equal to $\sqrt{3}d_{c-c}$ with d_{c-c} indicating *C-C* bond length. It is possible to calculate the diameter of the tube using the following equation:

$$D = \frac{\sqrt{3}d_{c-c}}{\pi}\sqrt{a^2 + ab + b^2}$$

Theoretically, it is important to note that for MWCNTs, the individual constituent layers can adopt any one of these different helicities and there are numbers of variations possible over the whole structure.

1.3 Synthesis of Carbon Nanotubes

There are different procedures for the growth of carbon nanotubes. However, in its most basic sense, the growth of CNTs involves vaporizing a carbon source in the presence of a suitable catalyst for growth. In many cases, this happens to be a transition metal. Chemical vapor deposition (CVD) method of growth is discussed in detail below.

CVD is perhaps the most versatile, commonly used and published method of growth. The process involves placing a catalytic material in the tubular section followed by passing hydrocarbon vapor for around 15-60 min. The catalytic material inside the tube is at a very high temperature, perhaps around 600-1200º C, since to decompose the hydrocarbon it has to be at a

very high temperature. Thus, the CNTs are grown in the reactor, which is collected upon the completion of the experiment. If liquid source of hydrocarbon is used, i.e. forms of benzene, alcohol etc. the inert gas is purged through the liquid after the liquid has been heated to high temperatures, which in turn carries the hydrocarbon vapor into the reaction zone. Also, if solid source of hydrocarbon is used, it is directly kept in low temperature zone of the reactor tube. It is important to note that, just like there can be many forms of carbon source that is used in CVD growth process, many different forms of catalyst can also be used. Solid, liquid or gas catalyst can be used and it can be fed from outside of the reactor tube or be kept inside the reactor tube. Pyrolysis of the catalyst vapor at a suitable temperature liberates metal nanoparticles in-situ (such a process is known as floating catalyst method). Alternatively, catalyst-coated substrates can be placed in the hot zone of the furnace to catalyze the CNT growth. Figure 1.2 provides an image of the CNTs grown using Chemical vapor deposition method.

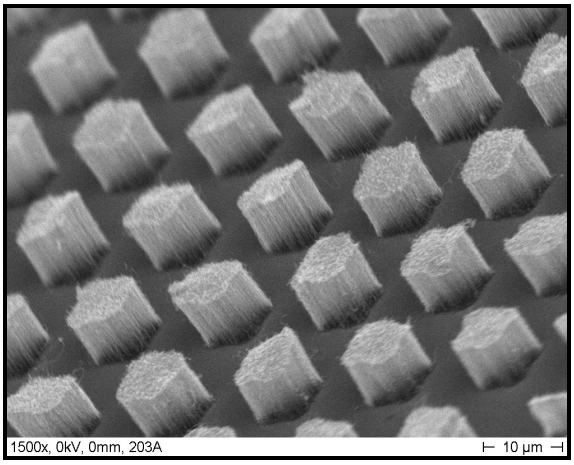

Figure 1.2 SEM Images of CNTs grown using CVD technique

Though one of the most commonly used growth techniques, there are many parameters that need to be controlled in the case of growth using the CVD technique. Some of the parameters include, choice of hydrocarbon, choice of catalyst, temperature, pressure, gas-flow rate, deposition time, reactor geometry. Since there exists a large number of parameters for growth in CVD, the method offers the advantage of tuning the final product i.e. the CNTs according to very specific needs and design. At the same time it also means that various parameters need to be adjusted when employing this growth technique. The main disadvantage to the CVD method is that the carbon products tend to be less highly graphitised. The increased incidence of defects means the CNTs exhibit inferior properties, particularly decreased mechanical strengths.

1.4 Characterization of Carbon Nanotubes

There is a need to characterize the growth of CNTs upon completion of the growth process. This is crucial in order to determine the effect of various parameters used in growth.

The main methods involved in characterizing the CNTs include direct imaging through microscopy. Optical microscopy, closely related to electron microscopy, involves a beam of light that is focused onto the sample and then a lens or a combination of lens is used for scattering and refracting the light to form an image. Optical microscopy is performed with a compound microscope that involves a condenser lens to focus incident beam, an objective lens to refocus the scattered beam into an image and finally a third lens for enlarging the image that can be captured. The typical resolutions achieved are around 0.2μm or 1500x magnification. On

the other hand, with electron microscopy, rather than focusing a beam of light onto a sample, a beam of high-energy electrons is used.

With electron microscope, typically used lens are replaced with electromagnets, which alter the magnetic field and aid in obtaining a precise image. In the case of electron microscope, the resultant image cannot be viewed by naked eye since it is composed by a beam of electrons. Thus, the beam is projected onto a suitable detector such as a scintillator detector, phosphor screen, photographic film, or charge-coupled device.

1.4.1 Transmission electron microscopy

Transmission electron microscopy, more commonly known as TEM, is a commonly used form of imaging for carbon nanotubes. In TEM, a beam of high energy electrons (generally hundreds of keV) is directed through a thin sample film and a cross sectional image of the transmitted electrons is produced on the other side. The image formed consists of a combination of dark and light regions representing the heavy nuclei scatter and light nuclei scatter. This is because, the heavy nuclei scatter the beam more intensely that the light nuclei region. One of main advantages offered by TEM is the fact that in transmission electron microscopy, the beam passes through the sample to generate a cross-sectional view, thus providing information on internal structure. This is very useful since the objective in many cases is not only to obtain a 1-D image but also to gain knowledge about the internal structure. Further, because of using the high voltage beam, the image resolution can be very high at large magnifications, e.g. about 0.2 nm at magnifications of about 2,000,000x. Some of the high end TEM equipment can even use a

large, million-volt transmission electron microscope to resolve separations less than 0.05 nm and achieve magnifications of up to 50,000,000x, enough to discern individual atoms.

1.4.2 X-Ray microscopy

Using the data and images obtained, one can also use this information for X-ray spectroscopy, also known as EDS or EDAX, to determine the elemental composition of the specimen. This is because an electron from a higher energy orbit can drop to a lower energy orbit to fill a vacant spot. When this happens, the released energy is of the form of an X-ray. The emitted X-rays have specific discrete energies equal to the drop in energy of the electron and the distribution of these energies is characteristic of particular atoms. As a result, the elemental composition of the specimen is obtained. Figure 1.3 provides example of TEM images of CNTs while Figure 1.4 provides a sample of EDAX of CNTs grown on Silicon with Aluminum and Copper metal decoration.

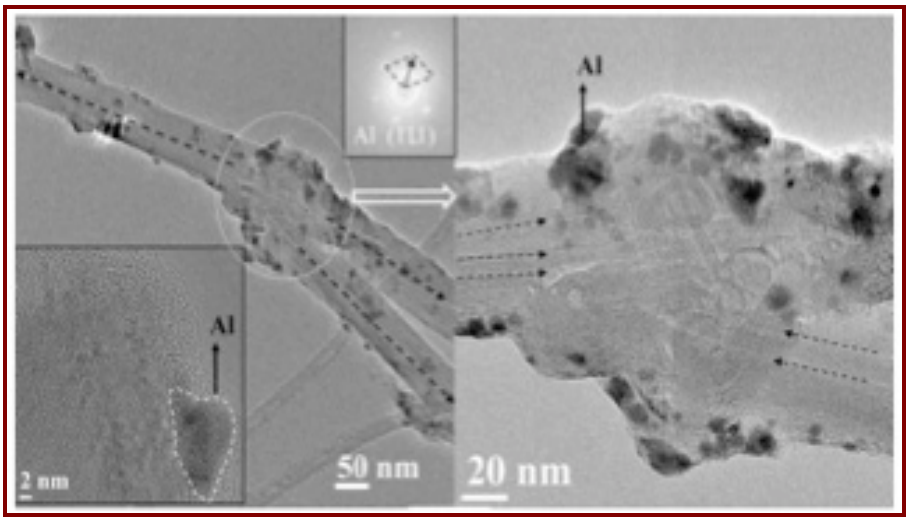

Figure 1.3 TEM images of CNTs grown on Silicon

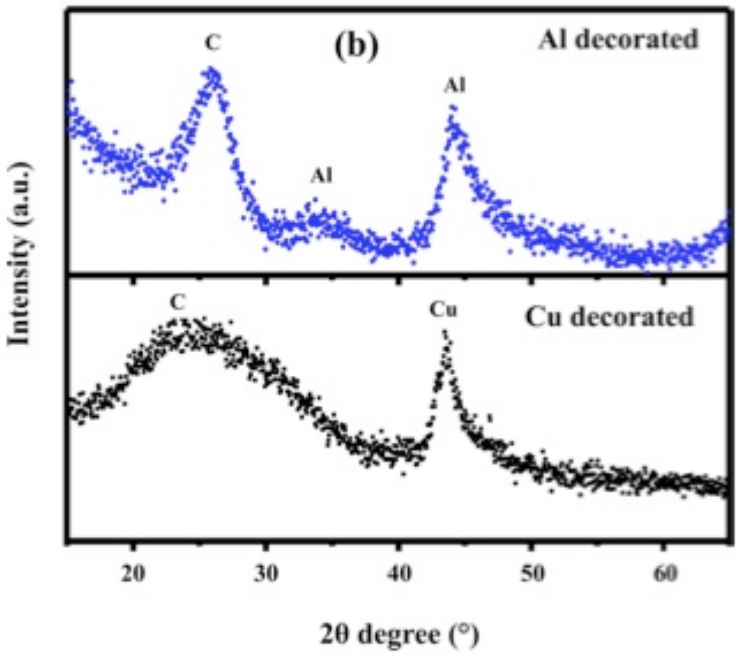

Figure 1.4 EDAX of CNTs grown on Silicon with Aluminum and Copper metal decoration

1.4.3 Scanning electron microscopy

Another form of microscopy commonly used for the characterization of CNTs is Scanning electron microscope, more commonly known as SEM. In this form of microscopy, a beam of electron is scanned across the sample area. The electrons present in the incident beam collide with the electrons in the sample and as a result, transfer of energy occurs between the two sets of electron also known as inelastic scattering. Thus, the secondary electrons are ejected from their orbit and these ejected electrons can then strike a scintillator detector placed near the specimen where it is converted into a digital, grey-scale image, as in secondary electron imaging (SEI). Normally, these secondary electrons originate from near the surface and the detection of these electrons is dependent on the topography of the specimen. SEM is perhaps one of the best ways to study the topology of a sample given its ability to scan over a large surface. Figure 1.5 provides a sample of an SEM image of CNTs at 1500X magnification.

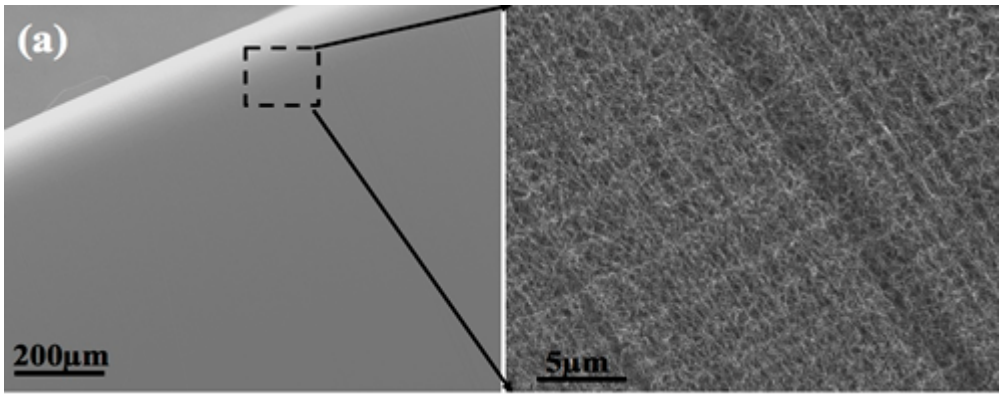

Figure 1.5 SEM image of CNTs at different magnifications

1.4.4 Raman spectroscopy

Micro-Raman spectroscopy is usually performed to investigate the vibrational properties of the synthesized structures, which allows us to draw further conclusions about their crystallography or morphology. All spectra from CNTs show at least the two significant peaks at 1580 cm^{-1} and at 1347 cm^{-1}, which become broader at higher temperatures and overlap. Crystalline graphite due to the presence of sp2 hybridized carbon domains leads to a sharp vibration mode at 1580 cm^{-1} [14] which is and is named as the first-order G band. The peak at approximately 1350 cm^{-1} describes the disordered structure and is known commonly as the D (disordered) band [15]. It is noteworthy to mention that due to the selection rules, in a perfect graphite crystal the first- order vibrational mode of the D band is almost forbidden. Bending of the lattice fringes or decreasing the particle size may activate this ban. Sometimes, we do get the second-order D peak (2.D) for nanotubes grown at lower temperatures and it appears at approximately 2700 cm^{-1}. However, by increasing the deposition temperature this peak may disappear. The signal strength becomes weaker for the structures deposited at higher

temperatures and therefore the noise level at those elevated temperatures becomes more and more visible in the spectra. It is known (e.g. [16,17]) that structural imperfections and smaller particles will broaden the first-order peaks from graphite. As a result, one can estimate the order of crystallinity in the material from the corresponding half-width (FWHM). If there is more amorphous content, then, that leads typically to a half-width (FWHM) of approximately 200 cm^{-1} [17]. In the case of nanotubes deposited at 650°C, sharp peaks (FWHM ~90 cm^{-1}) reveal the purity of CNTs and shows that they have a much higher degree of crystalline perfection. CNTs grown through catalyst deposition can be characterized as nano-crystalline structure but disordered graphite-like system where the level of disorder increases with the preparation temperature. Interestingly, the relative height of the peak at about 1050 cm^{-1} increases with temperature.

1.5 Specific properties of Carbon Nanotubes

As mentioned previously, CNTs possess a wide range of properties and one of the reasons why researchers are interested in them is because of their unique electrical, thermal and mechanical properties. In the following sections, different properties of CNTs are examined in detail.

There has been immense interest in the conductive nature of CNTs. Depending on how much the nanotube has been twisted, conductivity can highly vary and so does the metallic nature of the CNTs. Nanotubes can be either metallic or semi-conducting. Because of the highly sensitive electronic properties of carbon nanotubes, they make good semiconductor and

are often used in the preparation of metal–semiconductor, semiconductor–semiconductor and metal–metal junctions. It has been demonstrated that the introduction of pentagon–heptagon pair of defects into the hexagonal network of a carbon nanotube can change the chirality of the tube and change its electronic properties. Also, frequently chemical doping occurs in order to form an on-tube junction. Further, these nanotube junctions can be successfully used as a building element in many nanoscale devices. There is generally no change in current across different parts of metallic single-walled nanotubes. The behavior of the ropes of semi-conducting single walled nanotubes is different, in that the transport current changes abruptly at various positions on the CNTs.

The strength and elasticity of CNTs is exceptionally great. As discussed previously, carbon atoms in the graphite layer are connected through a strong chemical covalent bond to three neighboring atoms. Because of these strong bonds, the basal plane elastic modulus of graphite is one of the largest of any known material. Using atomic force microscopy, the unanchored ends of a freestanding nanotube can be pushed out of their equilibrium position, and the force required to push the nanotube can be measured. The current Young's modulus value of single walled nanotubes is about 1 TPa, but this value has been widely disputed, and a value as high as 1.8 TPa has been reported.

Another very important property of CNT is its' high thermal conductivity and in fact is even thought as one of the best heat-conducting material ever known. In some cases, superconductivity below 20K has been observed by single walled nanotubes. While the carbon-carbon bond is very strong and allows for little in-plane expansion, large inter-plane expansion of single walled nanotubes occurs and results in high flexibility against non-axial strains. Also,

the large surface area and high absorbency of CNTs make them ideal candidates for use in air, gas, and water filtration.

Carbon Nanotubes have a very high aspect ratio. This means that lower loading of CNTs is needed compared to other conductive additives to achieve the same electrical conductivity. Because of the lower loading, toughness is preserved at low temperatures and other factors affecting performance is also preserved. CNTs possess an aspect ratio of about 1000:1 and impart electrical conductivity at much lower temperatures when compared to carbon black, chopped carbon fiber, or stainless steel fiber.

Apart from these properties, carbon nanotubes also posses excellent field emission properties. The focus of this work is to study the field emission properties of carbon nanotubes. Before proceeding to the details of this work, it is important to understand the basics terms associated with field emission. This is provided in the following sections of this chapter.

1.6 About electron emission

Electron emission is defined as liberation of free electron from a surface of a substance caused by the external energy transferred to the electrons as shown in Figure 1.6.

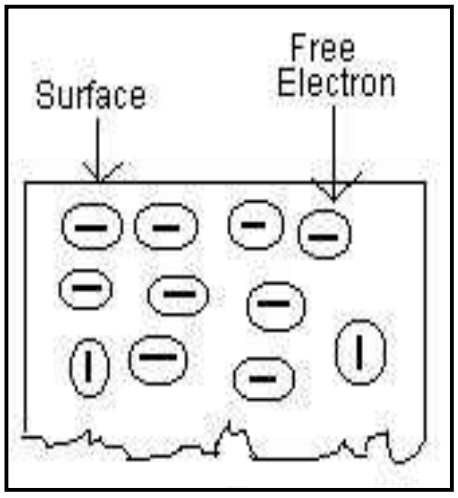

Figure 1.6 Electron Emission

Electron emission tends to occur on metal, because metal is a substance with much free electron in between its molecule. In order to emit from the metal surface these free electrons require additional external energy. The amount of outside energy required by electron to emit from the metal surface is known as work function. The work function is usually defined in electron volt unit (eV). The additional external energy required by the electron to emit from the metal surface could come from sources such as heat energy, kinetic energy or light energy.

1.6.1 Thermionic Emission

In this method the additional energy comes to the electron in the from of heat energy. The energy is transferred into kinetic energy. As the kinetic energy of electron increase its movement become uncertain and then finally there will be electrons that leave out from the metal surface.

The substance where the electrons emit from, is known as emitter or cathode. In case of vacuum tube it is called as cathode. And the substance that receives electron is known as the plate or the anode.

Material used for cathode must have the following properties:
(a) Low work function - Hence, electron emission can occur using only small amount of energy.
(b) High melting point - As the thermionic emission occurs at high temperature, the substance used as cathode must have high melting point.
(c) High mechanical strength - To withstand the bombardment of positive ions. No matter how careful the evacuation is in a vacuum tube, there are still gas molecules always present which may be in the form of ion by impact with electron. Under the influence of electric field these positive ions will strike the cathode and if a high voltage is being used, the cathode is subject to considerable bombardment and can be damaged.

1.6.2 Field Emission

In this type of emission additional energy comes in the form of electric field. When a conductor is put in a place very close to high voltage conductor, the electric field from the conductor will exert attractive force on the free electron in metal. If the positive field is big enough the free electron will succeed in overcoming restraining of the metal surface and it will emit from the metal surface. Very intense electric field is required to produce field emission.

Usually a voltage of the order of a million volts per centimetre distance between the emitting surface and the positive conductor is necessary to cause field emission.

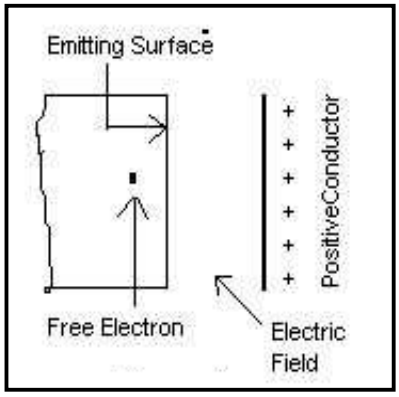

Figure 1.7 Field emission

Field emission can be obtained at temperature much lower than required for thermionic emission and therefore it is also sometimes called as cold cathode emission or auto electronic emission.

Here electrons tunnel through the surface potential barrier of a metal- vacuum interface and float in the vacuum region during the presence of an extremely high electric field.

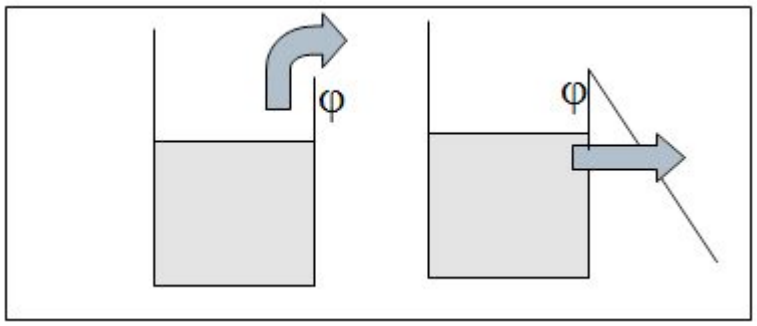

Figure 1.8 Thermionic and Field emission

Different from thermionic emission, electron field emission occurs without emitter heating (cold cathode). As a result, a field emission electron source has several prominent

advantages: less power consumption, fast turn on times, low thermionic noise, high current density (typically 100A/cm^2 for field emission, 0.5A/cm^2 for thermionic emission), high coherence, low energy spread, miniature volume. Vacuum tubes based on thermionic emission require several minutes to warm up before they can be used; by contrast, the function of field emission devices is effectively instantaneous, allowing switching times of many megahertz.

This quantum mechanical tunneling of electrons is an important mechanism for thin surface potential barriers, just like those in heavily doped semiconductor – metal junctions. This phenomenon is highly dependent on both the properties of the material and the shape of the particular cathode, so that higher aspect ratios produce higher field emission currents. However, if the cathode surface has a point or a protrusion, electrons may be extracted at a considerable lower applied gap field. This is because the lines of force converge at a sharp point and the physical geometry of the tip provides a field enhancement. Fowler-Northeim Equation governs the current density produced by a given electric field.

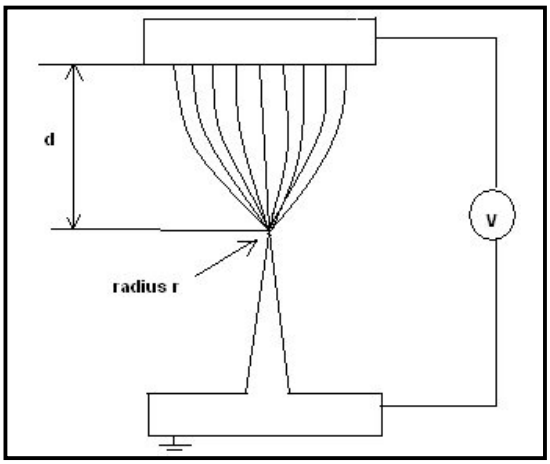

Figure 1.9 Illustration of field electron emission from a tip

1.7 Field emission micro tips

Micro fabrication is commonly used to produce sharp micro tips. Since the current generated from a single microtip is quite small, arrays of emitters are produced for application in large area electronics. In order to enhance the lifetime of micro fabricated emitters, it is prudent to operate them at low current level. Micro fabricated emitters may be broadly divided into four types including Molybdenum, Silicon, Diamond and Carbon Nanotubes.

1.7.1 Cold cathode materials

An ideal material for the field emitter should have a high mechanical strength and melting point, excellent electrical conductivity and thermal conductivity, a low work function and stable chemical productivity. Field emitter should also be able to deliver a high current density at a low electric field.

Metal tips were used to study the field emission in the early days. The metal tips are prepared by electrochemical etching. This leads to an intensification of the electric field. Among various metals, such as tungsten, molybdenum is utilized for field emitters because of their high melting temperatures and mechanical robustness to high mechanical stress. An emitter coated with a thin film of low work function such as Cs can render lower operating voltage but the chemically reactive Cs becomes easily oxidized reducing the current density.

1.8 Emitter material

1.8.1 Metal tip

In early days, metal tips were used to study Field emission (prepared by electrochemical etching. Amongst various metals, refractory metals such as Tungsten and Molybdenum are utilized for field emitters. The advantages of such metal tips were:

- High Melting temperature
- Mechanical robustness to high electrical stress

But these tips suffered from the following disadvantages:

- High Work function
- Low Field Enhancement factor of about 10 requires an ultrahigh vacuum environment.
- Suffer from emission degradation due to sputter erosion and chemical contamination. Hence require high vacuum environment operation

1.8.2 Why CNT emitters ??

A good field emitter should possess the following characteristics:

- Low turn-on voltage

  It gives low power dissipation

  Easy integration with low operating voltage

- High current density

  It implies high brightness

- Uniformity

  It's important for mass production

Best known in this category is carbon nanotubes. They meet a host of requirements of FE applications, unavailable in the traditional emitter materials. The tip of carbon nanotubes typically has radius of curvature in the nanometer scale (tube radius) and the lengths can be > 1μm, consequently the aspect ratio is very high. This attribute of CNTs allows a very high field enhancement at the tip apex. The geometrical field enhancement factor (β) of currently available CNTs can be >1000. Moreover such natural nanotip arrays may be grown using far simpler deposition techniques, compared to say diamond films. These make them very attractive for producing cold cathodes

Advantages of CNT as emitter:

- High aspect ratio, produce high current densities at low voltages.
- Stable electron emission and sufficient luminance.
- Good chemical stability and great mechanical property.
- Low work function.
- High Melting point.
- High Thermal and Electrical conductivity.
- Chemical inertness to be immune to the residual gases.
- Cheap cost and suitable mass scale fabrication.

1.9 CNT Based field emission configurations

Work on CNT based Field Emission devices have been configured in two modes till date :

(1). FE Diode

(2). FE Triode

But, in this research, all of the experiments were conducted in diode mode.

The Diode configuration is depicted in Fig.1.10. Initially the wafer is prepared by standard cleaning steps followed by CNT growth The CNT's grown on the substrate act as the **Cathode** while Stainless steel/Glass is taken as **Anode**. The two electrodes are separated using **Alumina spacers** as per experimental requirement as shown in the Fig.1.10.

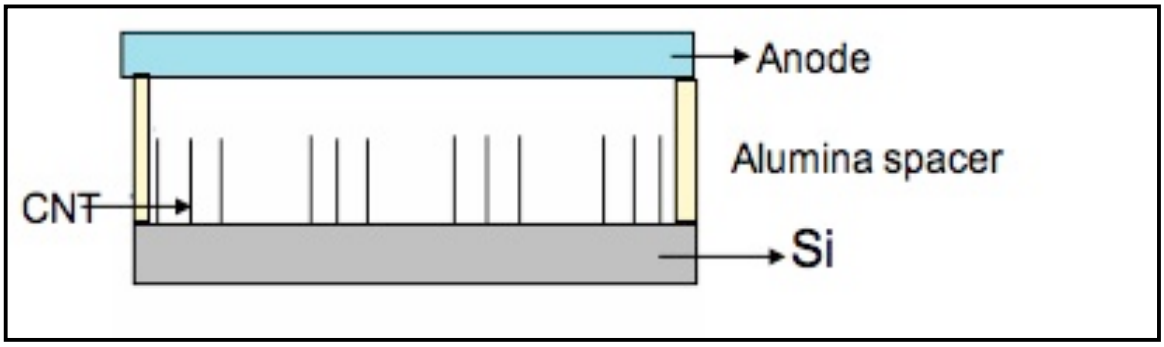

Figure 1.10 Diode configuration

The apparatus is enclosed in a vacuum of 10^{-7} Torr and voltage is applied due to which electric field is generated. A high Electric field (V/d) achieved by Field amplification effect i.e. electric field lines concentrated around a sharp object

$$F_{applied} = \frac{V}{d}$$

$$F_{tip} = \beta * F_{applied}$$

Due to high Beta (H/r) ratio >1000, CNT exhibit very high field amplification

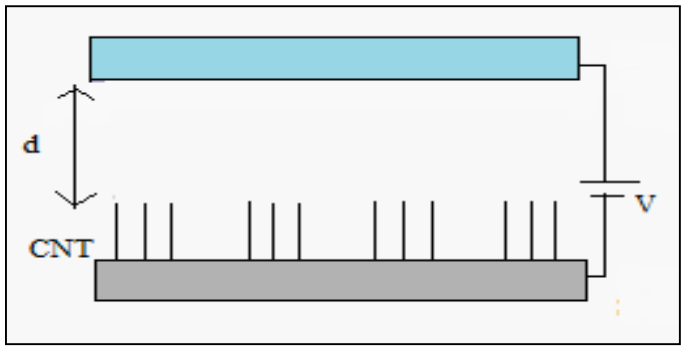

Figure 1.11 Voltage applied to Diode configuration

As the cathode is at a negative potential while anode at a positive potential, the latter exerts a strong attractive force and electrons are forced to emit from cathode (CNT's) towards the anode. Thus in Diode configuration the anode is responsible for electron extraction and acceleration.

1.10 Terminology related to CNT field emission

1.10.1 Electron work function

The electron work function is an energy threshold where electrons start to be emitted into vacuum from a metal conduction band, that is, the difference of energy between vacuum and the fermi levels. The work function varies with different metals, and ranges from 2 to 6 eV.

1.10.2 Field enhancement factor

The local field enhancement factor β, also called the geometrical enhancement factor, reflects the enhancement of an electric field at the emitter surface by an electrode configuration. It is represented as:

$$E_{local} = \beta d E_{macro}$$

Where E_{local}: Local field intensity

E_{macro}: Macroscopic field intensity

d : distance between the cathode and anode.

As shown in Figure 1.24, high electric field is achieved at lower voltages in case of sharp tips as compared to flat surfaces due to high field enhancement factor.

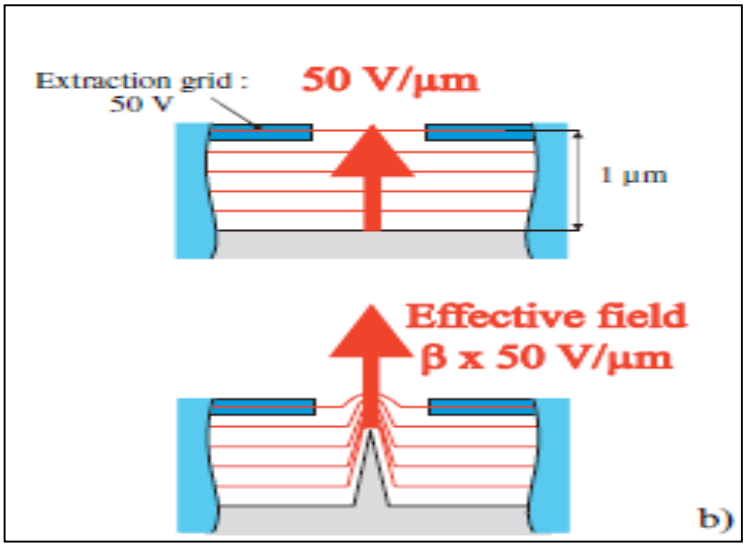

Figure 1.12 Effective Field at Flat and Sharp tips

The field enhancement factor β is obtained by either the slope of FN curve or the aspect ratio of the emitter.

$$\beta \sim h/r$$

Where h: height of the carbon nanotube tip.

r: radius of the carbon nanotube tip.

1.10.3 Screening effect

Screening of the applied electric field on the apex of a CNT by the neighboring CNTs comes into effect when inter-CNT spacing decreases from twice the CNT height. Screening effect restrains the field penetration. It was found that the films that have medium density have strong emission and better uniformity. If the density was too low or too high, the emission was not strong and not inhomogeneous. The former may not have enough emitters, and the latter may be due to the screening effect. Screening effect can be reduced if the site density of carbon nanotubes can be controlled.

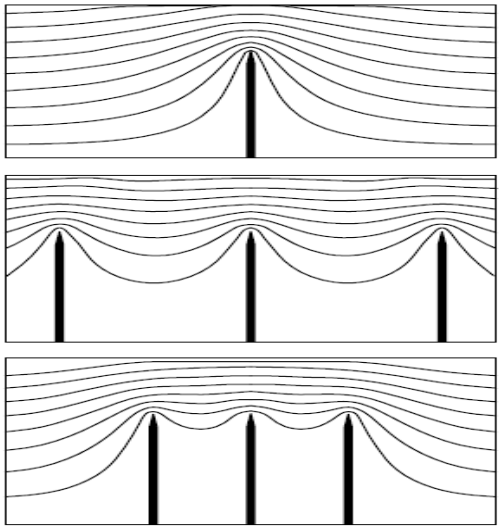

Figure 1.13 Screening of the applied electric field on the apex of a CNT by the neighboring CNTs

1.11 Focus of this work

The focus of this work is to synthesize CNTs for improved field emission properties. Because of their high aspect ratio, CNTs are often used as field emitters. In its simplest sense, field emission is the emission of electrons from the surface of the conductor, in this case, CNTs, under the influence of current or electromagnetic field. This often takes place in vacuum and sometime the conductor can even be in liquid or gaseous form. A general diagram of the field emission set up is provided in Figure 1.22.

After providing an overview of what field emission is, we move on to discussing the effects of Titanium (Ti) buffer layer on field emission results in Chapter 2. In chapter 3, we explore the effect of the thickness of buffer layer. Since the density of CNTs is an important factor affecting the screening effect during field emission, Chapter 4 deals with this in detail. Chapter 5 provides detailed information on the field emission results of CNTs grown on superalloy Inconel. Chapter 6 focuses on a simple and scalable process that results in metal decorated CNTs with ultra-low turn on voltage. During the course of this research, an unique one step process has been developed for the infiltration of iron particles into CNT forest. This is discussed in detail in Chapter 7.

1.12 References

1. Iijima, S., *Nature* 1991, *354*, 56-8
2. Radushkevich, L. V.; Luk'yanovich, V. M., *Zh. Fiz. Khim.* 1952, *26*, 88-95.
3. Baker, R. T. K.; Barber, M. A.; Waite, R. J.; Harris, P. S.; Feates, F. S., *J. Catal.* 1972, *26*, 51-62.
4. Oberlin, A.; Endo, M.; Koyama, T., *J. Cryst. Growth* 1976, *32*, 335-349.
5. Boehm, H. P., *Carbon* 1973, *11*, 583-586.
6. Kroto, H. W.; Heath, J. R.; Obrien, S. C.; Curl, R. F.; Smalley, R. E., *Nature* 1985, *318*, 162-163.
7. Wiles, P. G.; Abrahamson, J., *Carbon* 1978, *16*, 341-349.
8. Iijima, S.; Ichihashi, T., *Nature* 1993, *363*, 603-5.
9. Bethune, D. S.; Kiang, C. H.; de Vries, M. S.; Gorman, G.; Savoy, R.; Vazquez, J.; Beyers, R., *Nature* 1993, *363*, 605-7.
10. Ebbesen, T. W.; Ajayan, P. M., *Nature* 1992, *358*, 220-222.
11. Yakobson, B. I.; Brabec, C. J.; Bernholc, J., *Phys. Rev. Lett.* 1996, *76*, 2511-2514.
12. Lu, J. P., *Phys. Rev. Lett.* 1997, *79*, 1297-1300.
13. Hernandez, E.; Goze, C.; Bernier, P.; Rubio, A., *Phys. Rev. Lett.* 1998, *80*, 4502-4505.

14. F. Tuinstra, J. L. Koenig, Raman spectrum of graphite, J. Chem. Phys. 53 (1970) 1126.
15. R. O. Dillon, J. A. Woollam, V. Katkanant, Use of Raman-scattering to investigate disorder and crystallite formation in as-deposited and annealed carbon-films, Phys. Rev. B 29 (1984) 3482.
16. D. S. Knight, W. B. White, Characterization of diamond films by Raman spectroscopy, J. Mater. Res. 4 (1989) 385.
17. D. Beeman, J. Silverman, R. Lynds, M. R. Anderson, Modeling studies of amorphous-carbon, Phys. Rev. B 30 (1984) 870.

CHAPTER II

Titanium buffer layer for improved field emission

2.1 Introduction

Carbon nanotubes (CNTs) have recently emerged as an attractive cold cathode material due to their excellent field emission properties since their discovery by Iijima in 1991 [1]. CNTs, because of its unique physical and chemical properties such as low turn-on field, high current density, and long-term stability, have been considered as a potential material for various applications, such as electronic devices [2], flat panel displays [3], scanning probes [4], etc. Flat panel displays fabricated using CNTs as electron emitters have been recognized as one of the most promising display technologies of the future [5]. After the results published about Fowler–Nordheim tunneling in 1928 [6,7], many materials and device structures have been developed to realize efficient field emitters [8] since then. Due to the high aspect ratio, low work function, high mechanical strength and high thermal conductivity, CNTs are considered to be a wonderful electron emitting sources in field emission displays. However, some critical issues such as screening effect, adhesion of CNTs with the substrate, reliability, high contact resistance and stability have to be addressed while using CNTs as electron emitters in field emission applications. In other words, the adhesion of CNTs with the substrate has to be increased and the contact resistance between the CNTs and the substrate has to be lowered for improved device performance.

To synthesize CNTs more effectively, as mentioned in the previous chapter, various techniques like the arc discharge method, laser ablation, chemical vapor deposition (CVD) and

plasma enhanced chemical vapor deposition (PECVD) have been developed so far [9,10]. However, catalytic CVD is the most preferred method because it combines the advantages of easy setup and operation with the possibility of patterning the substrate as well. However, unlike conventional catalytic CVD in which the hot-wire is the catalyst, usually transition metal catalyst, such as Ni, Fe, Co and their alloys, is necessary to grow carbon nanostructures with a graphite structure. As explained in the earlier chapter, the CNT or the CNF-growth in a CVD process involves the dissociation of hydrocarbon molecules catalyzed by the transition metal, which is then followed by the dissolution and saturation of carbon atoms in the metal nanoparticles. Finally, the precipitation of carbon from the saturated metal particle leads to the formation of tubular carbon solids in a graphite structure [11,12]. Since most of the CNT growth involves the use of transition metal catalyst, it is worth emphasizing that the preparation and pre-conditioning of transition metal catalysts can have a significant role on the growth of carbon nanostructures since it is a catalyst- assisted process.

2.2 Overview of previous works

Many parameters can affect the quality of the CNTs, including buffer layer, substrate, type of carbon feedstock gas, catalyst composition, partial pressure of feedstock gas, effect of inert gas, annealing temperature, etc [13-25]. According to the work of Lu et al. [22], higher partial pressure is required for the nucleation of larger diameter nanoparticle which in turn results in larger diameter nanotubes. It has been further proved in this work that by lowering the temperature in addition to lowering the rate of flow of carbon feedstock, small diameter single

wall CNTs could selectively be grown from a large distribution of catalyst nanoparticle. In the CVD technique when using a Si substrate, the formation of metal silicides as a result of the preheating, will poison the synthesis process. For that reason prior to the catalyst deposition different buffer layers are usually deposited on top of the substrates [26,27]. In order to actually modify the characteristics of the grown CNTs, the incorporation of an intermediate layer plays a significant role. Various materials, such as Al, Al_2O_3, Ti, TiO_2, TiN, MgO, SiO2, W and Cr can be used as barrier layers [28-34]. The role of these buffer layers are: (i) improve the adhesion of CNTs to the substrate; (ii) can prevent the diffusion of catalyst atoms into the substrates and (iii) influence the characteristics of the resulting CNTs. A considerable amount of work related to the use of buffer layer during the growth of CNTs has been carried out. It has been reported that the supporting layer can tune the shapes and curvatures of the catalyst particles [35]. Kyung et al., in their work, used Cr, W, and Ti as buffer layer during CNT growth and obtained a maximum current density of 0.78 mA/cm^2 at 7 V/μm [36]. Chuang et al., in their work reported that the carbon atoms for CNT growth were supplied from Ni catalyst particles at an early stage and from Ti interlayer at a later stage in the growth process [37]. Huang et al. obtained well-aligned CNT growth with the use of Ti buffer layer [38]. 1 mA/cm^2 current density was obtained at the field of 3.5 V/μm by Sato et al. [39]. In all these works, the current density obtained was not that good though there was improvement of adhesion of CNT with the substrate.

As field emission electron sources, for better field emission performance and stable electron emission, CNTs must have excellent electrical conductivity to the electrode and good adhesion with the substrate. Wang et al. attributed the instability in emission current to the

structural damage during emission [40]. Bonard et al. ascribed the failure of a CNT to the resistive heating at the point of contact with the substrate [41]. More investigations had shown that emitting CNT would encompass a self-heating process resulting in subliming and melting of a CNT and eventually caused a failure in field emission [42,43]. Xu et al., addressed the issue of self-heating of CNTs due to the physical mechanism responsible for the breakdown [44]. The instability of electron emission because of thermal injury of bad contact to substrate is an urgent issue to be addressed.

This chapter focuses on the efforts made to increase the CNT tip density and improve the adhesion of CNTs with the substrate so as to make the CNT based cold cathodes suitable for high power microwave vacuum devices application, which require high current densities. To address the adhesion issue, substrate heating because of high contact resistance and shielding effect, we deposited titanium buffer layer on silicon substrate since it has been very recently reported that the field emission properties of CNT film have been improved by depositing CNTs onto the titanium (Ti)-coated Si substrate [45]. In our work, the CNTs were grown using CVD technique [46]. Scanning Electron Microscopy (SEM) was employed to study the effect of titanium buffer layer towards the adhesion. The adhesion between CNTs and substrate was greatly improved because of the strong binding between titanium and the substrate. This prevented the CNTs from pulling off from the substrate by the strong electro-static force at high electric field. Emission current density of 30 mA/cm^2 at a field of 4 V/mm was achieved. This suggests great promise for achieving higher current densities at practical electric fields.

2.3 Experimental Procedure

N-type silicon {100} wafers with a low resistivity of 4–6 Ωcm were used as substrates. A 10µm x 10µm square openings with 10µm interspace was formed on the silicon wafers by photolithography process. After the formation of an array, 30-nm-thick Ti was deposited by sputtering as a buffer layer and a thin layer of iron (Fe) was deposited subsequently as a catalyst. Photoresist was removed by a lift-off process. Then, the sample was loaded into the thermal-CVD furnace to grow carbon nanotubes. H_2, NH_3 and C_2H_2 were used as carrier and source gases. Growth temperature was kept around 850ºC and typical growth time was 10 min. SEM characterization was done using model JEOL JSM 840.

In the field-emission measurements, silicon substrate with CNTs was used as cathode and stainless steel plate as anode. The entire sample assembly was kept inside a vacuum chamber evacuated to vacuum better than 1 x 10^{-6} Torr. The cathode and anode were kept 600µm apart, using micrometer screw gauge arrangement and a suitable DC voltage was applied across the cathode and anode using a high voltage power supply.

2.4 Results

2.4.1 SEM morphology

Figure 2.1 (a) and (b) are the SEM images of the CNTs grown without and with the Ti buffer layer (30 nm in thickness) under the Fe catalyst layer respectively. From the morphology

observed, it can be seen that individual CNT bundles grew almost vertically via a self-supporting mechanism, due to the extremely high density of the CNTs. The buffer layer did affect the CNT growth density. It can be seen that the density of CNTs grown with Ti buffer is less when compared with the CNTs grown without Ti buffer. Probably, when grown without Ti buffer, number of catalyst particle sites available for CNT growth will be more when compared with the sample grown with Ti buffer. This is because small portion of Fe particles will be reacting with Ti for improving the adhesion and so the number of Fe particles available for the growth of CNTs will be comparatively reduced resulting in the reduction of CNT tube density.

2.4.2 Bonding of the transition metals with carbon

It is well known that in bulk materials, various metals exhibit different interactions with carbon. Normally, the ability of the bonding of the transition metals with carbon atoms increases as the number of unfilled d-orbital increases. Since the metals such as Au, Al and Pd have no d-vacancies, they have negligible affinity for carbon. Metals with limited d-vacancies such as Fe, Ni, and Co exhibit finite solubility for carbon in certain temperature ranges. On the other hand, 3d and 4d metals with many d- vacancies such as Ti and Nb can form strong chemical bonds with carbon and thus form highly stable carbide compounds. Dai et al., [47] systematically investigated the interaction between various transition metals and CNTs, which shed some light on electrical coupling between nanotubes and metal. Electrons pass the metal–CNT junction by means of quantum tunneling, which in turn increases the contact resistance. However, at the growth temperature of CNTs which is normally around 700 ºC, Ti forms covalent bond carbide

TiC with CNTs. The conductive titanium carbide interlayer will thin or remove the interface barrier.

SEM image shown in Figure 2.1 (a) clearly shows that the adhesion of CNTs with the substrate is not good when grown without the Ti buffer. On the other hand, the use of titanium buffer has improved the adhesion as seen in Figure 2.1 (b).

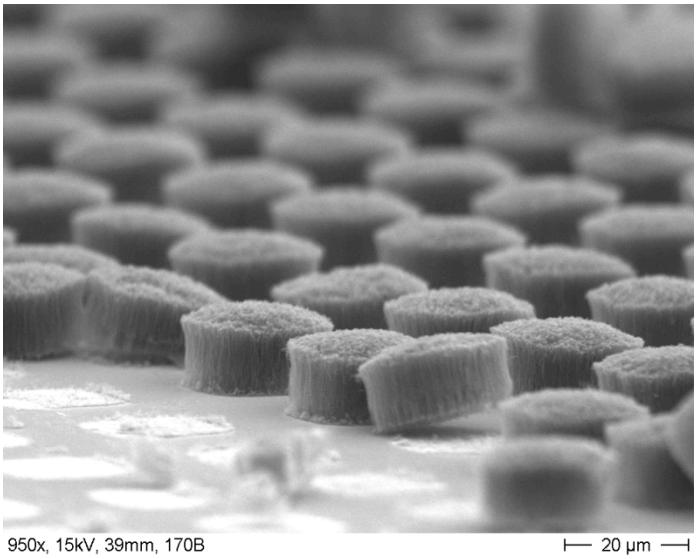

Figure 2.1 (a) SEM images of CNTs grown without Ti buffer.

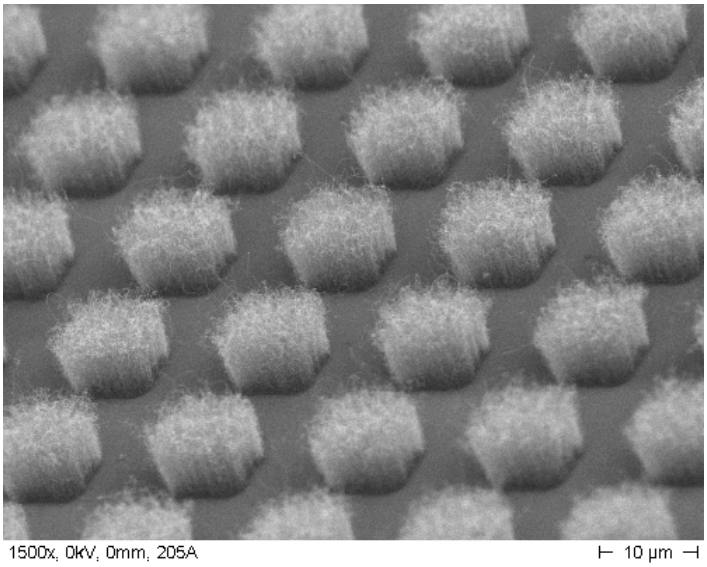

Figure 2.1 (b) SEM images of CNTs grown with Ti buffer.

2.4.3 Improvement in current density

From the J–E curve (Figure 2.2), we observe that there is an increase in the current density in the sample with the titanium buffer layer. Field-emission measurement data of the CNT array shows that the sample grown with the Ti buffer layer gave a better field emission result. The field emission current density increased from 10 mA/ cm^2 to 30 mA/cm^2 at an electric field of 4 V/µm. This observed increase in the emission current density in case of the sample with Ti buffer layer could be attributed to much less dense growth of CNTs of smaller diameter. Both these factors are expected to improve the geometrical field enhancement factor by way of increased aspect ratio and reduced shielding effect of one emitter (CNT) over other. The increased geometrical field enhancement factor ultimately results in lowering of the threshold field and improved field emission current. This increase in current density and field emission stability can also be attributed to the increase in the number of available emitters due

to their strong adhesion with the substrate to support high field in addition to their difference in enhancement factor due to the change in the morphology of the CNT growth.

2.4.4 Mechanism of Ti buffer layer in improving the adhesion

For the sample without a thin Ti buffer layer, part of carbon nanotubes could be pulled off from the substrate due to poor adhesion during field emission experiment. This shows a mechanical destruction during electrical breakdown. The paper of Okai et al., suggests that a strong static electric force may be the main reason of the electrical breakdown in field emission measurements [48].

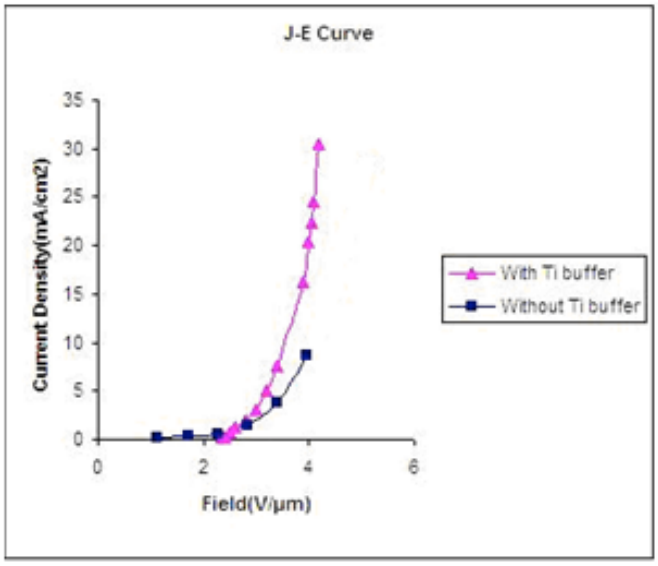

Figure 2.2 J–E curves of CNTs with and without Ti buffer layer

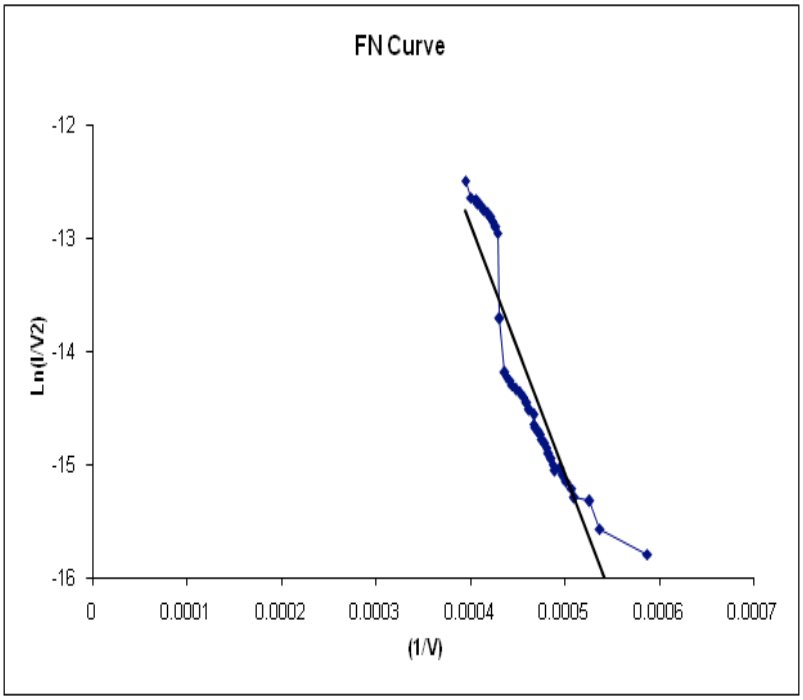

Figure 2.3 F–N curve of CNTs grown with Ti buffer layer

2.4.5 Two different regimes in F-N curve

A rapid increase in the current is observed when the electric field is higher than 3 V/μm. When plotted in a Fowler–Nordheim representation (Figure 2.3), two different regimes of emission are observed. The cathodes can reach currents of a few mA before showing degradation. When degradation of the cathode does occur, the field emission properties are not completely lost, but rather the voltage required to achieve a given current is merely increased. This suggests that either the emitting sites are not completely destroyed or they are replaced by other nanotubes in the film. The requirement for initial break-in of new cathodes and the hysteresis often observed in field emission data suggest a CNT reorganization within the film when an electric field is applied, giving the film a configuration more favorable for field

emission. This reorganization is also interpreted as a cause of the robust behavior or strong adhesion of the cathodes.

As the electric field between the anode and the cathode is increased, the dipole resulting from the concentration of electrons in the tips of carbon nanotubes will enhance the static electric force and pull the carbon nanotubes off from the substrate leading to an abrupt drop of emission current. This phenomenon is attributed to poor adhesion between carbon nanotubes and the substrate. With a thin Ti buffer layer, there is no obvious electrical breakdown as the electric field is increased. This may be due to the better adhesion between catalytic nanoparticles and carbon nanotubes which could have resulted from the thin Ti buffer layer.

2.4.6 Formation of TiC barrier layer

As for CNT films on Ti, because of the formation of conductive TiC, on the CNT–Ti junction, the interface barrier layer was removed (as exhibited in Figure 2.4) making the electrons to pass through this junction without any obstacle. So, during the whole field emission, electrons needed to overcome CNT-vacuum barrier only, as shown in Figure 2.5. Therefore, a very small voltage would result in considerable good electron emission.

Figure 2.4 Formation of conductive TiC barrier layer

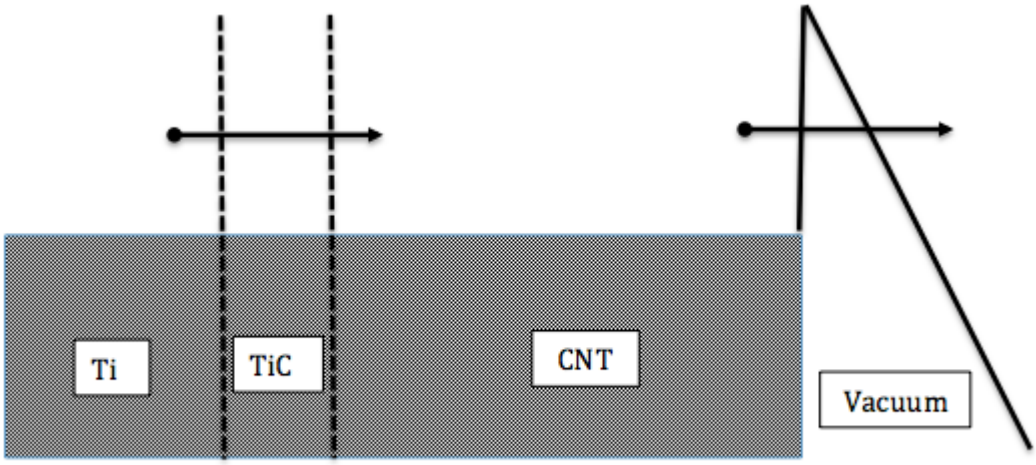

Figure 2.5 Band structure of cathode for CNT films on Ti. (Interface barrier layer was removed due to TiC formation)

This could have been due to the following reasons: (i) the roots of CNTs bond strongly with the Ti layer underneath; (ii) the adhesion of the CNTs to the substrate is dramatically promoted because titanium has an excellent adhesion property to Si and (iii) the titanium carbide could have formed which not only can reduce the effective work function, but also can protect the emitters from the attack of ionized molecules and thereby improving the field emission stability. Since in our lab it is not possible to perform scratch tape test to check adhesion, indirect way of exposure to higher field is adopted.

2.4.7 Stable emission

During FE measurements at high electric fields, vacuum remained moreover stable suggesting reduced substrate heating due to reduction in contact resistance. The emission

current stability has also been examined and a typical time trace of the emission current density at a fixed field of 4 V/μm is shown in Figure 2.6. It was found that there was stable emission for more than 50 minutes due to Ti buffer layer. Efforts are being made to optimize the thickness of Ti buffer layer to get an emission current density of about 1 A/cm^2 at practical field. It was also observed that initially the emission current was a bit unstable which got stabilized by conditioning the sample.

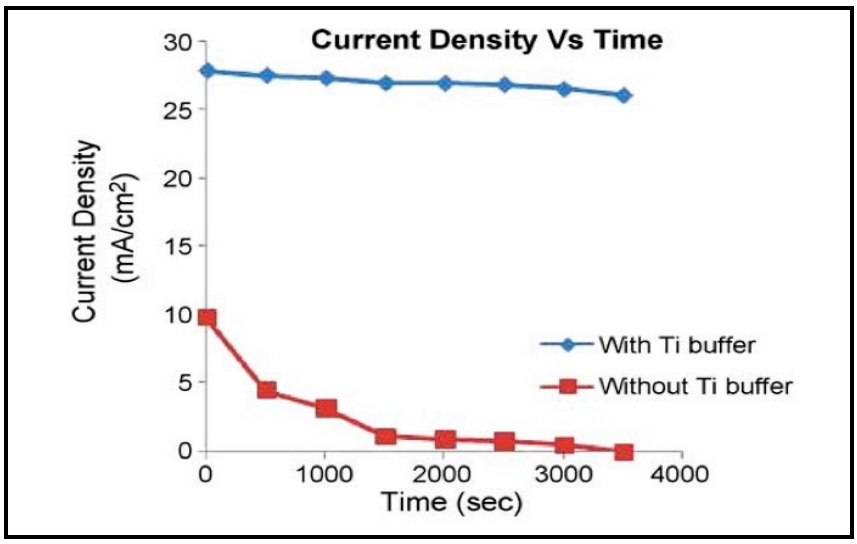

Figure 2.6 Time trace of current density at the fixed field of 4 V/μm

The stability of the emission current was also found to depend upon the vacuum conditions during the measurement. In our earlier experiment [49], when the field was just raised above 5 V/μm, a fluctuation in vacuum reading was observed possibly due to substrate heating. It could happen if some sort of change in state had occurred either due to local evaporation [50], burning or melting of CNTs or Si [51] or both. The debris of CNTs was found all over the substrate. This kind of destructive phenomenon can also be due to Joule heating. Bonard et al. [52] have reported that at high emission current density, a high contact resistance

caused by the bad interface between the CNTs and the substrate will result in Joule heating and lead to local evaporation of CNTs. The sample with the titanium buffer layer might have reduced the contact resistance between CNTs and the substrate. This may in turn suppress the Joule heating.

2.5 Conclusion

Using titanium buffer layer during CNT growth, the density of carbon nanotubes was efficiently modified to promote the electrical characteristics of field emission. The field emission current density increased from 10 mA/cm^2 to 30 mA/cm^2 at electric field of 4 V/μm with the help of the buffer layer. Also better adhesion of CNTs with the substrate was achieved which in turn suppressed the mechanical destruction and prevented the emitters from the electrical breakdown. Thus, stable emission of electron was realized for a longer duration without vacuum degradation. With some refinement in the growth parameters, we can certainly increase the current density of the emitter to a considerable extent.

2.6 References

1. S. Iijima, Nature (Lond.) 354 (1991) 56.
2. R. Martel, et al. Appl. Phys. Lett. 73 (1998) 2447.
3. H. Dai, N. Franklin, J. Han, Appl. Phys. Lett. 73 (1998) 1508
4. H. Dai, J.H. Hafner, A.G. Rinzler, D.T. Colbert, R.E. Smalley, Nature (Lond.) 388 (1997) 756
5. K. Shibayama, M. Hiraki, Y. Saito, A. Hosong, Jpn. J. Appl. Phys., Part 1 42 (2003) 3698
6. R.H. Fowler, L. Nordheim, Proc. R. Soc. Lond., Ser. A 119 (1928) 173
7. T.E. Stern, B.S. Grossling, R.H. Fowler, Proc. R. Soc. Lond., Ser. A 124 (1929) 699
8. D. Temple, Mater. Sci. Eng., R. 24 (1999) 185
9. Y. Huh, J.Y. Lee, C.J. Lee, Jpn. J. Appl. Phys. 42 (2003) 7154.
10. A.V. Melechko, V.I. Merkulov, T.E. McKnight, M.A. Guillorn, K.L. Klein, D.H. Lowndes, M.L. Simpson, J. Appl. Phys. 97 (2005) 041301.
11. Hongjie Dai, in: M.S. Dresselhaus, G. Dresselhaus, Ph. Avouris (Eds.), Carbon Nanotubes: Synthesis, Structure, Properties, and Applications, Springer-Verlag, Berlin, 2001, p. 33.
12. N.M. Rodriguez, A. Chambers, R.T.K. Baker, Langmuir 11 (1995) 3862.
13. H. Kataura, Y. Kumazawa, Y. Maniwa, Y. Ohtsuka, R. Sen, S. Suzuki, Y. Achiba, Carbon 38 (2000) 1691–1697.
14. R.H. Hauge, C.L. Pint, S.T. Pheasant, A.N.G. Parra-Vasquez, C. Horton, Y.Q. Xu, Journal of Physical Chemistry C 113 (2009) 4125–4133.

15. G.Eres,A.A.Kinkhabwala,H.T.Cui,D.B.Geohegan,A.A.Puretzky,D.H.Lowndes, Journal of Physical Chemistry B 109 (2005) 16684–16694.

16. T. Saito, S. Ohshima, T. Okazaki, S. Ohmori, M. Yumura, S. Iijima, Journal of Nanoscience and Nanotechnology 8 (2008) 6153–6157.

17. R. Xiang, E. Einarsson, J. Okawa, Y. Miyauchi, S. Maruyama, Journal of Physical Chemistry C 113 (2009) 7511–7515.

18. A.R. Harutyunyan, G.G. Chen, T.M. Paronyan, E.M. Pigos, O.A. Kuznetsov, K. Hewaparakrama, S.M. Kim, D. Zakharov, E.A. Stach, G.U. Sumanasekera, Science 326 (2009) 116–120.

19. B.G.Sumpter,V.Meunier,J.M.Romo-Herrera,E.Cruz-Silva,D.A.Cullen,H.Ter- rones, D.J. Smith, M. Terrones, ACS Nano 1 (2007) 369–375.

20. H. Liu, G. Cheng, R. Zheng, Y. Zhao, C. Liang, Surface and Coatings Technology 202 (2008) 3157–3163.

21. C.L. Cheung, A. Kurtz, H. Park, C.M. Lieber, Journal of Physical Chemistry B 106 (2002) 2429–2433.

22. C. Lu, J. Liu, Journal of Physical Chemistry B 110 (2006) 20254–20257

23. M.G.Hahm,Y.K.Kwon,E.Lee,C.W.Ahn,Y.J.Jung,JournalofPhysicalChemistry C 11 (2008) 17143–17147. [

24. S.P. Patole, P.S. Alegaonkar, J.H. Lee, J.B. Yoo, Europhysics Letters 81 (2008), 38002-

1–38002-6

25. S.P. Patole, P.S. Alegaonkar, H.C. Lee, J.B. Yoo, Carbon 46 (2008) 1987–1993.

26. Merkulov VI, Melechko AV, Guillorn MA, Lowndes DH, Simpson ML. Effects of spatial separation on the growth of vertically aligned carbon nanofibers produced by plasma-enhanced chemical vapor deposition. Appl Phys Lett 2002;80:476–9.

27. Teo KBK, Chhowalla M, Amaratunga GAJ, Milne WI, Pirio G, Legagneux P, et al. Characterization of plasma-enhanced chemical vapor deposition carbon nanotubes by Auger electron spectros- copy. J Vac Sci Technol B 2002;20:116–21.

28. Cao A, Ajayan P M, Ramanath G, Baskaran R and Turner K 2004 *Appl. Phys. Lett.* **84** 109–11

29. de los Arcos T, Garnier M G, Seo J W, Oelhafen P, Thommen V and Mathys D J 2004 *J. Phys. Chem.* B **108** 7728–34

30. de los Arcos T, Garnier M G, Oelhafen P, Mathys D, Seo J W, Domingo C, Garcia-Ramos J V and Sanchez-Cortes S 2004 *Carbon* **42** 187–90

31. de los Acros T, Wu Z M and Oelhafen 2003 *Chem. Phys. Lett.* **380** 419–23

32. XiongGY,WangDZandRenZF2006*Carbon***44**969–73

33. ChiuCC,TsaiTY,TaiNHandLeeCY2006*Surf.Coat. Technol.* **200** 3215–33

34. LeeHC,AlegaonkarPS,KimDY,LeeJH,LeeTY, Jeon S Y and Yoo J B 2008 *Thin Solid*

Films **516** 3646–50

35. Y. Wang, B. Li, P.S. Ho, Z. Yao, L. Shi, Appl. Phys. Lett 89 (2006) 183113.
36. K.H. Park, J.H. Yim, S. Lee, K.H. Koh, Thin Solid Films 501 (2006) 233–237.
37. Chuang, et al. Surf. Coat. Technol. 202 (2008) 2121–2125.
38. Huang, et al. IVNC 2004 (2004) 34–35.
39. H. Sato, et al. IVNC 2004 (2004) 210–211.
40. Wang ZL, Gao RP, de Heer WA, Poncharal P: In situ imaging of field emission from individual carbon nanotubes and their structural damage. Appl Phys Lett 2002, 80:856-858.
41. Bonard JM, Klinke C, Dean KA, Coll BF: Degradation and failure of carbon nanotube field emitters. Phys Rev B 2003, 67:115406.
42. Dean KA, Burgin TP, Chalamala BR: Evaporation of carbon nanotubes during electron field emission. Appl Phys Lett 2001, 79:1873-1875.
43. Purcell ST, Vincent P, Journet C, Binh VT: Hot nanotubes: stable heating of individual multiwall carbon nanotubes to 2000 K induced by the field- emission current. Phys Rev Lett 2002, 88:105502.
44. Huang NY, She JC, Chen J, Deng SZ, Xu NS, Bishop H, Huq SE, Wang L, Zhong DY, Wang EG, Chen DM: Mechanism responsible for initiating carbon nanotube vacuum breakdown. Phys Rev Lett 2004, 93:075501.
45. Y. Qin, M. Hu, Appl. Surf. Sci. 255 (17) (2009) 7618S–7622S.

46. P. Chaturvedi, S. Pal, Lamba, A.B. Dhaulakhandi, D.S. Rawal, M. Bal, Harsh, S.K. Agrawal, IWPSD Chennai (2003) 974.

47. Zhang Y, Franklin NW, Chen RJ, Dai H. Metal coating on suspended carbon nanotubes and its implication to metal–tube interaction. Chem Phys Lett 2000;331:35–41.

48. M. Okai, T. Fujieda, K. Hidaka, T. Muneyoshi, T. Yaguchi, Jpn. J. Appl. Phys., Part 1 44 (2005) 2051.

49. P. Verma, S. Gautham, P. Kumar, P. Chaturvedi, J.S. Rawat, s. Pal, R. Chaubey, H.P. Harsh, P.K. Vyas, Bhatnagar, J. Vac. Sci. Technol. B 25 (2007) 1584.

50. A.T. Sowers, B.L. Ward, S.L. English, R.J. Nemanish, J. Appl. Phys. 86 (1999) 3973.

51. J.C. She, et al. Appl. Phys. Lett. 83 (2003) 2671.

52. J.-M. Bonard, C. Klinke, Phys. Rev. B 67 (2003) 115406.

CHAPTER III

Effect of buffer layer thickness on the field emission of CNTs

3.1 Introduction

In the previous chapter, it was proved that there was improvement in the field emission properties of the CNTs with the use of buffer layer. We explained the efforts made to improve the adhesion of CNTs with the substrate so as to make the CNT based cold cathodes suitable for high power microwave vacuum devices application. This chapter focusses on the effect of the buffer layer thickness on the field emission properties of the CNTs. To address the adhesion issue and substrate heating because of high contact resistance, we deposited titanium buffer layer of different thicknesses below a thin layer of iron catalyst layer on a patterned silicon substrate. The CNTs were grown using chemical vapor deposition (CVD) technique [14]. Scanning Electron Microscopy (SEM), Transmission electron microscopy (TEM) and EDS analysis was employed to study the effect of titanium buffer layer towards the adhesion. Field emission experiments were performed for the sample with 10nm and 20nm thick Ti buffer layer and the emission current density of the sample with 20nm thick titanium found to be 200 times more than those with 10nm thick titanium buffer layer. This is because the adhesion between CNTs and substrate was greatly improved because of the strong binding between titanium and the substrate. We expected that this will prevent the CNTs from pulling off from the substrate by the strong electro-static force at high electric field. The field emission measurements

showed that the CNT array with the 20nm of Ti buffer layer gave a reasonably good FE characteristics because of the reduction in the shielding effect between the CNTs.

3.2 Experimental procedure

N-type silicon <100> wafers with a low resistivity of 4-6Ωcm wafer was used as substrate. 10μmx10μm square openings with 10μm interspace were formed on the silicon wafer by photolithography process. After the formation of an array, 10nm and 20-nm-thick Ti was deposited by sputtering as a buffer layer and a thin layer of iron (Fe) was deposited subsequently as a catalyst in the same sputtering system followed by lift-off. Then, the sample was loaded into the CVD furnace to grow carbon nanotubes. $H_{2,}$ NH_3 and C_2H_2 were used as carrier and source gases. Growth temperature was kept around 850ºC and typical growth time was 10 minutes. The morphology of CNTs on substrate were observed and investigated by transmission electron microscopy (TEM) , high-resolution transmission electron microscopy (Technai G-20-stwin, 200 KV) and scanning electron microscopy (JEOL JSM 840).

In the field emission measurements, silicon substrate with CNTs was used as cathode and stainless steel plate as anode. The entire sample assembly was kept inside a vacuum chamber evacuated to vacuum better than $1x10^{-6}$ torr. The cathode and anode were kept 500μm apart, using micrometer screw gauge arrangement and a suitable DC voltage was applied across the cathode and anode using a high voltage power supply.

3.3 Results and Discussion

3.3.1 Morphology of CNTs

Figure 3.1 (a and b) are the SEM images of the CNTs grown with about 10nm and 20nm thick Ti buffer layer under the Fe catalyst layer. Figure 3.1 (c) is the SEM image of the sample grown without Ti buffer layer. From the morphology observed, it can be seen that the sample with 10nm thick titanium buffer layer may not be suitable for field emission applications. When grown with 20nm thick titanium buffer layer, individual CNT bundles grew almost vertically due to the extremely high density of the CNTs. It is also evident from the SEM images that the CNTs nucleate and grow well when grown with optimum thickness of titanium as a buffer layer.

3.3.2 Formation of Ti capping layer

As shown in Fig. 1(b), Fe was observed at the tips of CNTs grown on Fe/Ti film, as a buffer layer. Probably, small portion of Fe which was not alloyed with Ti film (and was easily separated from it), was found to be lifted up to the top of the CNTs. As suggested by Young et al [15], acetylene molecules are catalytically adsorbed on the metal domains. As carbon atoms are further supplied, a carbon-metal eutectic alloy can be formed, decreasing the melting temperature of the alloy. Formation of carbon-metal eutectic alloy enhances the diffusion of carbon in the metal alloy, initiating carbon aggregations which act as a nucleation seed for nanotube growth. The carbon diffusion is limited by the domain size within the metal particles and thus the diameter of nanotubes should be smaller than the domain size. As the nanotube grows further, part of the metal domain is pushed upward, forming a metal cap.

3.3.3 TEM and HRTEM results

The HRTEM and TEM image of the sample with 30nm thick titanium buffer layer in Figure 3.2 (a) and (b) respectively shows that the CNTs are 20–50 nm in diameter and up to several microns in length. As shown in Figure 3.2 (b), Fe nanoparticles were observed at the tip of the CNT. Further the HRTEM image, it is clear that the CNT are multi-walled, centrally hollow tube. An EDS analysis in Figure 3.2 (c) shows the component of the particle in the carbon nanotube. The EDS spectrum exhibits well resolved signals from the characteristic K-shell ionization edges of carbon at 0.28 keV confirming the CNT. The peaks of copper are from the copper grid, which is used to hold the carbon nanotubes in TEM system. From the TEM images and the EDS analysis, Ti seems not to be involved into the catalytic nanoparticle and there is no obvious destructive effect on the crystallinity of the multiwall structure.

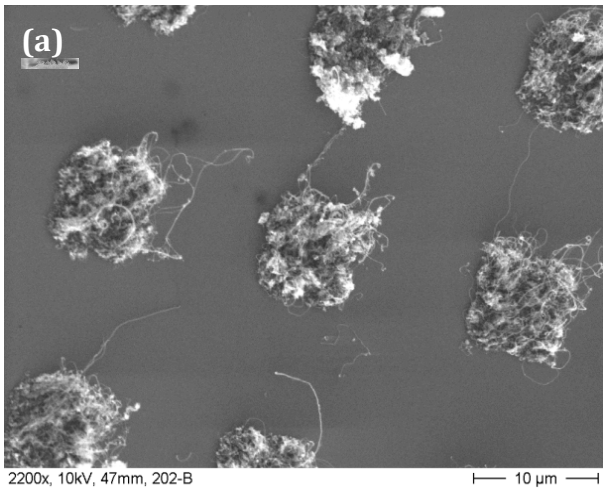

Figure 3.1 (a) CNTs grown with 10nm thick Ti

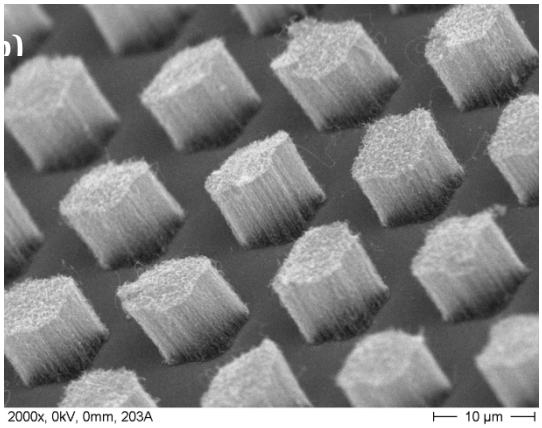

Figure 3. 1 (b) CNTs grown with 20nm thick Ti

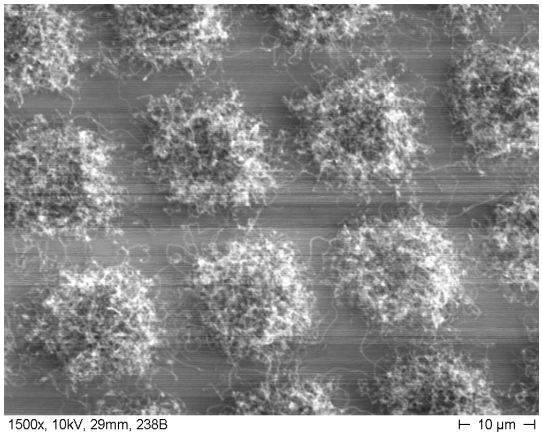

Figure 3.1 (c) CNTs grown without Ti

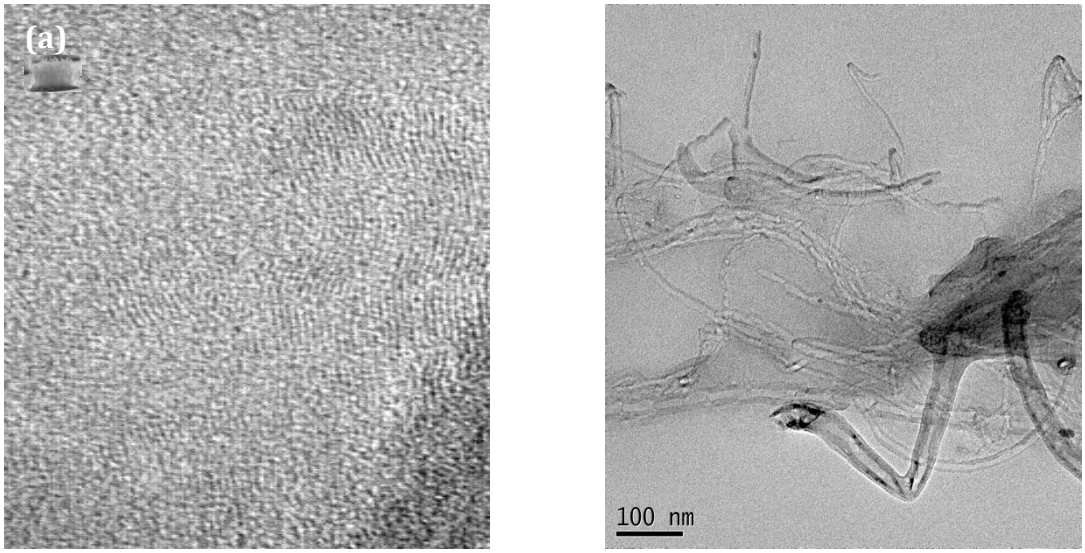

Figure 3. 2(a) HRTEM and (b)TEM images of the CNT

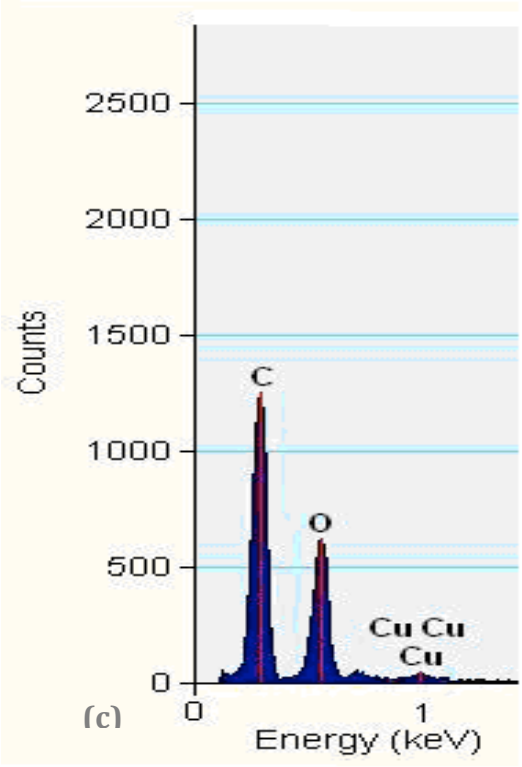

Figure 3. 2 (c) EDS spectrum of the grown CNT

3.3.4 Field emission characteristics

The field emission characteristics of the prepared CNT emitter arrays were measured in the diode structure. A typical plot of emission current density versus electric field (J-E curve) of the samples with 20nm, 10nm thick Ti and without Ti are shown in Figure 3.3 (a - b). The turn on field E_{to}, defined as the electric field to produce a current density of $10\mu A/cm^2$, of the sample with 20nm thick Ti, compared with the sample of 10nm thick Ti, reduced from 3.7V/µm to 2.9V/µm and the field emission current density at 5V/µm increased from $25.5\mu A/cm^2$ to $5.09mA/cm^2$. Hence the emission current density of the sample with 20nm thick titanium has increased around 200 times than those with 10nm thick titanium buffer layer.

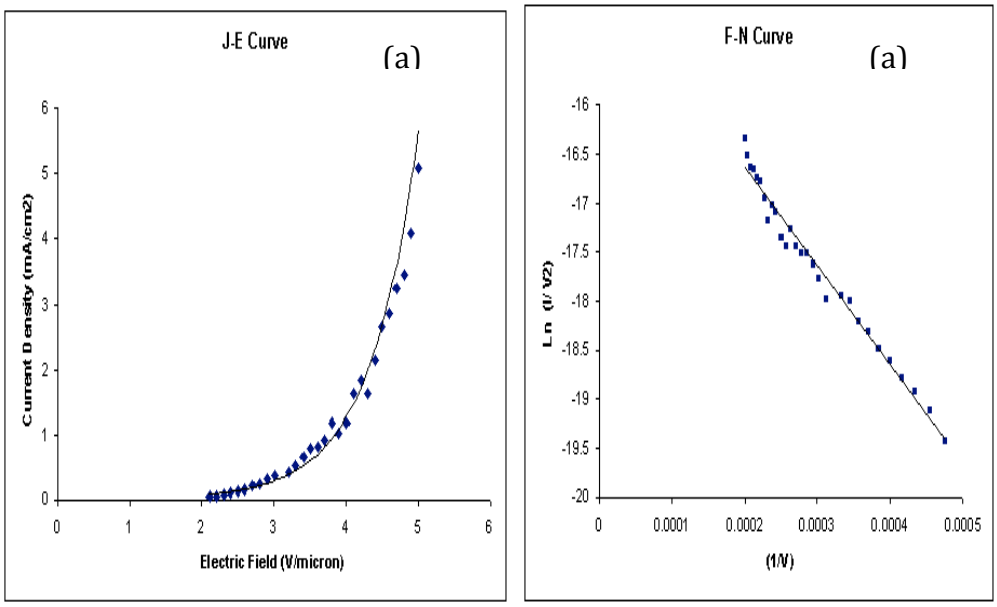

Figure 3.3 (a) Current vs. voltage characteristics and the corresponding Fowler–Nordheim plot [Of the sample with 20nm thick Ti buffer layer]

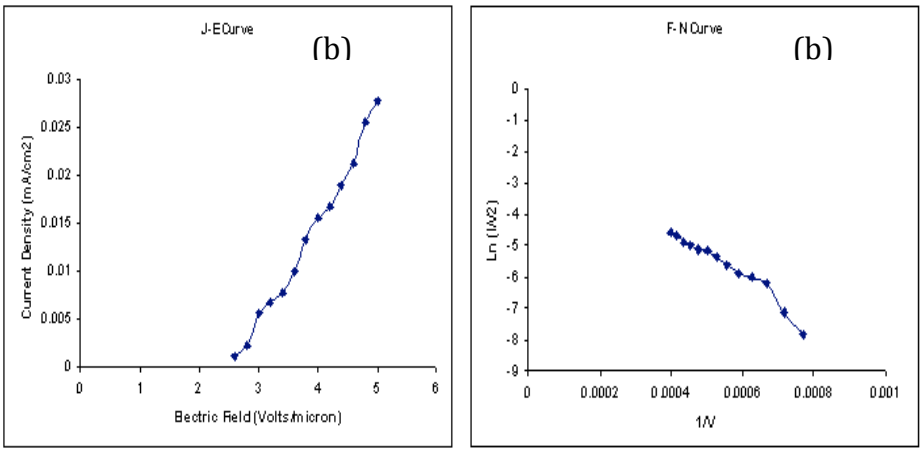

Figure 3.3 (b) Current vs. voltage characteristics and the corresponding Fowler–Nordheim plot [Of the sample with 10nm thick Ti buffer layer]

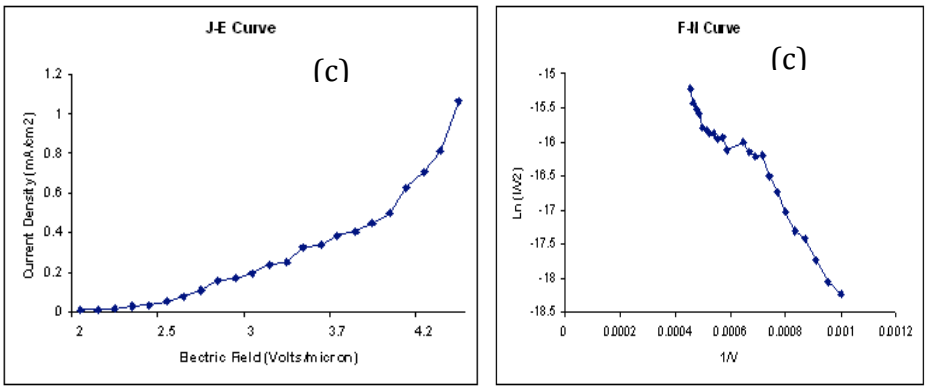

Figure 3.3 (c) Current vs. voltage characteristics and the corresponding Fowler–Nordheim plot [Of the sample without Ti buffer layer]

The E_{to} and the emission current density of our samples were comparable to the corresponding values in literatures [16-18]. As explained in the previous chapter, we believe that TiC could have formed by the reaction between Ti and C. Investigations are being carried out about this and we'll report the same in our future publication. Ti must have been decomposed and subsequently carbonated during CNT growth. It has been proved that the

titanium carbide has very low work function of about 3.5 eV [19]. So, the effective work function of CNTs emitters could be reduced due to the formation of the titanium carbide on the surface of CNTs. That is, the electron tunneling barrier for the titanium carbide-modified CNTs was reduced effectively, which might help the electron emission at considerably low turn-on electric field.

3.3.5 F-N characteristics and enhancement factor

The linear behavior of the FN curves (Figure 3.3) indicated that the measured current was generated by field emitted electrons. Taking the work function of CNTs the same as that of graphite, i.e., 5 eV [20], the field enhancement factor β of the sample with 20nm thick titanium buffer of 8871 was calculated by using the slope of the straight region. The rather high β value, which is still comparable to those in literatures [21-23], should have some contribution from the enhanced conductivity between the CNTs and titanium buffer layer.

3.3.6 Study of emission current degradation

In our earlier study [24], when the field was just raised above 5V/μm, a fluctuation in vacuum reading was observed. To address this issue, we performed another experiment without Ti buffer layer for field emission studies where we could not even go up to 5V/μm as shown in Figure 3.3 (c). Similar to our previous report, in this experiment too, when the current density was about 1mA/cm^2, arcing started which in turn resulted in fluctuation in the vacuum. It could have happened if some sort of change in state had occurred either due to evaporation, burning or melting of the CNT's or silicon or both. In order to study the emission current degradation

phenomena, which is a slow degradation of current when a constant electric field is applied for a long time, a high voltage of 5V/µm was applied between the anode and cathode for more than an hour. In this experiment, we increased the field from 4 V/µm to 5 V/µm. The emission current density was found to be stable in the case of the sample with 20nm thick Ti buffer but dropped to almost zero in a very short time in the sample with 10nm

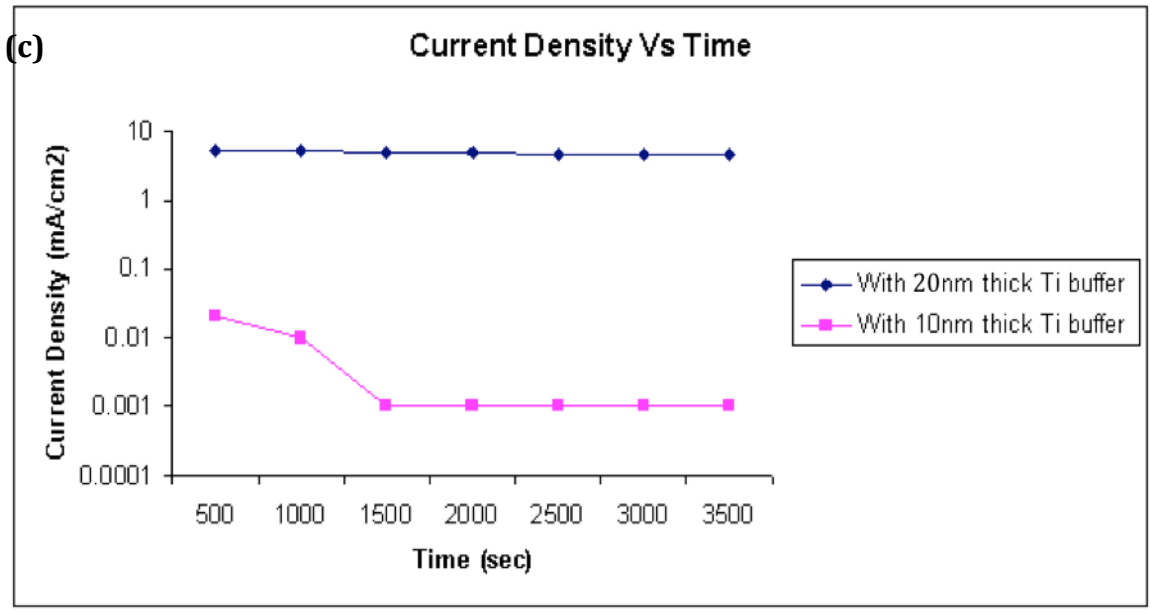

Figure 3.4 Time trace of the current density at a fixed applied voltage of 5V/ µm

thick Ti buffer (Figure 3.4). This can be attributed mainly due to the formation of titanium carbide. As titanium carbide has extremely high melting point and good chemical inertness, the titanium carbide formed on the root of CNTs not only can reduce the effective work function, but also can protect the emitters from peeling off from the substrate giving rise to stable emission. Thus, the experiment clearly indicated that the use of titanium buffer layer of optimum thickness has certainly improved the adhesion of CNT with the substrate giving rise to

a stable emission for prolonged duration. This increased CNT-substrate adhesion could avoid CNTs efficaciously to be overheated by joule heating and prevent the early current saturation of the CNT emitter [25].

3.4 Conclusion

Vertically aligned CNT emitter arrays was synthesized using titanium buffer layer. Reasonably good current density at reduced turn on field was achieved and there was excellent improvement in the adhesion of CNT with the substrate giving rise to stable emission for more than an hour. With some refinement in the growth parameters, we can certainly increase the current density of the emitter to a considerable extent. If instead of diode, triode configuration is used for the field emission experiment, the emitter tips shall be able to extract electrons at much lower gate voltage. Taking into account the fine field emission property and the simple procedure for the synthesis, CNT based emitters with titanium buffer layer of optimum thickness should be a promising electron source for potential applications.

3.5 References

1. S. Iijima, Nature (London) 354, 56 (1991).
2. H. Dai, J. H. Hafner, A. G. Rinzler, D. T. Colbert, and R. Smalley, Nature (London) 384, 187 (1996).
3. L. Forro and C. Schnonenberger, *(*Springer, New York, 2001), p. 329.
4. T. Hertel, R. Martel, and P. Avouris, J. Phys. Chem. B 102, 910 (1998).
5. M. A. Guillorn, A. V. Melechko, V. I. Merkulov, E. D. Ellis, M. L. Simpson, L. R. Baylor, and G. J. Bordonaro, J. Vac. Sci. Technol. B 19, 2598 (2001).
6. C. Bower, W. Zhu, D. Shalom, D. Lopez, L. H. Chen, P. L. Gammel, and S. Jin, Appl. Phys. Lett. 80, 3820 (2002).
7. K. B. Teo, M. Chhowalla, G. A. Amaratunga, W. I. Miline, P. Legagneux, G. Pirio, L. Gangloff, D. Pribat, V. Semet, V. T. Binh, W. H. Bruenger, J. Eichholz, H. Hanssen, D. Friedrich, S. B. lee, D. G. Hasko, and H.Ahmed, J. Vac. Sci. Technol. B 21, 693 (2003).
8. J. M. Planeiz, N. Coustel, B. Coq, V. Brotons, P. S. Kumbhar, R. Dutartre, P. Geneste, P. Bernier, and P. M. Ajayan, J. Am. Chem. Soc. 116, 7935, (1994).
9. C. Dillon, K. M. Jones, T. A. Bekkedahl, C. H. Kiang, D. S. Bethune, and M. J. Heben, Nature, (London) 386, 377 (1997).
10. G. E. Gadd, M. Blackfold, S. Moricca, N. Webb, P. J. Evans, A. M. Smith, G. Jacobsen, S. Leung, A. Day, and Q. Hua, Science 277, 933 (1997).
11. S. S. Wong, J. D. Harper, P. T. Lansbury, and C. M. Lieber, J. Am. Chem. Soc. 120, 603 (1998).

12. Teresa de los Arcos T, Vonau F, Garnier MG, Thommen V, Boyen HG, Oelhafen P M. Düggelin, D. Mathys, and R. Guggenheim., Appl. Phys. Lett. 80, 2002, 80, 2383–5.
13. Merkulov VI, Melechko AV, Guillorn MA, Lowndes DH, Simpson ML.. Appl Phys Lett 2002, 80, 476–9.
14. P. Chaturvedi, S. Pal, S. Lamba, A. B. Dhaulakhandi, D. S. Rawal, M. Bal, Harsh and S. K. Agrawal, IWPSD Chennai, 2003, 974.
15. Young Chul Choi, Dae Woon Kim, Tae Jae Lee, Cheol Jin Lee, Young Hee Lee, Synthetic Metals 117 (2001) 81-86
16. Y. Sun, C.Z. Gu, W. Liu, Z.S. Jin, Diam. Relat. Mater. 13 (2004), 1187.
17. J.H. Han, T.Y. Lee, D.Y. Kim, J.B. Yoo, C.Y. Park, J.J. Choi, T. Jung, I.T. Han,
18. J.M. Kim, Diam. Relat. Mater. 13 (2004) 987.
19. Y. Chen, D.T. Shaw, L.P. Guo, Appl. Phys. Lett. 76 (2000) 2469.
20. Y. Qin, M. Hu , Applied Surface Science 254 (2008) 3313–3317
21. J.H. Han, T.Y. Lee, D.Y. Kim, J.B. Yoo, C.Y. Park, J.J. Choi, T. Jung, I.T. Han, J.M. Kim, Diam. Relat. Mater. 13 (2004) 987.
22. M.A. Guillorn, A.V. Melechko, V.I. Merkulov, D.K. Hensley, M.L. Simpson, D.H. Lowndes, Appl. Phys. Lett. 81 (2002) 3660.
23. Y. Saito, S. Uemura, Carbon 38 (2000) 169.
24. P. Verma , S. Gautham, P. Kumar, P.Chaturvedi, J.S. Rawat, s. Pal, R. Chaubey, Harsh, H.P. Vyas and P.K. Bhatnagar , J. Vac. Sci. Technol B 25, 1584 (2007)
25. Bonard J and Klinke C 2003 Phys. Rev. B 67, 115406.

CHAPTER IV

Density control of CNTs for better field emission

4.1 Introduction

For CNTs to be used in field emission application, uniform, and large emission current over the CNT film is required at low threshold electric field. It has been reported that the density of CNTs play a crucial role in determining the field emission properties. The growth process described in the Chapter 3 and 4 yielded high density of CNTs. Several reports in the literature show emission current density ranging from 50 mA/cm^2 to 4 A/cm^2 with single-walled nanotubes and multi walled CNTs on a patterned Fe film grown on Si substrate [1-6]. The excellent field emission characteristics of CNTs can be attributed to their high aspect ratios of the length to the diameter resulting in the enhancement of electric field at the CNT tip. [7-12]. Emission current depends on several parameters such as catalyst metal, adhesion layer, structure, and density of CNTs [13,14]. In high density CNT films, the screening effect reduces the field enhancement to a larger extent which in turn affects the emitted current [15,16]. According to the work of Nilson et al., [15], the emission current can be maximized when the intertube distance is around twice the height of the CNTs.

However, most growth methods used today afford a high density of CNTs on the substrate. The disadvantage of such high-density growth is the high turn-on field because of the large screening effect. There are several reports on controlling the growth density of CNTs by

plasma treatment, wet etching, thin-film capping layer, etc. [17-19]. But, most of the methods will increase the complexity in their synthesizing technique.

4.2 Methods used for reducing the density of CNTs

Groning et al. [20] has reported by the simulation of an electric field that the best density of carbon nanotubes with 1μm is approximately 3 x 10^7 cm^{-2} to suppress the screening effect and obtain an optimized emission current density. Unfortunately, the density of carbon nanotubes synthesized through CVD technique is much higher than $10^7 cm^{-2}$. Several methods, such as electron beam lithography [21], ultraviolet photolithography, [22] pulse current electro-chemical deposition [23], SiOx capping [24], plasma post-treatment [25], catalytic particle size control [26] etc., have been reported to reduce the density of CNTs grown by CVD technique to suppress the screening effects. Although some of these methods can effectively control the density of carbon nanotubes, destruction of crystallinity results in many cases and also high cost is involved in the above mentioned complex processes.

4.2.1 Electrical breakdown and emission current degradation

During field emission, electrical breakdown which is nothing but an abrupt drop of emission current when the electric field between anode and cathode is increased [27] and emission current degradation which is a slow degradation of emission current when a constant electric field is applied between anode and cathode for a long period [28,29] are two important aspects to be considered for reliability. The work of Okai et al.[27] proved that the electrical breakdown may result from a mechanical destruction of carbon nanotubes caused by a strong

static electric force. From Bonard and Klinke's work [29], the high contact resistance results due to weak interface between the CNTs and the substrate. It has also been reported in their work that when there is a passage of high emission current density through the CNTs, Joule heating results which may in turn cause the local evaporation of CNTs. We must increase the adhesion and reduce the contact resistance between the carbon nanotubes and the substrate to suppress these two phenomena.

In this chapter, we discuss a simple method to control the density of CNTs, which will not only reduce the turn-on field but can also improve the adhesion of CNTs to the substrate, and reduce the contact resistance between substrate and CNTs. In our experiment, a barrier layer of Ti is first sputtered on the substrate to improve the adhesion of CNTs. On top of the barrier layer, a layer of Fe (which catalyses the growth of CNTs) is sputtered. Over this, sputtering of a thin capping layer of Ti of varying thickness is carried out in order to suppress the screening effect. By varying the thicknesses of the capping layer, the density of carbon nanotubes can be controlled effectively without serious damages to their crystallinity.

4.2.2 Experiment

N-type silicon {100} wafers with a low resistivity of 4–6 Ωcm were used as substrates. A 10μm x 10μm square openings with 10μm interspace was formed on the silicon wafers by photolithography process. After the formation of an array, 30-nm-thick Ti was deposited by sputtering as a buffer layer and a layer of iron (Fe) (5nm) was deposited subsequently as a catalyst. Photoresist was removed by a lift-off process. After this, the sample was pretreated in the thermal-CVD furnace in atmospheric pressure at 700°C with H_2 (500 sccm) for 5 min in

order to form catalytic iron nanoparticles. After the formation of catalytic nanoparticles, a thin titanium capping layer with different thicknesses 10, 20 and 40 Å was deposited over the catalyst nanoparticle in a sputtering system. Then, the samples were loaded into the thermal-CVD furnace to grow carbon nanotubes. H_2, NH_3 and C_2H_2 were used as carrier and source gases. Growth temperature was kept around 800°C and typical growth time was 10 min. SEM characterization was done using model JEOL JSM 840.

In the field emission measurements, silicon substrate with CNTs was used as cathode and stainless steel plate as anode. The entire sample assembly was kept inside a vacuum chamber evacuated to vacuum better than $1x10^{-6}$ torr. The cathode and anode were kept 500μm apart, using micrometer screw gauge arrangement and a suitable DC voltage was applied across the cathode and anode using a high voltage power supply.

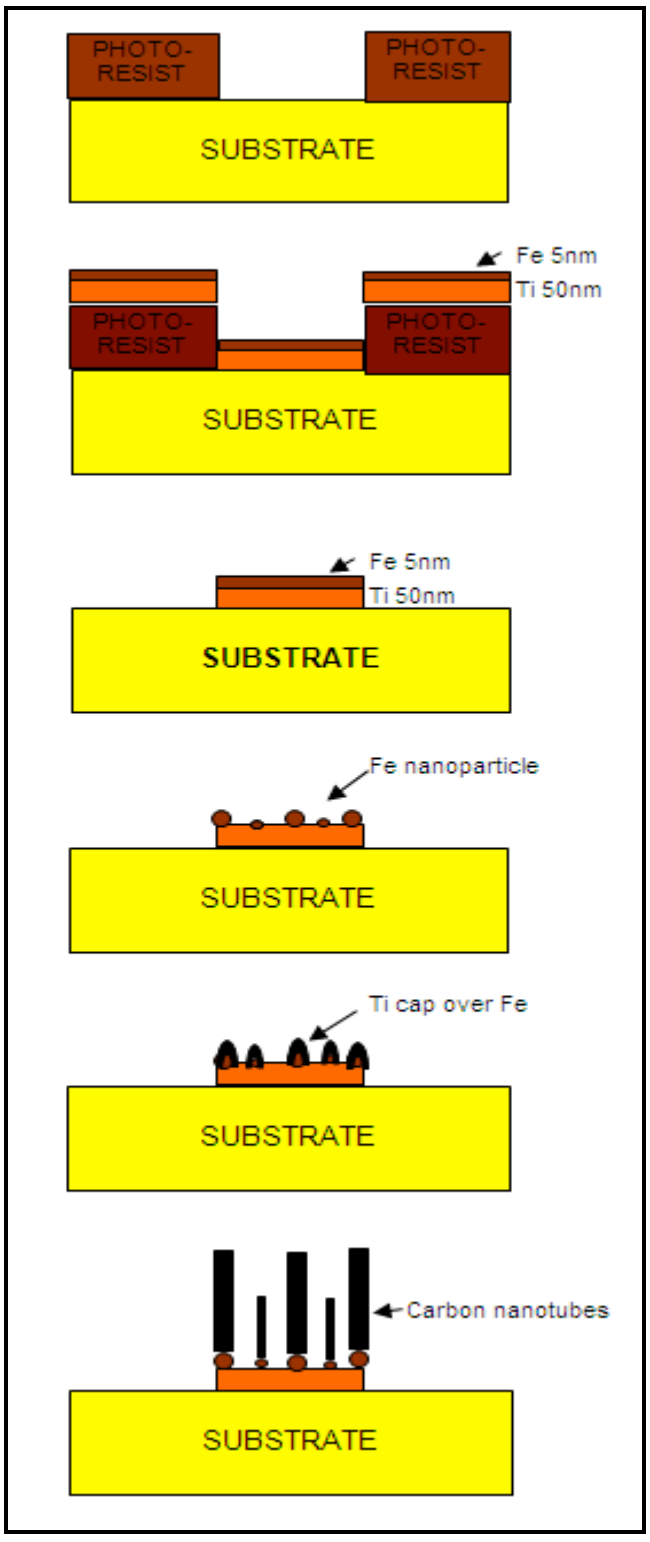

Figure 4.1 Schematic procedure of the experiment

4.3 Results and discussion

4.3.1 Catalyst nanoparticle after Ti capping of different thickness

The schematic procedure of the experiment is given in Figure 4.1. The SEM images of hydrogen-pretreated iron catalytic nanoparticles without any Ti capping and with three different thicknesses of the thin Ti capping layer (10 Å, 20 Å and 40 Å) are shown in Figure 4.2. Figures 4.2 (a-d) clearly reveal that part of catalytic nanoparticles remained and the other particles become unobvious when the thickness of thin Ti capping layer is increased from 0 to 40 Å. This could be due to the fact that the catalytic nanoparticles with very small size are buried under the increased Ti capping layer.

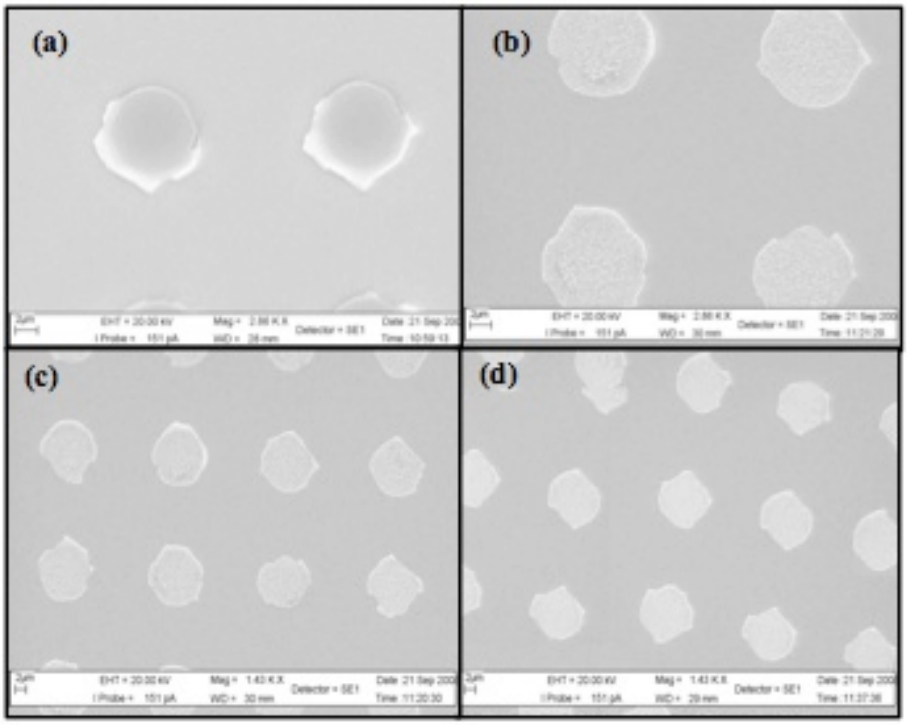

Fig 4.2. SEM images of catalyst surface on substrate (a) without Ti capping and (b) with Ti capping of 10 Å, (c) With Ti capping of 20 Å and (d) with Ti capping of 40 Å

4.3.2 Morphology of the CNTs grown after Ti capping

After the deposition of the thin Ti capping layer, the samples were loaded into the thermal-CVD to grow carbon nanotubes. Figure 4.3 shows the morphologies of subsequently-grown CNTs. From the SEM images [Figures 4.3 (a-d)], it can easily be observed that the density of carbon nanotubes decreases with the increase in the thickness of the thin Ti capping layer. This shows that the thin Ti capping layer on pretreated catalytic nanoparticles can restrain the growth of CNTs and the density of CNTs can be controlled by changing the thickness of the thin Ti capping layer.

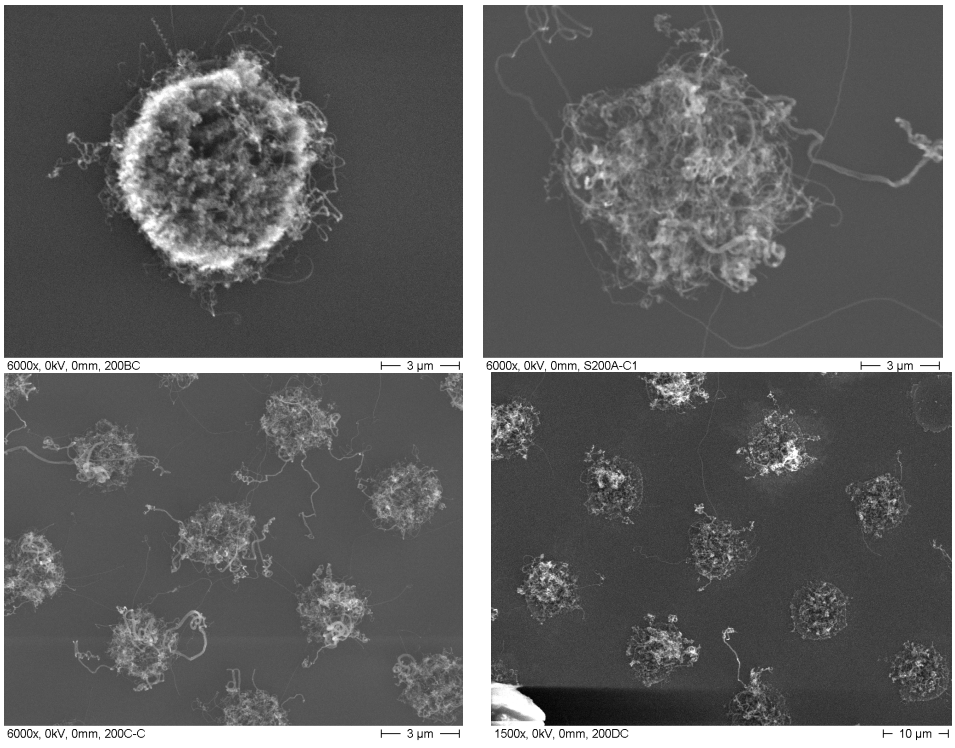

Figure 4.3 Clockwise starting to left - SEM images (top view) of CNTs grown without Ti capping, with Ti capping of 10 Å, with Ti capping of 20 Å and with Ti capping of 40 Å

As a speculation, the thin Ti capping layer could have blocked the carbon radicals from diffusing into the catalytic nanoparticles and hence the growth of CNTs is suppressed and there by altering the density. It is very clear from the side view given in Figure 4.4 that the density of the CNTs with 20 Å thick Ti capping is much less than those grown without Ti capping.

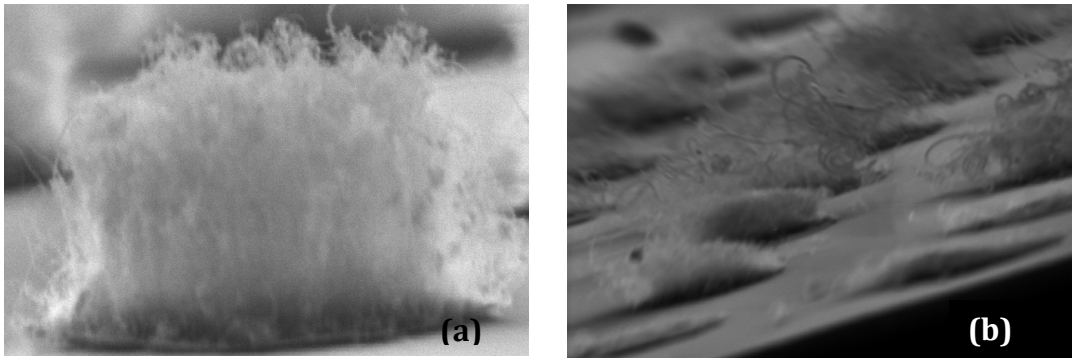

Figure 4.4 SEM images (side view) of CNTs grown (a) without Ti capping and (b) with Ti capping of 20Å.

4.3.3 J-E curve and F-N curve

Figure 4.5 (a) shows the curves of emission current density versus electric field (J-E curve, which shows that the emission current density is relative to the thickness of the thin Ti capping layer. The corresponding Fowler-Nordheim plot (F-N plot) displayed in Figure 4.5 (b) shows that the measured emission current is a Fowler-Nordheim tunneling phenomenon. Although field emission did occur in the samples with thin Ti capping layer of 40 Å, it was almost negligible compared with samples to thin Ti capping layers below 40 Å.

From the J-E curve in Figure 4.5 (a), it is very clear that the threshold field for the sample with 20 Å thick Ti capping is less than the sample with 10 Å thick Ti capping. This

could have been possible due to the reduction in the screening effect when there is an increase in the thickness of Ti capping layer as shown in Figure 4.5.

.

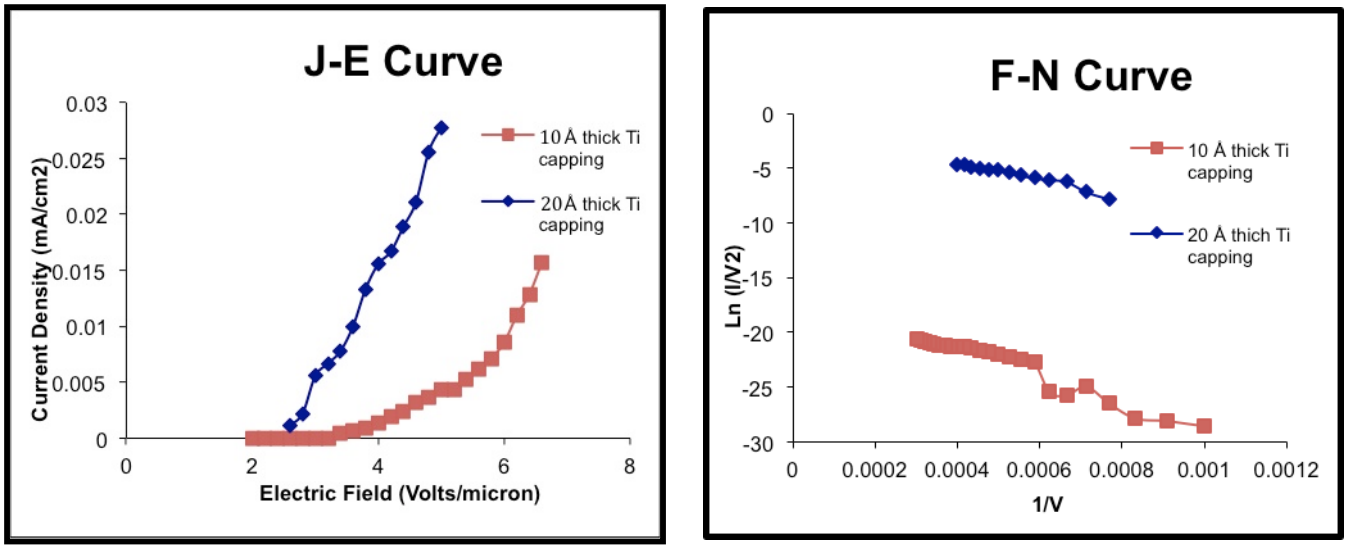

Figure 4.5 (a) Current vs. voltage characteristics and (b) the corresponding F-N plot [Of the sample with 10nm and 20nm thick Ti buffer layer]

4.3.4 Absence of arcing

In our earlier experiment, when the field was just raised above 5V/µm, a fluctuation in vacuum reading was observed. As predicted by Verma et al.,[30], it could have happened if some sort of change in state had occurred either due to burning, evaporation, or melting of the CNT's or silicon or both. SEM analysis clearly showed the debris all around the substrate. The reasons for such a kind of behavior was attributed to vacuum arcing. The arcing is due to the formation of a conduction path between closely spaced electrodes and also depends upon the

vacuum to an extent. On the other hand, no arcing was observed while using Ti capping and Ti buffer layer even when the field was 6 V/ μm.

4.4 Conclusion

By depositing a thin Ti capping layer on the hydrogen-pretreated catalytic nanoparticles, the density of carbon nanotubes can be effectively modified to promote the field emission characteristics of CNTs. From the experimental results, 20 Å thick Ti capping is found to be the optimum thickness as it reduces the threshold field from 3.8 volts/micron to 2.6 volts/micron. We were able to get stable emission for a longer duration without any arcing. These improvements in the field emission properties of CNTs is due to the reduction in the screening effect between the CNTs which is in turn due the density control by Ti capping of optimum thickness.

4.5 References

1. Z. F. Ren, Z. P. Huang, D. Z. Wang, J. G. Wen, J. W. Xu, J. H. Wang, L. E. Calvet, J. Chen, J. F. Klemic and M. A. Reed, Appl. Phys. Lett. 75, 1086 (1999).
2. [D-H. Kim and H-R. Kim, J. Korean Phys. Soc. 44, L208 (2004).
3. K. B. K. Teo, M. Chhowalla, G. A. J. Amaratunga, W. I. Milne, G. Pirio, P. Legagneux, F. Wyczisk, D. Pribat and D. G. Hasko, Appl. Phys. Lett. 80, 2011 (2002).
4. M. Chhowalla, C. Ducati, N. L. Rupensignhe, K. B. K. Teo and G. A. J. Amaratunga, Appl. Phys. Lett. 79, 2079 (2001).
5. J. H. Choi, S. H. Choi, J-H. Han, J-B. Yoo, C-Y. Park, T. W. Jung, S. G. Yu, I-T. Han a nd J. M. Kim, J. Appl. Phys. 94, 487 (2003).
6. J-M. Bonard, M. Croci, C. Klinke, R. Kurt, O. Noury and N. Weiss, Carbon 40, 1715 (2002).
7. W. A. de Heer, A. Chatelain, and D. Ugarte, Science 270, 1179 (1995).
8. Y. Saito, K. Hamaguchi, T. Nishino, K. Hata, and K. Tohji, Jpn. J. Appl. Phys., Part 2 36, L1340 (1997).
9. J. M. Bonard, J. P. Salvetat, T. Stockli, L. Forra, and A. Chatelain, Appl. Phys. A: Mater. Sci. Process. 69, 245 (1999)
10. C. J. Edgcombe and U. Valdre, J. Microsc. 203, 188 (2001).
11. V. Filip, D. Nicolaescu, and F. Okuyama, J. Vac. Sci. Technol. B 19, 1016 (2001).
12. C. H. Adessi and M. Devel, Phys. Rev. B 65, 075418 (2002).
13. H. Murakami, M. Hirakawa, C. Tanaka, and H. Yamaiawa, Appl. Phys. Lett. 76, 1776 (2000).

14. M. Rao, D. Jacques, R. C. Haddon, W. Zhu, C. Bower, and S. Jin, Appl. Phys. Lett. 76, 3813 (2000).

15. L. Nilsson, O. Groening, C. Emmenegger, O. Kuettel, E. Schaller, L. Schlapbach, H. Kind, J-M. Bonard, and K. Kern, Appl. Phys. Lett. 76, 2071 (2000).

16. J-M. Bonard, N. Weiss, H. Kind, T. Stockli, L. Forro, K. Kern, and A. Chatelain, Adv. Mater. ~Weinheim, Ger.! 13, 184 (2001)

17. J.H. Choi et al. Thin Solid Films 435, 318–323 (2003)

18. Chuan-Ping Juan, Chun-Chien Tsai, Kuei-Hsien Chen, Li-Chyong Chen and Huang-Chung Cheng, Japanese Journal of Applied Physics 44 8231 (2005)

19. T.G. De Monsabert et. al. Carbon 43, 2441-2452, (2005)

20. O. Gröning, O. M. Küttel, Ch. Emmenegger, P. Gröning, and L. Schlapbach, J. Vac. Sci. Technol. B, 18, 665 (2000).

21. L. Dong, A. Subramanian, B. J. Nelson, and Y. Sun, in Intelligent Robots and Systems 2005, p. 3598 (2005).

22. Z. F. Ren et al., Appl. Phys. Lett. 75, 1086 ~1999!.

23. Y. Tu, Z. P. Huang, D. Z. Wang, J. G. Wen, and Z. F. Ren, Appl. Phys. Lett. 80, 4018 (2002).

24. C.-P. Juan, K.-J. Chen, C.-C. Tsai, K.-C. Lin, W.-K. Hong, C.-Y. Hsieh, W.-P. Wang, R.-L. Lai, K.-H. Chen, L.-C. Chen, and H.-C. Cheng, Jpn. J. Appl. Phys., Part 1, 44, 365 (2005)

25. C.-P. Juan, C.-C. Tsai, K.-H. Chen, L.-C. Chen, and H.-C. Cheng, Jpn. J. Appl. Phys., Part 1, 44, 8231 (2005).

26. Y. C. Choi, Y. M. Shin, S. C. Lim, D. J. Bae, Y. H. Lee, and B. S. Lee, J. Appl. Phys., 88, 4898 (2000).

27. M. Okai, T. Fujieda, K. Hidaka, T. Muneyoshi, and T. Yaguchi, Jpn. J. Appl. Phys., Part 1, 44, 2051 (2005).

28. K. A. Dean, T. P. Burgin, and B. R. Chalamala, Appl. Phys. Lett., 79, 1873 (2001).

29. J.-M. Bonard and C. Klinke, Phys. Rev. B, 67, 115406 (2003)

30. P. Verma, S. Gautham, P. Kumar, P. Chaturvedi, J.S. Rawat, s. Pal, R. Chaubey, H.P. Harsh, P.K. Vyas, Bhatnagar, J. Vac. Sci. Technol. B , 25 1584 (2007)

CHAPTER V

Enhanced field emission properties from CNT arrays synthesized on Inconel super alloy

5.1 Introduction

Since the reports made by Heer et al. [1] and Rinzer et al., [2] on the field emission from films and individual MWCNTs, respectively, large number of experimental studies on the field emission of MWCNTs grown using various techniques on different substrates have been pursued [3-15]. As mentioned in the previous chapters, reliability and reproducibility are the biggest aspects needing improvement when using CNTs in field emission devices; electrical breakdown and current degradation are the two major limiting aspects of the reliability of CNT based field emitters. Chapter 4 and 5 also explained about the electrical breakdown which is nothing but a sudden discharge caused by an avalanche of charged particles above a certain threshold field. The process is associated by the evaporation of electrode materials and/or surface adsorbed impurities as a consequence of electron bombardment of the anode, resistive heating of the sharp cathode or simple desorption of surface impurities so that a low pressure vapor forms in the proximity of the electrodes [16]. Above the threshold field, the vapor undergoes ionization and sparking, similar to that in ordinary low pressure gases [17]. On the other hand, the emission current degradation is a slow process that occurs below the threshold

field. Heating by the emission current and subsequent evaporation of the electrode materials results in a gradual loss, structural collapse and deterioration of the cathode.

5. 2 Importance of robust electrical contact

Apart from thermal and electrical stability of the electrode materials, high quality robust electrical contacts (that are interfacing the emitter back side) are also vital for multiple reasons. Firstly, the contact must be uniform along the entire interface to allow optimal, uniform current densities throughout the joint area. This is especially important for carbon nanotube forests, to ensure each nanotube is in direct electrical contact with the substrate with similar contact resistance all around at the interface eliminating the formation of hot spots. Secondly, good ohmic contacts at the CNT-substrate interface introduce only minor series resistances in the emitter circuit thus resulting in higher emission currents or lower interfacial losses (when current regulated). Thirdly, mechanical strength, or good adhesion, between the nanotube/catalyst and the substrate interface is also an important criterion in order to minimize problems related to delamination of the emitter material from the back side contact [18-21].

5.3 Common technical approaches

The above list of requirements suggests two kinds of technical approaches that may offer feasible and reasonably simple solutions to meet the stringent thermal, mechanical and electrical boundary conditions. One solution is a solder transfer of CNT films to electrically conductive surfaces, which has been proven to be a robust and versatile method to obtain joints with excellent structural, thermal and electrical integrity [22-27]. The other, more feasible approach

is the direct growth of CNTs on conductive surfaces. Growing CNTs on metal substrates or on alloys containing one of the common catalyst metals can result in CNT films of high footprint density, which is electrically advantageous [28-30]. For intstance, Talapatra et. al. [31], estimated an average total contact resistance of aligned CNTs on Inconel to be about 500 Ω, while measurements carried out on similar structures by Halonen et al.[32] showed the contact resistance is as low as ~10 Ω (for a pattern footprint area of ~0.4 cm^2). Although relatively low turn-on fields are observed for such devices, the maximum emission current densities reported were typically not higher than 10 mA/cm^2 [32-36]. For CNTs to be used in field emission devices, it is not only essential to develop techniques to grow CNTs on conducting substrates but also to get good current density besides reducing the turn on and threshold voltages.

In this chapter, we report the growth of CNTs on Inconel and Si substrates in water assisted CVD and compared their field emission behavior. CNTs grown on Inconel exhibited excellent field emission properties: The maximum current densities from the produced emitters were around 100 mA/cm^2. Although CNTs on Si substrates also yielded high initial current densities (> 100 mA/cm^2), early arcing and rapid failure of the devices indicate their limited use in high current density applications. The results presented here may be adopted for CNT based cold cathodes suitable for high power microwave vacuum devices and also for long-life low-power applications.

5.4 Experimental section

Vertically aligned MWCNTs were synthesized using a water assisted CVD process on Si and Inconel substrates coated previously with 10nm Al buffer and 1.5nm Fe catalyst layers using e-beam evaporation. For CNT growth, the substrate is inserted into a quartz tube inside a furnace and initially purged with argon, then heated up to 775°C under Ar/H_2 (, 15% H_2/balance argon) Once the growth temperature is reached, Ar/H_2 is bubbled through water and the carbon source, ethylene, is flown into the reactor. The CNTs are grown for 30 minutes and finally the furnace is cooled under Ar.

5.5 Characterization

Scanning electron microscopy (SEM, FEI Quanta 400 ESEM FEG), transmission electron microscopy (JEOL 2100 F TEM) and Raman spectroscopy were used for sample characterization. For the field-emission measurements, the silicon (Si) and Inconel substrates with CNTs were used as the cathode and ITO coated glass plate as the anode. The cathode and anode mounting stands are machine ground to ensure that they are perfectly parallel. The whole sample assembly was kept inside a vacuum chamber evacuated to at least $2 \cdot 10^{-6}$ Torr and the distance between the cathode and the anode was maintained at 200 μm through a spring loaded micrometer gauge. The CNT sample is mounted on the cathode stand and I–V measurements are done using a Keithley 2410 instrument.

5.6 Results and discussion

5.6.1 Difference in morphology of CNTs grown on Si and Inconel

Figure 5.1 (a & b) display SEM images of the CNTs grown on Si and Inconel, respectively. From the morphology observed, it can be seen that the CNTs are vertically aligned via a self-supporting mechanism. According to scanning and transmission electron microscopy analyses, the CNTs grown on Inconel are somewhat more tangled and have smaller diameters compared to those grown on Si. Since the same amount of iron is deposited on both substrates, the catalyst interaction with the surface is the only plausible explanation for the differences. One main reason is the different surface roughness of the two substrates. The smooth polished single crystal of Si, in contrast with the rolled foil of the polycrystalline metal alloy of Inconel, ensures that the nanotubes grow parallel with each other. On the other hand, the different chemical qualities and thus surface energy of the two substrates influence the wetting properties of the catalyst metals which affect the catalyst island morphology, size and surface density when heating the samples to the growth temperature resulting in differences in the nanotube diameter distributions for the two substrates. Furthermore, the Inconel substrate itself can also act as an additional catalyst resulting in thinner and denser CNTs.

It can be seen that the CNTs on Si are longer when compared with those grown on Inconel most probably due to the partial tangling of the nanotubes and more efficient diffusion of the Al/Fe catalyst into the polycrystalline metal than the single crystal Si surface.

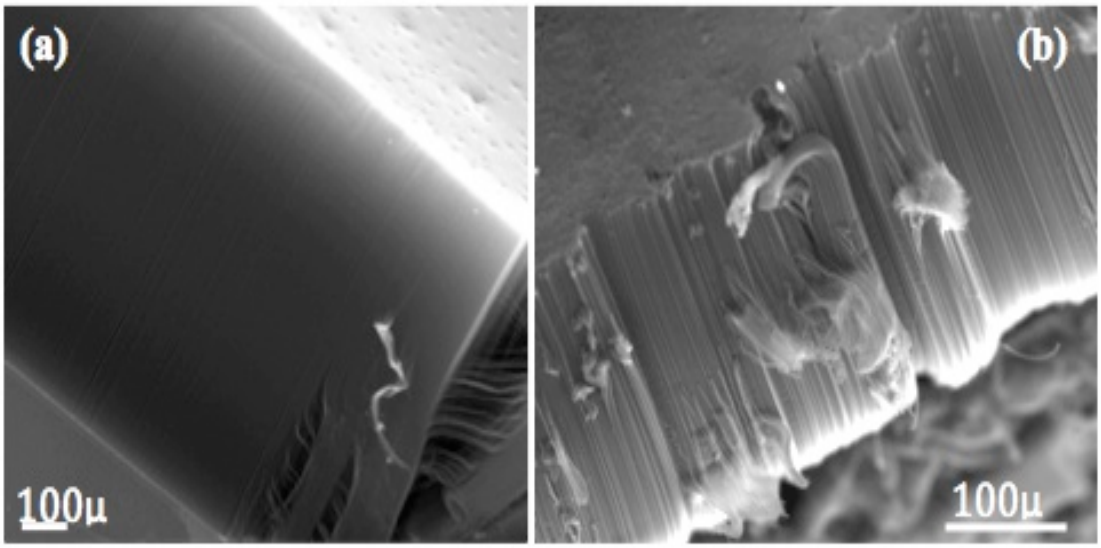

Figure 5.1 SEM images of CNT films grown on (a) Si and (b) Inconel substrates showing that the CNTs on Si are longer when compared with those on Inconel.

5.6.2 Raman spectroscopy analysis

Raman analysis in Figure 5.2 shows the usually observed 3 main distinct bands, the D-band (disorder) around 1350 cm^{-1}, the G-band (graphitic peak) around 1580 cm^{-1} and the G'-band (long range order) around 2700 cm^{-1} for the CNTs on both types of substrates. There is a minor shift in the D band and G band positions for the CNTs grown on the two substrates due to their different diameter distribution and the number of walls (Figure 2e and 2f). The D peak arises due to the formation of sp^3 and dangling sp^2 bonds on the CNT side walls as well as from the deposition of amorphous carbon; the G peak arises from graphitic sp^2 carbon in the nanotubes; the G' peak is the indicator of long range order present within the CNTs. For these CNTs, we obtained the intensity ratio I_D/I_G of 0.78 and 0.91 for Inconel and Si, respectively and the values are very close to the values reported earlier for CNTs synthesized on Inconel [37].

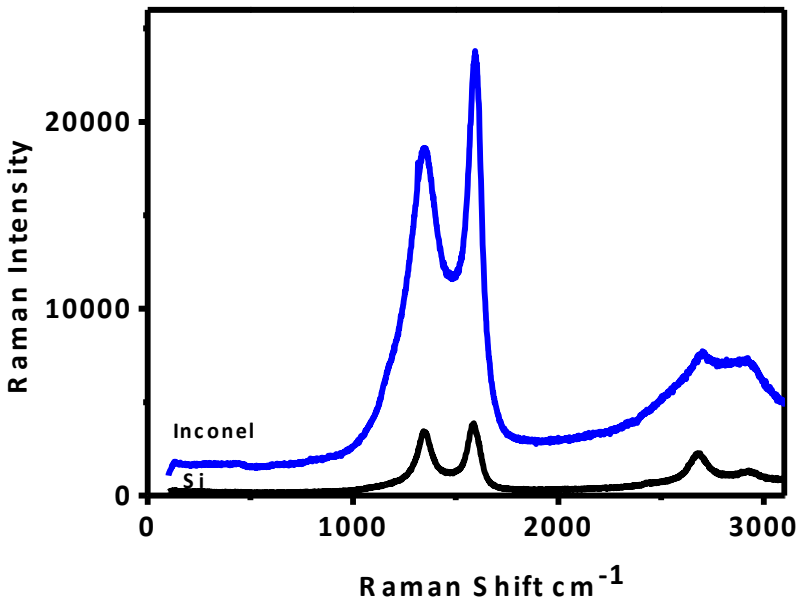

Figure 5.2 Raman spectra of films synthesized on the two different substrates

5.6.3 Contact resistance measurement

Electric impedance spectroscopy measurements performed for CNTs grown on both Si and Inconel substrates suggest the structures are sufficiently conductive for emitter applications (Figure 5.3). It can be seen from the Nyquist plots that the contact resistance between the CNT and Si is ~320 Ω/cm^2 while for the CNT-Inconel contact it is ~90 Ω/cm^2. The semi-circles in the impedance spectra indicate the presence of a capacitive component most likely caused by the nanotube films of large specific surface area.

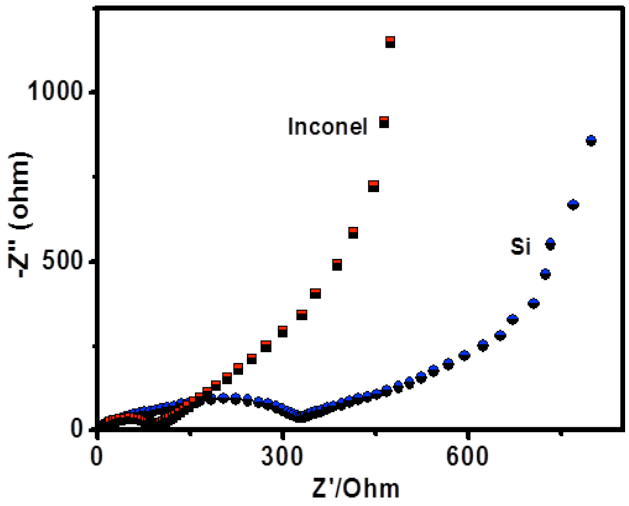

Figure 5.3 Nyquist plots of the films (on the substrates) measured by electrical impedance spectroscopy using electrochemical lithium half-cell of MWCNTs grown on silicon and Inconel as anodes.

5.6.4 TEM Analysis

From the TEM analysis (Figure 5.4 (a) - (e)), it is clear that the number of walls and also the average diameter of CNTs grown on Si are higher than those synthesized on Inconel. TEM analysis also reveals the presence of more amorphous carbon on the surface of the CNTs in the case of Si as compared to those grown on Inconel substrates.

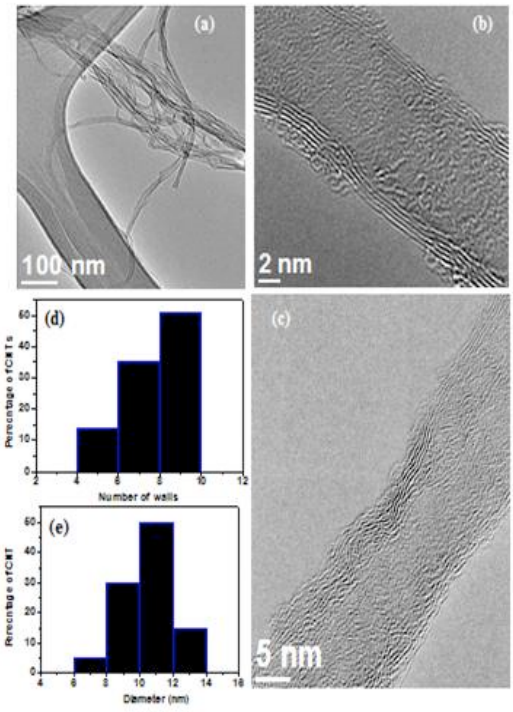

Figure 5.4(i) (a), (b) & (c) TEM of CNTs grown on Si

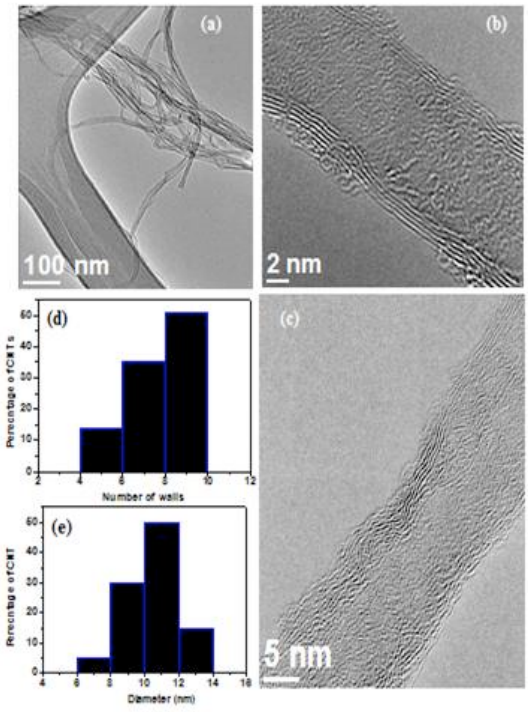

Figure 5.4(ii) (a), (b) & (c) TEM of CNTs grown on Inconel

Panels (d) and (e) display the nanotube diameter and wall number distribution plots, respectively

5.6.5 Field emission characteristics

Initially, the CNTs grown on both substrates demonstrated excellent field emission properties. From the J-E curves displayed in Figure 5.5, we observe that the initial current density of the CNT array grown on Si is higher than that for the corresponding sample obtained on Inconel (131 mA/cm^2 vs. 99 mA/cm^2). Initially, the turn on field (which is the field required to give a current density of 10 μA/cm^2) for the sample grown on Si (2.2 V/μm) is less than that for the nanotubes grown on Inconel (3.4 V/μm). However, the turn on field for the latter

samples decreased considerably from 3.4 to ~1.5 V/μm after arcing. The threshold field, the field required to reach a current density of 10 mA/cm^2, also shows similar tendencies. For the CNT films grown on Si, it gradually increases, meanwhile a significant decrease of the corresponding threshold value is observed for the samples synthesized on the metal alloy substrate (from ~5.0 to 2.8 V/μm).

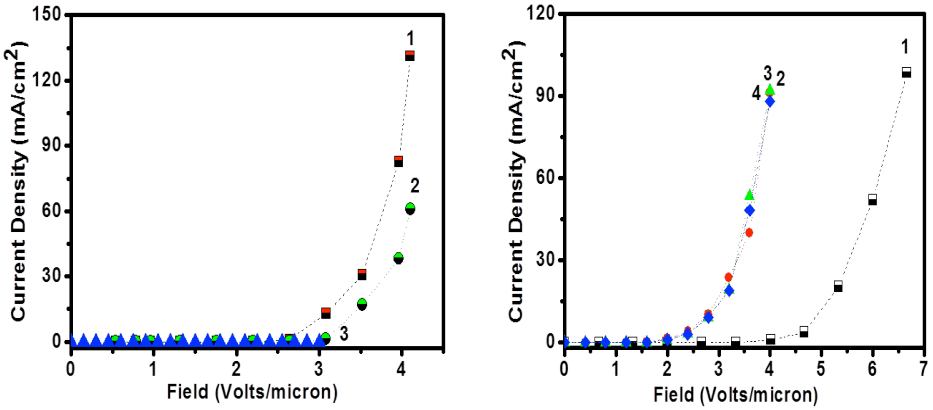

Figure 5.5 Plots of emission current density as a function of applied electric field in repeated experiments for CNTs grown on (a) Si and (b) Inconel

The increase in the turn on and threshold fields as well as the early device failure for the films grown on Si might be because of the structural damage of the emitters [38] as also indicated by the voids and fused CNTs visible in SEM images (Figure 5.6).

5.6.6 Current degradation on CNTs grown on Si

The causes of current degradation on the Si substrate can be associated with a number of different mechanisms: (1) Poor adhesion of CNTs to the substrate and consequent peeling, (2) high and/or inhomogeneous contact resistance between the CNTs and the substrate resulting in large local current densities and excessive joule heating and (3) at high electric fields, resistive

heating and related stress due to thermal expansion coefficient mismatch at the CNT-substrate junction causing mechanical failure.

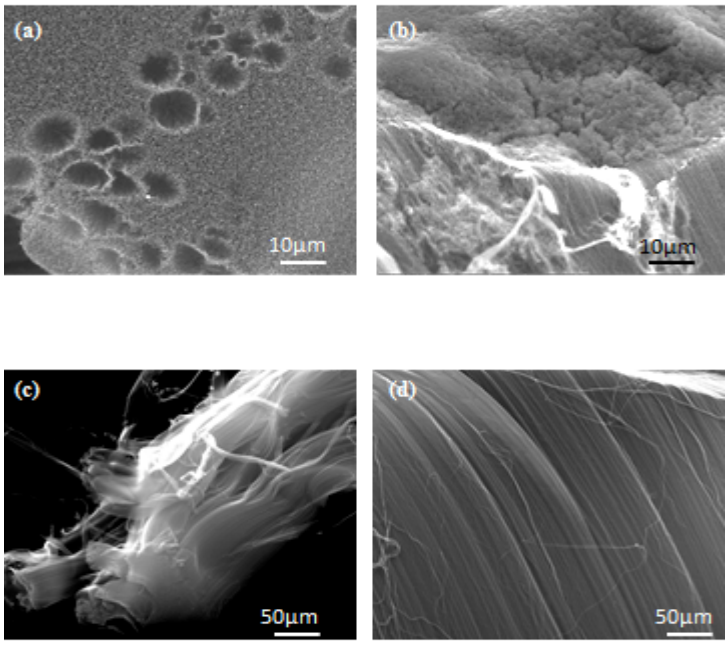

Figure 5.6 SEM images of the samples after field emission. CNT films (a) on Si, top view, (b) on Inconel, top view, (c) on Si side view and (d) on Inconel, top view.
Microscopic voids in the films on Si show the structural instability in contrast with the continuous surface of the films grown on Inconel.

According to Okai et.al. [18], the strong repulsive electrostatic forces may also be a reason for the electrical breakdown during field emission. As reported in our earlier work [39,40], when the electric field between the anode and the cathode is increased, the dipole resulting from the concentration of electrons in the tips of carbon nanotubes will enhance the static electric force and pull the carbon nanotubes off from the substrate leading to an abrupt drop of emission current. As noticed by Wang et al [38], the electrostatic force created by the flow of emission current acting in the tip of nanotube can induce a split or even burning of the emitters. On the other hand, there was no obvious electrical breakdown in the case of the sample

grown on Inconel while the emission threshold fields were improving with use. The superior field emission properties and reliability of the nanotube films grown on Inconel as compared to those on Si are inevitable and can be explained by the good electrical and thermal interface between the nanotubes and the metallic substrate. The excellent electrical contact ensures uniform current distribution in the entire cross-section of the emitter thus eliminating the formation of hot spots and also avoiding the evolution of excess Joule heat in local microscopic volumes at the nanotube-substrate interface as well as at the tips of the nanotubes. The improved overall field emission performance of the Inconel-supported films may be due to localized cleaning caused by mild arcing at the tips of the nanotubes. In addition, a uniform fusing of the CNT-catalyst-Inconel interface caused by the current might have also taken place by which the electrical and mechanical properties of the interfacial contact are improved.

5.6.7 Fowler-Nordheim plot

Another important aspect is the field enhancement factor (β) that describes how much the emitter tips amplify the macroscopic electric field around the sharp and highly curved apices. As predicted by Mc. Clain et. al. [41], as the diameter of the CNTs decreases (in our case the CNTs grown on Inconel), the emission field decreases with a corresponding increase in field amplification. The field enhancement factor, which describes the ability of the emitters to amplify the macroscopic field and in turn determines the total emission current, is dependent on the diameter of the CNTs. It increases with the decrease in the diameter of the CNTs. From the linearized form of the Fowler-Nordheim plot (i.e. by plotting $\ln(J/U^2)$ *versus* $1/U$ (Figure 5.7), where J is the current density and U is the voltage drop on the emitter, it is clear that the emission current is from the field emitted electrons. The slope of the linear curve is m =

$(Bd\phi^{3/2})/\beta$, where B is a constant with the value of $6.83 \cdot 10^9$ $VeV^{-3/2}m^{-1}$, ϕ is the work function of the emitter material (~5 eV for CNTs), and d is the distance between the cathode and the anode (200 μm in our case).

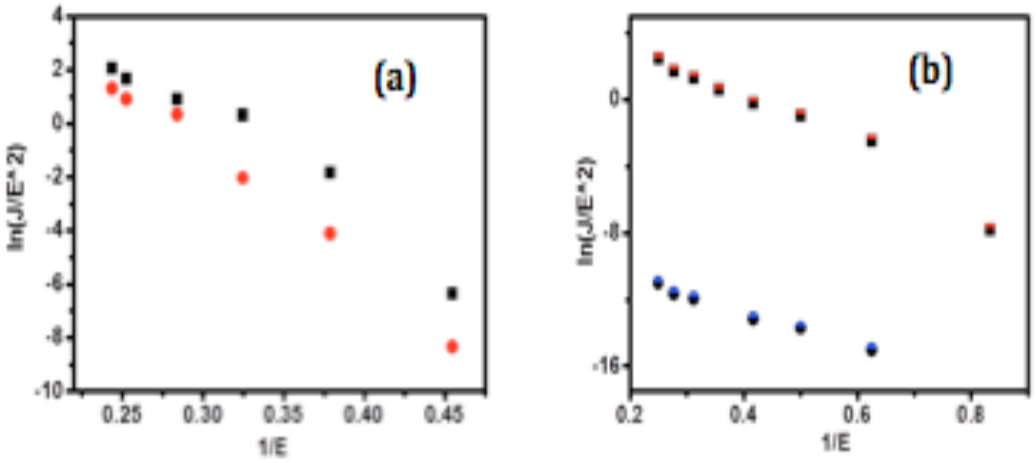

Figure 5.7 Fowler-Nordheim curves of the samples grown on (a) Si and (b) Inconel substrate

The enhancement factors for both types of emitter structures are very similar having values of ~2500. In the case of the Si-supported CNT films, this value remained unchanged as long as the emitters were functional. Interestingly, for the nanotube films synthesized on Inconel, this initial field amplification value was abruptly increased to ~7300 when repeating the measurement on the same device and then it kept the increased value in the subsequent tests. Such a substantial increase in the field amplification is a consequence of surface cleaning by the mild arcing in the course of the first emission experiment but also sharpening of the nanotube tips might have taken place as suggested by Talapatra and co-workers [31]. Although the initial values for β are rather close to the ones reported for nanotube films in the literature (i.e.

typically between 500-3000) [1,5,31,42,43], the improved enhancement factors are considerably higher than those.

5.7 Conclusions

In conclusion, vertically aligned CNTs on Inconel substrates grown via water assisted chemical vapor deposition have shown excellent field emission properties clearly outperforming similar films synthesized on Si substrates. The field emitter devices synthesized on the metallic substrate have low turn-on fields (~1.5 V/μm), enable high current operation (~100 mA/cm^2) and show very high local field amplification with factors up to ~7300. These properties, along with their increased reliability, make the demonstrated structures as a potential candidate for future flat panel displays based on CNT electron emitters.

5.8 References

1. W.A. de Heer, A. Chatelain, D. Ugarte, *Science* 1995, 270, 1179-1180

2. A.G. Rinzler, J.H. Hafner, P. Nikolaev, L. Lou, S.G. Kim, D. Tomanek et al., *Science*, 1995, 269, 1550-1553

3. Saito Y, Hamaguchi K, Hata K, Uchida K, Tasaka Y, Ikazaki F, Yumura M, Kasuya A, Nishina Y. *Nature* 1997, 389, 554–555.

4. Q.H. Wang, T.D. Corrigan, J.Y. Dai, R.P.H. Chang, A.R. Krauss, *Appl. Phys. Lett*. 1997, 70, 3308-3310

5. J. M. Bonard, F. Maier, T. Stockli, A. Chatelain, W. A. de Heer, J. P. Salvetat and L. Forro, *Ultramicroscopy* 1998, 73, 7-15

6. K. B. K. Teo, M. Chhowalla, G. A. J. Amaratunga, W. I. Milne, G. Pirio, P. Legagneux, F. Wyczisk, D. Pribat, and D. G. Hasko, *Appl. Phys. Lett*. 2002, 80, 2011

7. Y. Chen, Z. Sun, J. Chen, N.S. Xu, B.K. Tay, *Diam. Relat. Mater.* 2006, 15, 1462-1466

8. M.P. Siegal, P.A. Miller, P.P. Provencio, D.R. Tallant, *Diam. Relat. Mater.* 2007, 16, 1793

9. Archana Pandey, Abhishek Prasad, Jason P. Moscatello, Mark Engelhard, Chongmin Wang, Yoke Khin Yap, *ACS Nano* 2013, Vol 7 No 1 117

10. Juan Su, Deng-Zhu Guo, Ying-Jie Xing, and Geng-Min Zhang *Phys. Status Solidi A* 2013, 210, No. 2, 349

11. Haizhen Ren, Linfeng Yang and Yuguang Zhang *J. Phys.: Conf. Series* 2013,

12. Bhattacharya, S and De, D and Ghosh, S and Ghatak, KP *J. Comp. Theoretic. Nanosci.,* 2013, 10 (3). pp. 1-5

13. Gowtam Atthipalli, Rigved Epur, Prashant N. Kumta and Jennifer L. Gray, *J. Vac. Sci. Technol. B* 2011, 29, 04D102

14. Sun PC, Deng JH, Cheng GA, Zheng RT, Ping ZX, *J Nanosci. Nanotechnol.* 2012, Aug;12(8):6510-5.

15. Sarah Berhanu, Oliver Gröning, Zexiang Chen, Jacqueline Merikhi, Monja Kaiser, Nalin L. Rupesinghe, and Peter K. Bachmann *Phys. Stat. Sol. A* 2012, 209, No. 11, 2114

16. W.J. Wijker, *Appl. Sci. Res. Section B*, 1961, 9, 1-20

17. John E. Almy, *Phys. Rev. (Series I)* 1907, 24, 50–59

18. M. Okai, T. Fujieda, K. Hidaka, T. Muneyoshi, and T. Yaguchi, *Jpn. J. Appl. Phys.,* 2005, 44, 2051

19. J.-M. Bonard and C. Klinke, *Phys. Rev. B,* 2003, 67, 115406

20. G. Nessim, M. Seita,, K. O'Brien, A. Hart, R. Bonaparte, R. Mitchell, C. Thompson,

Nano Lett., 2009, 9, 3398

21. B. Kim, H. Chung, K.Chu, H. Yoon, C Lee, W. Kim, *Synth. Metals,* 2010, 160, 584

22. Y. Fu, N. Nabiollahi, T. Wang, S. Wang, Z. Hu, B. Carlberg, Y. Zhang, X. Wang, J. Liu, Nanotechnology 2012, 23 045304

23. K. Kordás, G. Tóth, P. Moilanen, M. Kumpumäki, J. Vähäkangas, A. Uusimäki, R. Vajtai, P. M. Ajayan, Appl. Phys. Lett. 2007, 90 123105-3

24. Y.F. Fu, Y.H. Qin, T. Wang, S. Chen, J.H. Liu Adv. Mater. 2010, 22 5039-5042

25. Kumar, V. L. Pushparaj, S. Kar, O. Nalamasu, P. M. Ajayan, R. Baskaran, Appl. Phys. Lett. 2006, 89 163120

26. G. Tóth, J. Mäklin, N. Halonen, J. Palosaari, J. Juuti, H. Jantunen, K. Kordás, W. G. Sawyer, R. Vajtai, P. M. Ajayan, Adv. Mater. 2009, 21 1-5

27. Jani Mäklin, Niina Halonen, Olli Pitkänen, Géza Tóth and Krisztián Kordás, 2013, submitted.

28. C. Masarapu & B. Wei, *Langmuir*, 2007, 23, 9046-9049 29.

29. C. Baddour, F.Fadlallah, D. Nasuhoglu, R Mitra, L. Vandsburger, J Meunier, *Carbon*, 2008, 47, 313

30. S. Benito, L. Lefferts, *Carbon*, 2010, 48, 2862

31. S. Talapatra, S. Kar, S. Pal, R. Vajtai, L. Ci, P. Victor, M. Shaijumon, S. Kaur, O. Nalamasu, Ajayan. *Nature Nanotechnol.*, 2006, 1, 112

32. Halonen N., Mäklin J., Rautio A.-R., Kukkola J., Uusimäki A., Toth G., Reddy L.M., Vajtai R., Ajayan P.M., and Kordas K., *Chem. Phys. Lett.* 2013, 583 (17): 87-91

33. W. Sung, W. Kim, H. Lee, Y. Kim, *Vacuum*, 2008, 82, 551

34. Lahiri, R. Seelaboyina, J. Hwang, R. Banerjee, W. Choi, *Carbon,* 2001, 48,1531

35. P. Mahanandia, V. Arya, P. Bhotla, S. Subramanyam, J. Schneider, K. Nanda, *Appl. Phys. Lett*, 2009, 95, 083108

36. W. Yi, & Q. Yang, *Diam. Relat. Mater.*, 2010, 19, 870

37. Gowtam Atthipalli, Hao Wang, Jennifer L. Gray, *Appl. Surf. Sci.* 2013, 273, 515

38. Z.L. Wang, R.P. Gao, W.A. Heer, and P. Pomcharal, *Appl. Phys. Lett.*, 2002, 80, 856

39. P. Verma, S. Gautham, P. Kumar, P. Chaturvedi, J.S. Rawat, s. Pal, R. Chaubey, H.P. Harsh, P.K. Vyas, Bhatnagar, *J. Vac. Sci. Technol. B* 2007, 25 1584.

40. S. Srividya, S. Gautam, P. Jha, P. Kumar, A. Kumar, U.S. Ojha, J.S.B.S. Rawat, S. Pal, P.K. Chaudhary, Harsh, R.K. Sinha, *Appl. Surf. Sci.* 2010, 256, 3563

41. Devon McClain, Mason DeRoss, Noel Tavan, Jun Jiao *Mater. Res. Soc. Symp. Proc.* 2006, Vol. 901E

42. M.A. Guillorn, A.V. Melechko, V.I. Merkulov, D.K. Hensley, M.L. Simpson, D.H. Lowndes, *Appl. Phys. Lett.* 2002, 81 3660-3662

43. Y. Saito, S. Uemura, *Carbon* 2000, 38 169-182

CHAPTER VI

Field emission with ultra low turn on voltage from metal decorated CNTs

6.1 Introduction

Due to the high aspect ratio, high mechanical strength and high thermal conductivity, CNTs are considered to be an ideal electron emitting sources in field emission displays [1-8]. Aligned and well-separated CNT cathode morphology is important for many potential applications, where a high electric-field is needed such as in field emission devices. As mentioned in the previous chapters, the growth in these cases is usually achieved by means of chemical vapor deposition (CVD). It is important to mention, however, the highly dense growth of CNTs by thermal CVD method may compromise the field emission properties, due to a field-screening effect caused by the proximity of neighboring tubes. Also some critical issues such as adhesion of CNTs with the substrate, reliability, and stability have to be addressed while using CNTs as electron emitters in field emission applications.

6.2 Methods used for improving field emission

To improve the field emission performance from CNT emitters, different methods such as doping of CNTs with nitrogen, [9,10] surface coatings with low work function materials such as LaB_6 or Ha for low turn on field [11,12] and decorations with ZnO and Ru [13–15] have been

investigated. Previous studies have also shown that tuning the structure of the CNTs such as the radius [16], geometry [17,18], structural change by oxygen plasma treatment [19] and improving their density [20] could improve the field emission property. Also by decorating the CNT walls with organic functional groups [21-23] or by inorganic semiconductor [24-31] the field emission properties of CNTs could be enhanced. Chi *et al.* [32] reported a threshold field of 0.9 V/ μm at 1 mA/cm^2 which correlated to a turn on voltage of 0.6 V/μm at 10 μA/cm^2 by growing CNTs on a mesh electrode. Also, Zuo *et al.* [33] demonstrated low turn on field of 0.63 V/μm at 10 μA/cm^2 by decorating the surface of the CNT with titanium nanoparticles. Pandey *et al.* [34] arrived at a threshold field of 0.8 V/μm in strontium titanate coated CNTs. On the other hand, Liu *et al.* [15] decorated CNTs with Ru nanoparticle and the turn on field reduced from 2.5 to 1.3 V/μm after Ru decoration. In the recent report of Zannin *et al.* [35] hybrid diamond-like carbon and CNT composite structures showed threshold field of 2 V/μm. In this chapter, we want to elaborate the process by which we could reduce the turn on and the threshold field which are very important properties for the CNTs to be used in the fabrication of next generation high-performance flat panel displays and vacuum microelectronic devices.

Electrophoretic deposition (EPD) technique is a common method used for decorating the CNTs with the desired metal particle to improve the field emission properties of the cold cathode. Fan *et al.* [36] used CNT/Ni composite and Chen *et al.* [37] fabricated CNT/Cu composite to enhance the field emission properties of the CNTs. But during the fabrication, the CNTs in the composites would be easily covered by the consequently deposited nanoparticles in the chemical process resulting in the decrease of effective field emitters in the CNT cathode. Another important issue of CNTs getting bundled together is also common in this process.

Once they are bundled, without the use of aggressive treatment like ultra-sonication or chemical functionalization, it is extremely difficult to achieve a stable dispersion or homogeneous mixture. These measures are known to damage the walls of the CNTs and degrade their electrical properties to a larger extent.

6.3 Screening effect and the distance between the CNTs

Moreover, the above mentioned process cannot alter the distance between the CNTs. Although it is important to lower the turn on and threshold voltage for better field emission results, reducing the screening effect is crucial for CNTs to be used in field emission application. It is well known that if the separation between the tubes, *"d"*, is much less than the tube height, *"h"*, in an array, the electrostatic shielding between the CNTs can drastically affect the field emission performance of the cold cathode. Numerical simulations show that if the distance between the CNTs is equal to or more than twice the height of the CNTs, then the screening effect can be considerably reduced which in turn could improve the field emission property of the cathode [38-40]. Electrostatic shielding becomes a significant hurdle for future device applications because of the exponential dependence of the emission current on the electric field in accordance with the Fowler-Nordheim theory.

Work has also been done on thermally evaporated nanoparticles on nanotubes [41-43]. The results in these work indicate that the morphology of the metal particle or the film on the CNTs is dependent on the intrinsic properties of the metal themselves than on the process parameters. On the other hand, the work of Muratore *et al*. [44] reported the effect of particle growth temperature and time on the decorated metal nanoparticles' density and morphology.

However, the sputtered metal nanoparticles were attached to the surface of the CNTs without penetrating in between the CNTs to change the inter tubular spacing of those.

This chapter focusses on a simple and scalable procedure for decorating the vertically aligned CNTs forest with metal nanoparticles for improved field emission properties. This process enabled the CNTs to bundle towards a metal particle forming a pattern due to which the CNT bundles are separated by almost 3 times the height of the bundle reducing the screening effect considerably. Further, by the deposition of metal nanoparticles on the surface of the nanotubes, emitting centers are obtained that ensure highly conductive paths for the electrons from the nanotubes towards the vacuum helping to by-pass the amorphous carbon impurities, known as one of the major hurdles in CNT based emitters. Thus, to the best of our knowledge, such low turn on field of 0.1 V/μm achieved in this work has not been reported so far.

6.4 Experimental Set-Up

First the CNTs were grown on Al coated silicon (Si) and Inconel as described elsewhere [45]. The grown CNTs were kept inside the CVD chamber with aluminum (Al) sheet of thickness 150 μm over them and the temperature of the system was gradually increased to 700°C for 10 minutes and cooled gradually. Since the melting point of Al is 660°C, it got melted and the CNTs were decorated with Al particles. As the sheet was kept over the array of CNTs, some of the Al particles penetrate in between the CNTs in the array. This process of annealing was done in the presence of Argon (Ar) at a low flow rate. The same procedure was repeated for the deposition of Cu particles using Cu sheet to obtain Cu decorated CNTs.

Though the melting point of Cu is 1085℃, the Cu got melted around 700˚C and the CNTs were decorated with Cu particles. Since the sheet was kept over the array of CNTs, some of the Cu particles went in between the CNTs in the array. This process of annealing was done in the presence of Argon (Ar) at a low flow rate.

6.5 Characterization

The surface morphologies were characterized using scanning electron microscopy (SEM, FEI Quanta 400 ESEM FEG) and high resolution transmission electron microscopy (HRTEM JEOL 2100 F TEM). The content of Al and Cu particles is identified using X-ray diffraction (Rigaku D/Max Ultima II Powder XRD with a Cu Kα source) and Raman spectroscopy (Renishaw in *Via* Raman Microscope). The area of the sample used was 1 cm^2. After the deposition with metal particles the sample was transferred to a vacuum chamber with vacuum better than 2 x 10^{-6} Torr, for field emission measurement. The silicon (Si) and Inconel substrates with CNTs were used as the cathode and indium tin oxide (ITO) coated glass plate as the anode. The cathode and anode mounting stands were machine ground to ensure that they are perfectly parallel. The distance between the cathode and the anode (100 μm) was adjusted using micrometer screw gauge arrangement and a suitable DC voltage (up to 400 V) was supplied using Keithley 2410 high voltage power supply.

The electron impedance spectroscopy (EIS) measurements were performed using a two electrode setup with the CNT on the substrate as the working electrode and lithium metal as the counter/reference electrode. In this, 1 M LiPF6 in 1:1 v/v mixture of ethylene carbonate (EC)

and dimethyl carbonate (DMC) are used as the electrolyte and glass micro-fiber filter membrane as the separator. The EIS measurements were conducted over 70 kHz to 10 mHz by applying a constant dc bias with sinusoidal signal of 10 mV.

6.6 Results and Discussion

6.6.1 Morphology Change due to Metal Decoration

(i) Silicon

A schematic of the morphology of CNTs grown on Si and Inconel substrate is shown in Figure 6.1. Figure 6.2 (a), (b) & (c) shows the scanning electron microscope (SEM) images of the multi-walled carbon nanotubes (MWCNTs) grown on Si with Al decoration on them. Before the metal decoration, the CNTs were vertically aligned *via* self-supporting mechanism as described in our previous work, [45] due to extremely high density of CNTs. Interestingly, after metal evaporation, the morphology of the CNTs changed completely. Groups of CNTs became linked together by their tips while attaching to the Al particles forming microscopic patterns in the nanotube forest. Accordingly, the CNTs are no longer individual strands for field emission; instead they are individual bundles.

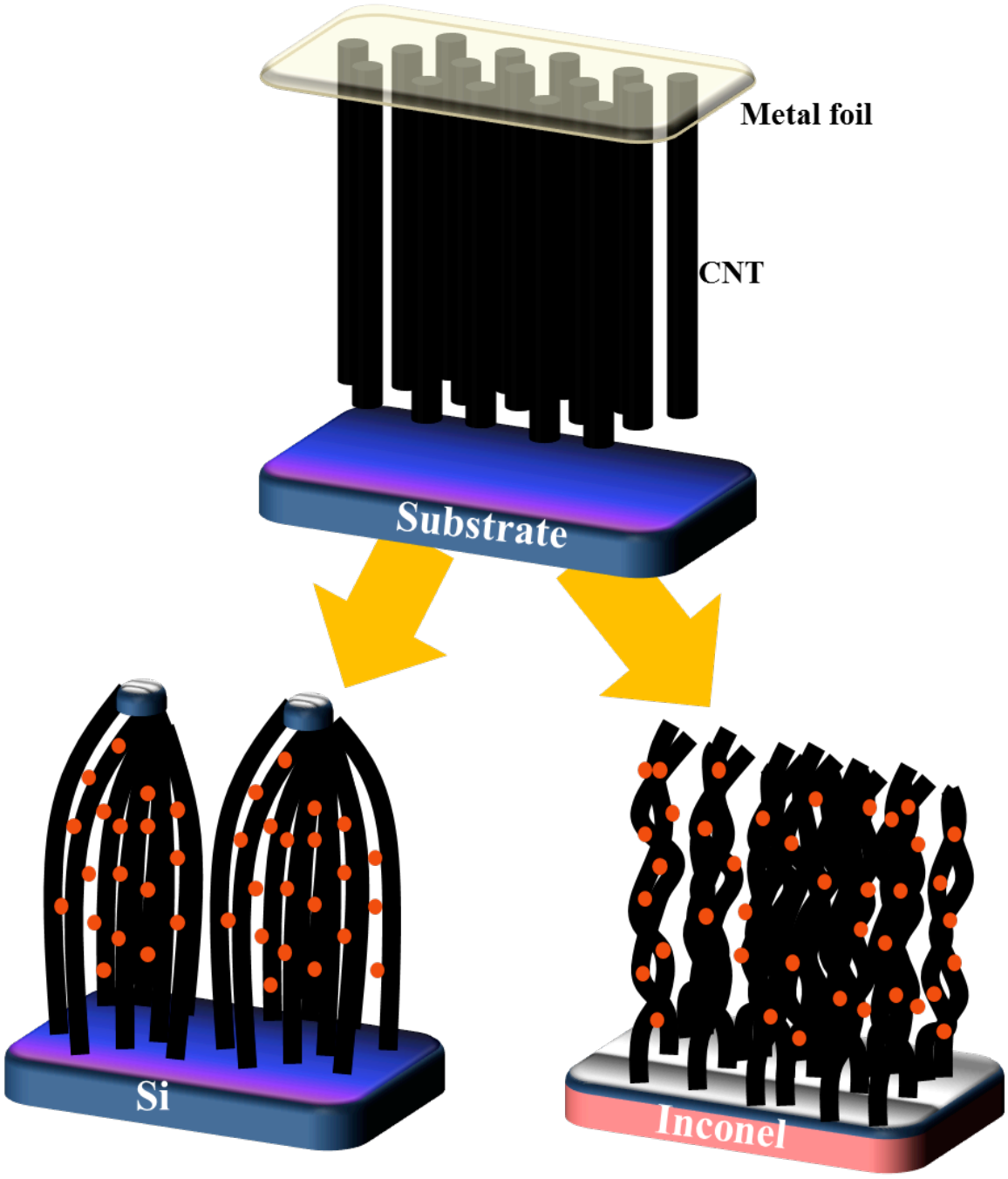

Figure 6.1 The schematic procedure for the fabrication of metal decorated CNTs

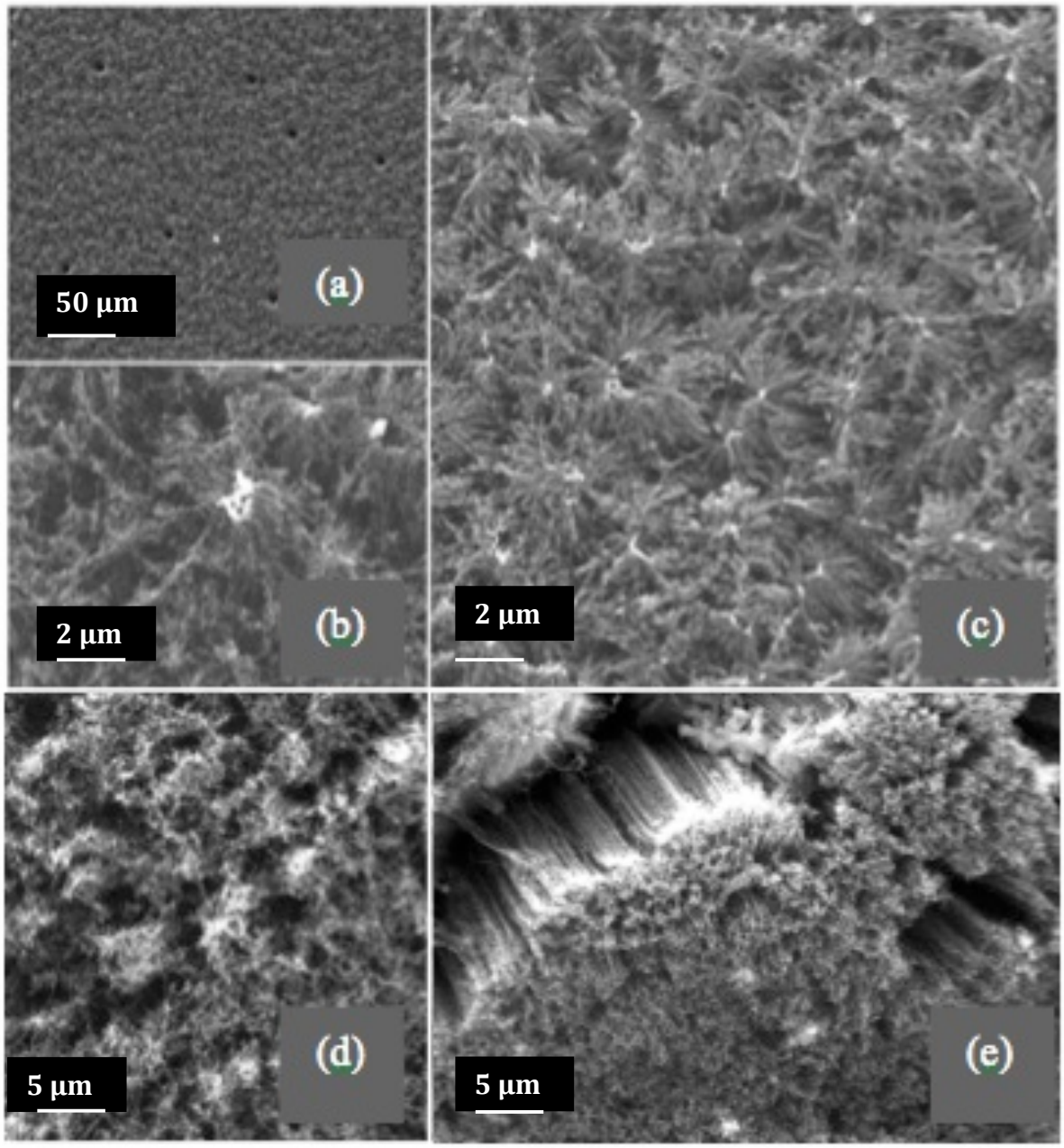

Figure 6.2 (a), (b) & (c) SEM image of CNTs grown on Si with Al decoration in different magnification. Figure 6.2(d) &(e) SEM image of the CNTs grown on Inconel with Al decoration on them in different magnification.

Choi. *et al.* [20] also observed similar morphology by H_2 plasma treatment. The surface morphology of vertically aligned MWCNTs changed from flat surface to sharp conical stacks of CNTs due to the post plasma treatment. They claimed that there was improvement in the field emission properties of the CNTs due to the formation of such stacks.

(ii) Inconel

Figure 6.2 (d) & (e) corresponds to the SEM images of Al decorated CNTs grown on Inconel. SEM images clearly show that the CNTs on Inconel are also no longer a uniform film after the metal deposition, however the surface texture of the forests are not the same as for the other CNTs grown on the other substrate material. The nanotubes in this case formed bundles which has in turn is expected to reduce the screening effect. Although the mechanisms responsible for the differing surface textures after evaporating the metals on the different films are not clear, a number of different reasons associated with the wetting behavior of the CNT forests with the molten metal (and/or with the condensing metal from the vapor phase) might explain our observations.

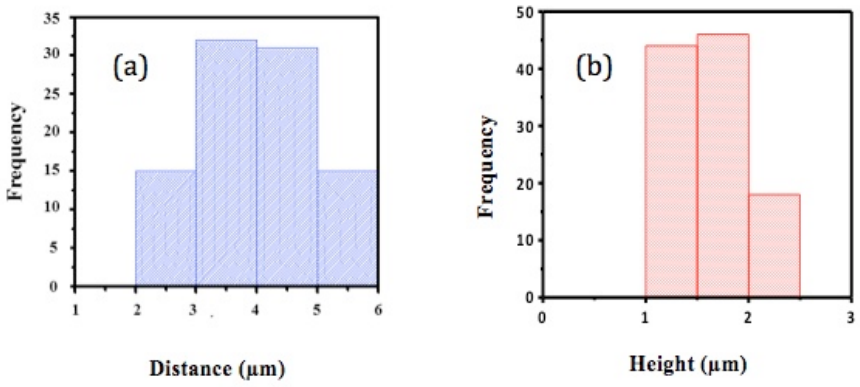

6.6.2 Di

Figure 6.3 (a) Histogram of distance distribution between the CNT bundles
Figure 6.3 (b) Histogram of vertical distance (height) of the CNT bundles

Figure 6.3 (a) and (b) show the distribution histogram of the number of CNTs with their height and the number of CNT bundles with the inter-bundle distance respectively. From the histogram, it is very clear that most of the CNT bundles are of around 2 μm in their height with inter bundle distances varying mostly between 3 and 5 μm. It was found that the inter bundle distance varies mostly between 3 μm and 5 μm. Some of the bundles are even separated by 6 μm. The height of majority of the bundles is around 2 μm. It is to be noted that bundled CNTs have the advantage of realizing the ideal ratio of inter tube distance to the height for achieving maximum field emission by reducing charge screening effects in adjacent CNTs in the forest [46]. According to Suh *et al.* [47] the field emission would be optimum when the tube height is similar to the inter-tube distance, while the results of Ren *et al*. [48] suggest 3-fold inter-tube distance in reference to CNT height to achieve maximum emitter efficiency. In our case, since most of the CNT bundles are separated by almost 3 times the height of the bundle and the bundle are emitting as a whole, the screening effect is reduced considerably and the emitter efficiency has increased substantially.

6.6.3 TEM and HRTEM characterization

Figure 6.4 (a) shows the transmission electron microscope images (TEM) and high resolution transmission electron microscope images (HRTEM) of CNTs grown on Si substrate with Al decoration on them. The low magnification image resembles a similar morphology as seen in SEM. The TEM observation of the CNTs revealed the formation of MWCNTs consisting of 4-6 graphite layers. It is clear that individual CNTs form bundles with adjacent nanotubes and share a metal tip.

The high magnification image at the point of joint in a bundle confirms the presence of metal particles and several CNTs are found to be tangled together. The high magnification image also reveals the nanoparticles embedded in the amorphous carbon layer are in reasonably close contact with the nanotubes, while the other side of the particles is unraveled.

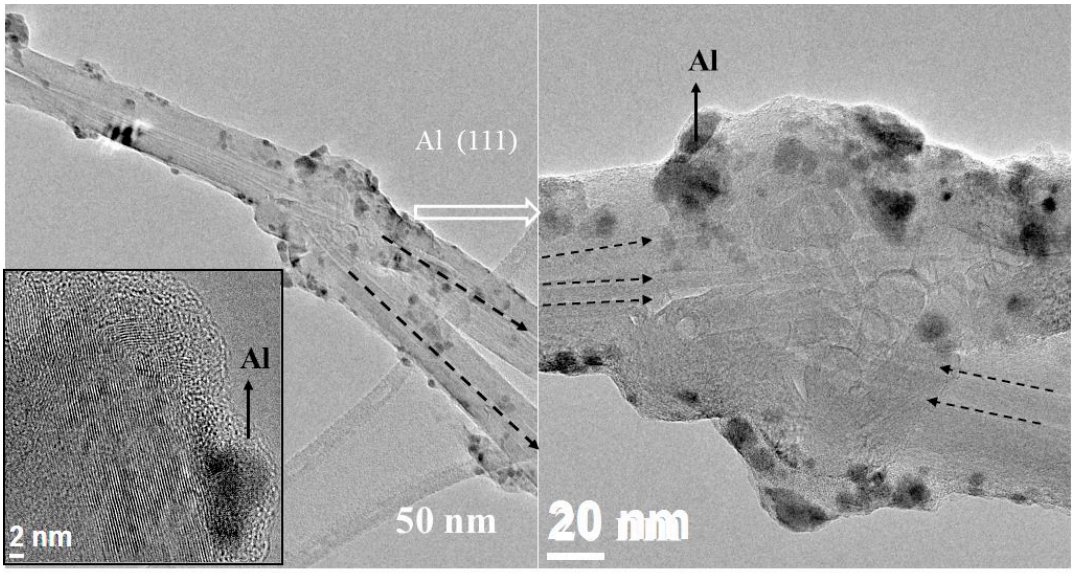

Figure 6.4 (a) TEM and HRTEM micrograph of the CNTs grown on Si substrate with Al decoration on them. It shows how the CNTs are joined together at the tip and the high magnification confirms the presence of metal particle.

The increase in wall diameter due to bundle formation is further verified with Raman measurements. The Al deposition on Inconel shows very similar morphology as shown in Figure 6.4 (b). Selected area diffraction (SAD) of the particle confirms these particles to be FCC plane (111) of Al. The large area SAD shows the presence of Al planes. The high magnification image shows an increase in diameter with a narrow distribution because of CNTs

joining together to form a bundle. The size of the metal nanoparticles was found to be 5-10 nm in diameter.

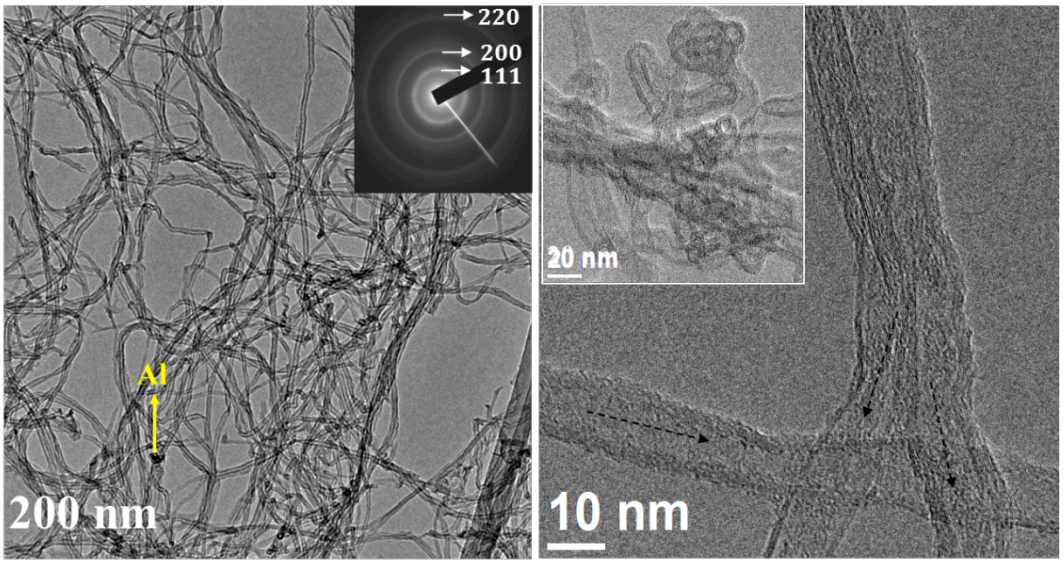

Figure 6.4 (b) TEM and HRTEM micrograph of the CNTs grown on Inconel

6.6.4 Raman spectroscopy

Raman spectra of the pristine CVD grown CNTs with and without metal deposition are shown in Figure 3a. Raman spectroscopy is the inelastic scattering of light usually associated with absorption or emission of phonons and is rich in information about the structure and chemical bonding of CNTs. Defects and sp^3 hybridized carbon atom give rise to D- band (1340 cm^{-1}) and height of this band is inversely related to the quality of the nanotube (*i.e.* presence of disorder in the graphitic material). The G- band (~1580 cm^{-1}) is associated with the sp^2 hybridized carbon atom in the nanotube wall and is a good measure of the graphitization of the sample. The G' or 2D peak (around 2600 cm^{-1}) arises due to two phonon second order

scattering process and indicates long range order in a sample. The ratio of the intensities of the defect or the disorder induced D-band to the symmetry allowed graphitic band or the G-band I_d/I_g characterizes the defect density or degree of disorder in sp^2 hybridized carbon material [49]. The ratio I_{2d}/I_g can be used for identifying the number of walls in the given MWCNT [50]. It is also to be noted that increase in the number of layer leads to a significant decrease in the peak intensity of the 2D peak and this peak becomes hardly distinguishable if the number of layer exceeds 5 [51].

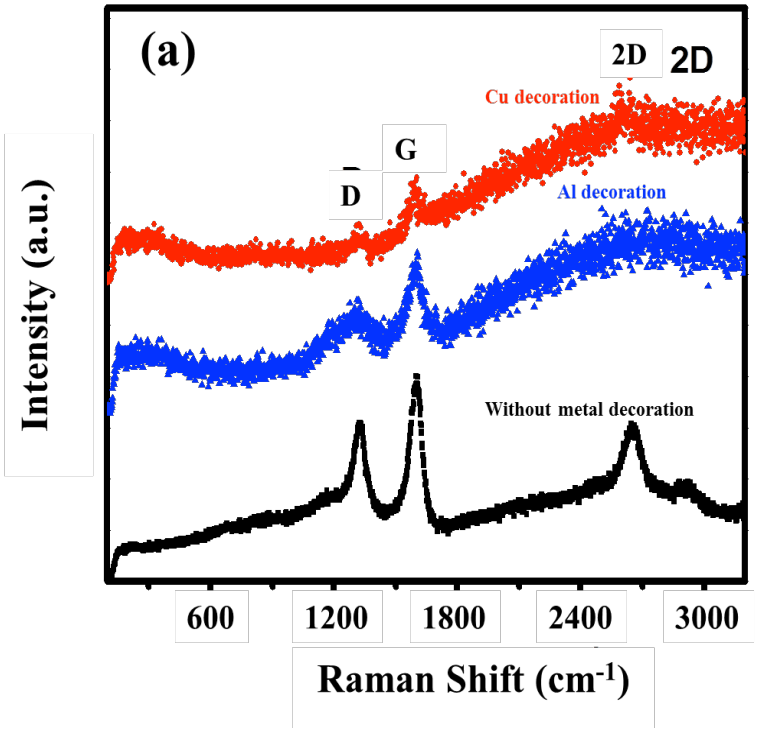

Figure 6.5 (a) Raman spectra showing 3 distinct peaks [dis-order peak D, graphitic peak G and 2D peak for Si without metal decoration, with Al decoration and Cu decoration.

The intensity ratios I_d/I_g and I_{2d}/I_g are given in Table 6.1. From the results, it is clear that the intensity ratio I_d/I_g of CNTs grown on Si substrate without any metal decoration and with Al

decoration was 0.78 and these values are very close to the values reported by Athipalli *et al.* [52]. For the CNTS grown on Si substrate with Cu decoration on them this ratio became 0.51. The lower the value of this ratio, lesser is the defect, which in turn means lesser amorphous carbon, and greater is the degree of graphitic crystallinity. Also, the 2D peak for Al decorated CNTs grown on Inconel was hardly distinguishable and hence the ratio I_{2d}/I_g became zero. As predicted by the work of Ferrari [51], the number of walls must have exceeded five and hence this peak became hardly distinguishable. This was also consistent with TEM, where it is clear that the CNTs join together thereby increasing the number of walls. From the above predictions, it is clear that the CNTs grown on Si with Cu decoration on them have higher graphitic crystallinity with lesser defect. The occurrence of sharp 2D peak on this sample indicates a good long range order in those samples.

Table 6.1: Values of I_d/I_g and I_{2d}/I_g ratio for different types of CNTs

Type of CNTs	I_d/I_g	I_{2d}/I_g
Si Grown	0.78	0.71
Inconel Grown	0.65	0.41
Si grown with Al decoration	0.78	0.80
Inconel grown with Al decoration	0.67	0.00
Si grown with Cu decoration	0.51	0.58
Inconel grown with Cu decoration	0.66	0.77

6.6.5 X-ray diffraction study

In order to characterize the phase deposited on the CNT forest, the samples are analyzed by X-ray diffraction. Figure 6.5b shows the representative image of the Al deposition and Cu deposition on Si. In the diffraction pattern we observe reflections at 2Θ=38° and 44° which can be assigned to the (111) and (200) planes of FCC phase of Al. The reflection at 2Θ=43° corresponds to the FCC plane (111) of Cu. These diffraction patterns confirm the presence of metallic particles of Al and Cu and absence of their crystalline oxides. The broadened reflections from the metals clearly reveals the small crystallite size of the metallic particles (~5 nm) supporting observations done with TEM.

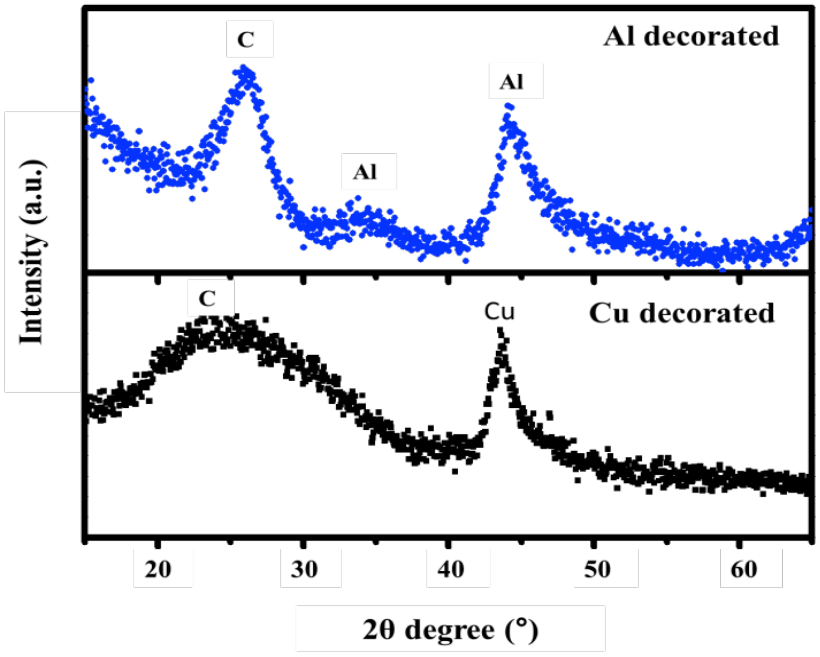

Figure 6.5 (b) XRD pattern on Si with Al decoration and XRD pattern on Si with Cu decoration. Al, Cu and C peak clearly prove that there is no oxide formation

6.6.6 Field emission characteristics

6.6.6.1 Turn on and threshold voltage

The field emission characteristics of the CNTs grown on Si with and without any metal decorations are shown in Figure 6.6. The turn on field E_{to}, which is the field required to obtain a current density of 1 μA/cm^2 and the threshold field E_{th}, which is the field required to obtain a current density of 100 μA/cm^2 (in our case) are summarized in Table 6.2. The data clearly reveals that Si grown CNTs with Al decoration on them gave the lowest E_{to} and E_{th}, 0.13 V/μm and 0.14 V/μm respectively. One of the explanation for our low E_{to} and E_{th} for Si grown CNTs with Al decoration on them is due to the lower work function of Al as predicted by Lee *et al*. [53]. Similar field emission characteristics were observed for CNTs grown on Inconel with and without any metal decorations on them. (Figure 4b) The J-E plot was repeatedly measured and it showed good reproducibility. No current saturation was observed over E_{th}.

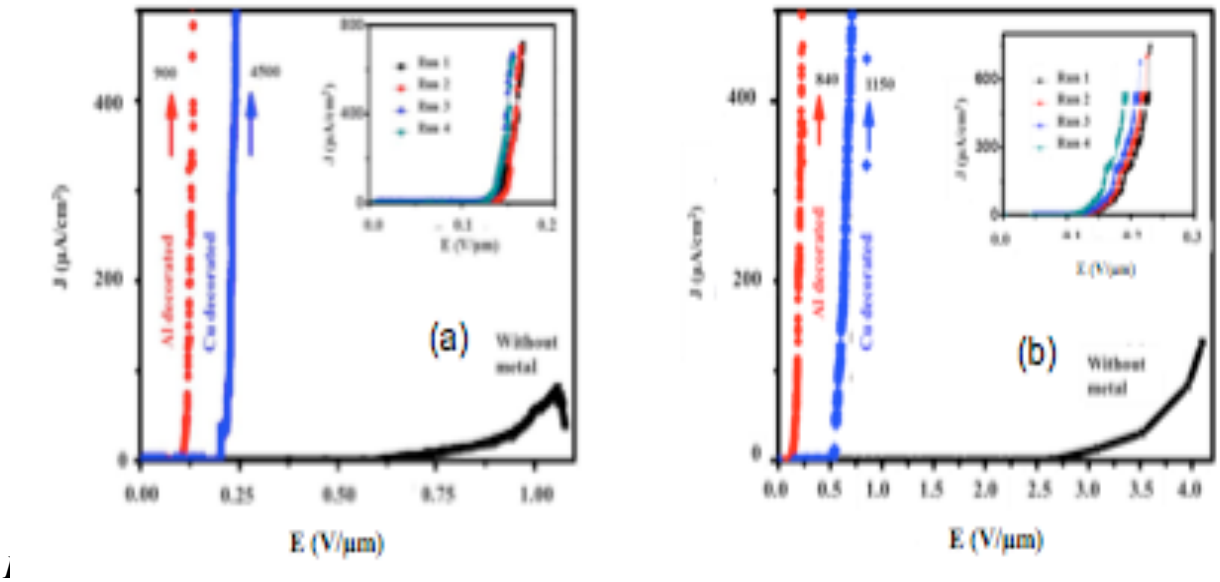

without any metal decorations. Inset in the JE plot shows emission stability

It is well known that during field emission, the electrons have to cross two barriers [54]. Barrier 1 is the barrier between the substrate and the CNT and the barrier 2 is the barrier between the CNT and the vacuum. Since the Inconel and Al coated Si substrates on which CNTs are directly grown have good electrical conductivity, barrier 1 is expected to be reduced substantially enhancing the overall field emission properties of our structures. The measured low contact resistance values for the CNT-substrate interfaces are in agreement with our assumptions as seen in Figure 6.8 (a &b).

Barrier 2 on the other hand has also improved. According to Tanaka *et al.* [55] the presence of amorphous carbon can increase the work function and the E_{th} to a larger extent. One of the explanations for the low E_{th} values for metal decorated CNTs can be due to the reduced amount of amorphous carbon [45]. Although the mechanism that would reduce the amorphous carbon content obtained after Cu decoration is not clear, a plausible explanation might be a partial dissolution of carbon by Cu at the process temperatures applied in the course of evaporation. Another, probably more important effect that helps electron emission is the promoted electron passage from the nanotubes towards the vacuum through the metal nanoparticles, which may reasonably explain why we observe significant reduction of E_{th} for both metals. The metal nanoparticles form highly conductive electrical paths for the electrons through the amorphous carbon layer (Figure 6.2 (a)) covering the nanotubes thus ensuring emission centers with clean surface towards the vacuum.

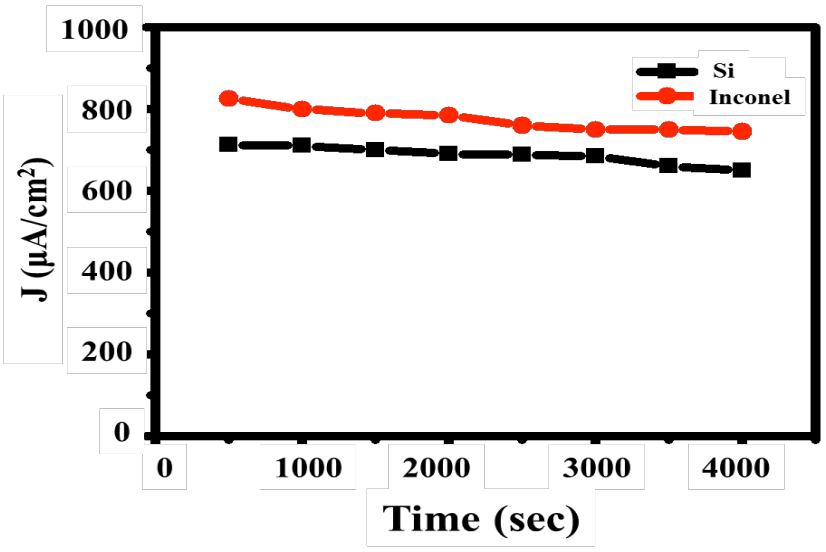

Figure 6.6 (c) Time trace of current density at the fixed field of 0.15 V/μm for Si grown CNTs and 0.25 V/μm for Inconel grown CNTs, both decorated with Al nanoparticles.

Table 6.2: Values of E_{to} and E_{th} for different type of substrates with and without metal decoration.

Type of CNTs	E_{to}	E_{th}
Si Grown	0.78	2.6
Inconel Grown	1.2	2
Si grown with Al decoration	0.13	0.14
Inconel grown with Al decoration	0.14	0.18
Si grown with Cu decoration	0.19	0.22
Inconel grown with Cu decoration	0.53	0.58

6.6.6.3 Edge effect

Furthermore, according to Fuji *et al.* [56], the electric field of the bundle is significantly higher at the edge than at the center when compared to the electric field of the flat film which is constant all over the emitter surface. In our samples, due to the metal decoration, the emitter surface is no longer a flat film; instead they are transformed into individual bundles since some of the Al particles went in between the CNTs, thereby increasing the number of edges. The CNTs at the periphery of the bundle formed due to metal decoration acted as a major emission sites. Thus, the excellent field emission property of our emitters can also be attributed to the edge effect.

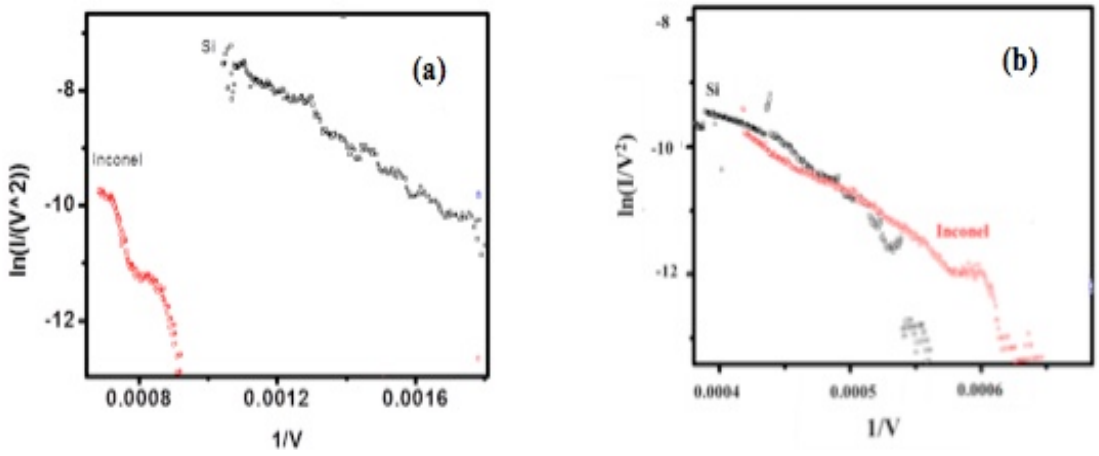

Figure 6.7 (a &b) F-N plot for the Al decorated CNTs grown on Si and Inconel showing two different regimes of emission

In addition to the improved field emission I–V characteristics, better emission uniformity is observed from the emission pattern of Al decorated CNTs grown on both Si and Inconel, as shown in the inset of the Figure 6.6 (a &b). This is because of the increase in the number of available emitters and reduced screening effect. Figure 6.6 (c) shows the time trace of current density at the fixed field of 0.15 V/μm for Si grown CNTs and 0.25 V/μm for Inconel

grown CNTs, both decorated with Al nanoparticles. It was found that there was stable emission for more than an hour due to metal decoration on the CNTs.

6.6.6.4 Deviation of Fowler-Nordheim plot

The Fowler-Nordheim (F-N) plot (Figure 6.7), which is between ln (I/V^2) and 1/V deviated from the linear behavior in this case. Though F-N model was originally developed for flat metallic surfaces, it has been extensively used for nanomaterials. As obtained by Choi *et al.* [20], in this work too, the F-N curve did not follow entirely the conventional F-N model during initial field emission range. As predicted by Zettl *et al.* [57], the nanotube tips may have localized states which are weekly coupled to the back of the tube. Also the F-N model assumes a single emitter, which is totally independent of its surroundings. But while using the model for nanotubes, we ignore the effect of multiple emitting tips of the nanotubes.

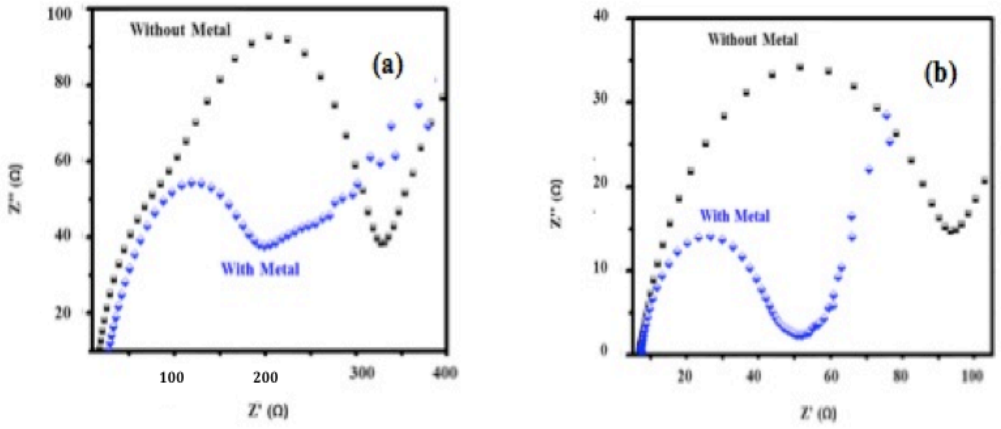

Figure 6.8 (a & b) Nyquist plots of EIS spectra collected from electrochemical lithium half cell of raw MWCNTs grown without any metal decoration and with Al decoration on CNTs grown on two different substrates, (a) Si and (b) Inconel

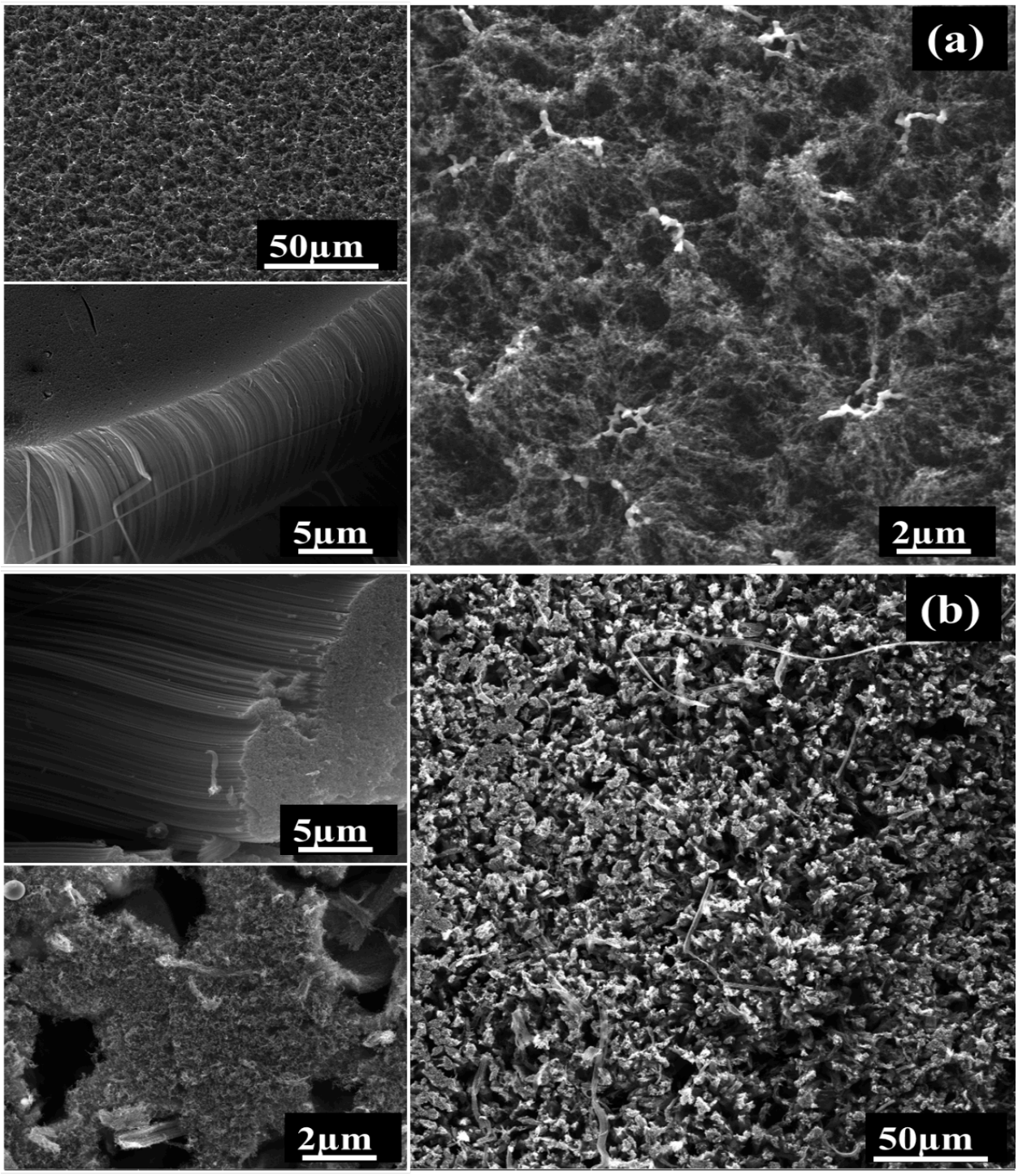

Figure 6.9 (a & b) (a) and (b) are the SEM images taken after field emission experiment on the CNTs grown on Si and Inconel respectively with Al decoration on them.

6.6.7 Contact resistance measurement

Electric impedance spectroscopy measurements performed for CNTs grown on both Si and Inconel substrates before and after the metal decoration suggests the structures are sufficiently conductive for emitter applications. It can be seen from the Nyquist plots that the contact resistance between the CNT and Si was ~331 Ω/cm^2 before the metal decoration and it got reduced to 194 Ω/cm^2 after the metal decoration. Similarly the contact resistance between the CNT and Inconel before and after the metal decoration was 93 Ω/cm^2 and 50 Ω/cm^2 respectively. The semicircles in the impedance spectra indicate the presence of a capacitive component and that is most likely caused by the nanotube films of large specific surface area.

6.6.8 After field emission

SEM images in Figure 6.9 (a & b) clearly shows that the metal decoration has not altered the morphology of the CNTs even after the field emission experiment. This proves the fact that the particles are strongly attached to the CNTs, which in turn increases the adhesion of the CNTs resulting in the enhancement in the field emission properties of the CNT.

6.7 Conclusions

In conclusion, vertically aligned CNTs grown on Al coated Si and Inconel substrates were decorated with Al and Cu particles using a simple and scalable process. The synthesized hybrid structures showed enhanced field emission properties with ultra low turn on and threshold voltages of 0.13 V/μm and 0.14 V/μm respectively measured for the Al decorated CNTs grown on Al coated Si. Contact resistance also got reduced substantially in the metal

decorated structures which resulted in stable emission for a longer duration without any current degradation. The excellent field emission properties of the metal decorated CNTs can be attributed to the edge effect, reduced screening effect, lower contact resistance, which may pave the road for future devices that require substantially lower bias than the currently existing ones.

6.8 References

1. Planeix, J. M.; Coustel, N.; Coq, B.; Brotons, V.; Kumbhar, P. S.; Dutartre, R.; Geneste, P.; Bernier, P.; Ajayan, P. M. Application of Carbon Nanotubes as Supports in Heterogeneous Catalysis. J. Am. Chem. Soc. 1994, 116, 7935–7936.
2. Fu, Y.; Zhang, L.; Chen, G. Preparation of a Carbon Nanotube-Copper Nanoparticle Hybrid by Chemical Reduction for Use in the Electrochemical Sensing of Carbohydrates. Carbon 2012, 50, 2563–2570.
3. Liu, Z.; Lin, X.; Lee, J. Y.; Zhang, W.; Han, M.; Gan, L. M. Preparation and Characterization of Platinum-Based Electrocatalysts on Multiwalled Carbon Nanotubes for Proton Exchange Membrane Fuel Cells. Langmuir 2002, 18, 4054–4060.
4. Sun, Y.; Wang, H. H. High-Performance, Flexible Hydrogen Sensors That Use Carbon Nanotubes Decorated with Palladium Nanoparticles. Adv. Mater. 2007, 19, 2818–2823.
5. Li, W.; Liang, C.; Zhou, W.; Qiu, J.; Zhou; Sun, G.; Xin, Q. Preparation and Characterization of Multiwalled Carbon Nanotube-Supported Platinum for Cathode Catalysts of Direct Methanol Fuel Cells. J. Phys. Chem. B 2003, 107, 6292–6299.
6. Reddy, A.; Ramaprabhu, S. Hydrogen Storage Properties of Nanocrystalline Pt Dispersed Multi-Walled Carbon Nanotubes. Int. J. Hydrog. Energy 2007, 32, 3998–4004.
7. Kong, J.; Chapline, M. G.; Dai, H. Functionalized Carbon Nanotubes for Molecular Hydrogen Sensors. Adv. Mater. 2001, 13, 1384–1386.

8. Teo, K. B. K.; Chhowalla, M.; Amaratunga, G. A. J.; Milne, W. I.; Pirio, G.; Legagneux, P.; Wyczisk, F.; Pribat, D.; Hasko, D. G. Field Emission from Dense, Sparse, and Patterned Arrays of Carbon Nanofibers. Appl. Phys. Lett. 2002, 80, 2011.
9. Stephan, O.; Ajayan, P. M.; Colliex, C.; Redlich, P.; Lambert, J. M.; Bernier, P.; Lefin, P. Doping Graphitic and Carbon Nanotube Structures with Boron and Nitrogen. Science 1994, 266, 1683–1685.
10. Golberg, D.; Bando, Y.; Bourgeois, L.; Kurashima, K.; Sato, T. Large-Scale Synthesis and HRTEM Analysis of Single-Walled B- and N-Doped Carbon Nanotube Bundles. Carbon 2000, 38, 2017–2027.
11. Zhang, J.; Yang, C.; Wang, Y.; Feng, T.; Yu, W.; Jiang, J.; Wang, X.; Liu, X. Improvement of the Field Emission of Carbon Nanotubes by Hafnium Coating and Annealing. Nanotechnology 2006, 17, 257–260.
12. Wei, W.; Jiang, K.; Wei, Y.; Liu, P.; Liu, K.; Zhang, L.; Li, Q.; Fan, S. LaB[sub 6] Tip-Modified Multiwalled Carbon Nanotube as High Quality Field Emission Electron Source. Appl. Phys. Lett. 2006, 89, 203112.
13. Min, Y.-S.; Bae, E. J.; Park, J. B.; Kim, U. J.; Park, W.; Song, J.; Hwang, C. S.; Park, N. ZnO Nanoparticle Growth on Single-Walled Carbon Nanotubes by Atomic Layer Deposition and a Consequent Lifetime Elongation of Nanotube Field Emission. Appl. Phys. Lett. 2007, 90, 263104.
14. Green, J. M.; Dong, L.; Gutu, T.; Jiao, J.; Conley, J. F.; Ono, Y. ZnO-Nanoparticle-Coated Carbon Nanotubes Demonstrating Enhanced Electron Field-Emission Properties. J. Appl. Phys. 2006, 99, 094308.

15. Liu, C.; Kim, K. S.; Baek, J.; Cho, Y.; Han, S.; Kim, S.-W.; Min, N.-K.; Choi, Y.; Kim, J.-U.; Lee, C. J. Improved Field Emission Properties of Double-Walled Carbon Nanotubes Decorated with Ru Nanoparticles. Carbon 2009, 47, 1158–1164.
16. Jonge, N. de; Allioux, M.; Doytcheva, M.; Kaiser, M.; Teo, K. B. K.; Lacerda, R. G.; Milne, W. I. Characterization of the Field Emission Properties of Individual Thin Carbon Nanotubes. Appl. Phys. Lett. 2004, 85, 1607.
17. Han, S.; Ihm, J. First-Principles Study of Field Emission of Carbon Nanotubes. Phys. Rev. B 2002, 66.
18. Kim, H.-S.; Lee, H.; Han, K.-S.; Kim, J.-H.; Song, M.-S.; Park, M.-S.; Lee, J.-Y.; Kang, J.-K. Hydrogen Storage in Ni Nanoparticle-Dispersed Multiwalled Carbon Nanotubes. J. Phys. Chem. B 2005, 109, 8983–8986.
19. Kim, J.-Y.; Jeong, T.; Baik, C.-W.; Park, S. H.; Han, I.; Kim, G.-H.; Yu, S. Field-Emission Performance and Structural Change Mechanism of Multiwalled Carbon Nanotubes by Oxygen Plasma Treatment. Thin Solid Films 2013, 547, 202–206.
20. Choi, H.; Ji Shin, Y.; Il Cha, S.; Ho Kang, I.; Bahng, W. Enhanced Field-Emission Capacity by Density Control of a CNT Cathode Using Post-Plasma Treatment. Solid State Commun. 2013, 171, 50–54.
21. Xiao, L.; Liu, P.; Liu, L.; Jiang, K.; Feng, X.; Wei, Y.; Qian, L.; Fan, S.; Zhang, T. Barium-Functionalized Multiwalled Carbon Nanotube Yarns as Low-Work-Function Thermionic Cathodes. Appl. Phys. Lett. 2008, 92, 153108.
22. Lyth, S. M.; Hatton, R. A.; Silva, S. R. P. Efficient Field Emission from Li-Salt Functionalized Multiwall Carbon Nanotubes on Flexible Substrates. Appl. Phys. Lett. 2007, 90, 013120.

23. Jin, F.; Liu, Y.; Day, C. M.; Little, S. A. Enhanced Electron Emission from Functionalized Carbon Nanotubes with a Barium Strontium Oxide Coating Produced by Magnetron Sputtering. Carbon 2007, 45, 587–593.
24. Feng, M.; Sun, R.; Zhan, H.; Chen, Y. Decoration of Carbon Nanotubes with CdS Nanoparticles by Polythiophene Interlinking for Optical Limiting Enhancement. Carbon 2010, 48, 1177–1185.
25. Wang, W.; Serp, P.; Kalck, P.; Silva, C. G.; Faria, J. L. Preparation and Characterization of Nanostructured MWCNT-TiO2 Composite Materials for Photocatalytic Water Treatment Applications. Mater. Res. Bull. 2008, 43, 958–967.
26. Haremza, J. M.; Hahn, M. A.; Krauss, T. D.; Chen, S.; Calcines, J. Attachment of Single CdSe Nanocrystals to Individual Single-Walled Carbon Nanotubes. Nano Lett. 2002, 2, 1253–1258.
27. Huang, C.-S.; Yeh, C.-Y.; Chang, Y.-H.; Hsieh, Y.-M.; Ku, C.-Y.; Lai, Q.-T. Field Emission Properties of CNT–ZnO Composite Materials. Diam. Relat. Mater. 2009, 18, 452–456.
28. Yang, M.; Liang, T.; Peng, Y.; Chen, Q. Synthesis and Characterization of a Nanocomplex of ZnO Nanoparticles Attached to Carbon Nanotubes. Acta Phys.-Chim. Sin. 2007, 23, 145–151.
29. An, G.; Na, N.; Zhang, X.; Miao, Z.; Miao, S.; Ding, K.; Liu, Z. SnO 2 /carbon Nanotube Nanocomposites Synthesized in Supercritical Fluids: Highly Efficient Materials for Use as a Chemical Sensor and as the Anode of a Lithium-Ion Battery. Nanotechnology 2007, 18, 435707.

30. Zhai, L.; Wei, Z.; Yang, Z.; Ni, X. Polymerization Initiated by ZnS Nanocrystals Anchored on Carbon Nanotubes. Mater. Lett. 2010, 64, 531–533.
31. Cho, N.; Roy Choudhury, K.; Thapa, R. B.; Sahoo, Y.; Ohulchanskyy, T.; Cartwright, A. N.; Lee, K.-S.; Prasad, P. N. Efficient Photodetection at IR Wavelengths by Incorporation of PbSe–Carbon-Nanotube Conjugates in a Polymeric Nanocomposite. Adv. Mater. 2007, 19, 232–236.
32. Li, C.; Ding, S.; Lei, W.; Zhang, X.; Wang, B. Enhanced Field Emission from Vertically Aligned Carbon Nanotubes on Metal Mesh Electrode. Appl. Surf. Sci. 2013, 285, 505–508.
33. Zuo, Y.; Ren, Y.; Wang, Z.; Han, X.; Xi, L. Enhanced Field Emission and Hysteresis Characteristics of Aligned Carbon Nanotubes with Ti Decoration. Org. Electron. 2013, 14, 2306–2314.
34. Pandey, A.; Prasad, A.; Moscatello, J. P.; Engelhard, M.; Wang, C.; Yap, Y. K. Very Stable Electron Field Emission from Strontium Titanate Coated Carbon Nanotube Matrices with Low Emission Thresholds. ACS Nano 2013, 7, 117–125.
35. Zanin, H.; May, P. W.; Hamanaka, M. H. M. O.; Corat, E. J. Field Emission from Hybrid Diamond-like Carbon and Carbon Nanotube Composite Structures. ACS Appl. Mater. Interfaces 2013, 5, 12238–12243.
36. Fan, Y. C.; Liu, Y. M.; Chen, Y. C.; Sung, Y.; Ger, M. D. Carbon Nanotube Field Emission Cathodes Fabricated with Chemical Displacement Plating. Appl. Surf. Sci. 2009, 255, 7753–7758.

37. Chen, Y.; Jiang, H.; Li, D.; Song, H.; Li, Z.; Sun, X.; Miao, G.; Zhao, H. Improved Field Emission Performance of Carbon Nanotube by Introducing Copper Metallic Particles. Nanoscale Res. Lett. 2011, 6, 537.
38. Nilsson, L.; Groening, O.; Emmenegger, C.; Kuettel, O.; Schaller, E.; Schlapbach, L.; Kind, H.; Bonard, J.-M.; Kern, K. Scanning Field Emission from Patterned Carbon Nanotube Films. Appl. Phys. Lett. 2000, 76, 2071.
39. Bonard, J.-M.; Dean, K.; Coll, B.; Klinke, C. Field Emission of Individual Carbon Nanotubes in the Scanning Electron Microscope. Phys. Rev. Lett. 2002, 89.
40. Bonard, J.-M.; Weiss, N.; Kind, H.; Stöckli, T.; Forró, L.; Kern, K.; Châtelain, A. Tuning the Field Emission Properties of Patterned Carbon Nanotube Films. Adv. Mater. 2001, 13, 184–188.
41. Bittencourt, C.; Ke, X.; Van Tendeloo, G.; Thiess, S.; Drube, W.; Ghijsen, J.; Ewels, C. P. Study of the Interaction between Copper and Carbon Nanotubes. Chem. Phys. Lett. 2012, 535, 80–83.
42. Gingery, D.; Bühlmann, P. Formation of Gold Nanoparticles on Multiwalled Carbon Nanotubes by Thermal Evaporation. Carbon 2008, 46, 1966–1972.
43. Charlier, J.-C.; Arnaud, L.; Avilov, I. V.; Delgado, M.; Demoisson, F.; Espinosa, E. H.; Ewels, C. P.; Felten, A.; Guillot, J.; Ionescu, R.; et al. Carbon Nanotubes Randomly Decorated with Gold Clusters: From Nano 2 Hybrid Atomic Structures to Gas Sensing Prototypes. Nanotechnology 2009, 20, 375501.
44. Muratore, C.; Reed, A. N.; Bultman, J. E.; Ganguli, S.; Cola, B. A.; Voevodin, A. A. Nanoparticle Decoration of Carbon Nanotubes by Sputtering. Carbon 2013, 57, 274–281.

45. Sridhar, S.; Ge, L.; Tiwary, C. S.; Hart, A. C.; Ozden, S.; Kalaga, K.; Lei, S.; Sridhar, S. V.; Sinha, R. K.; Harsh, H.; et al. Enhanced Field Emission Properties from CNT Arrays Synthesized on Inconel Superalloy. ACS Appl. Mater. Interfaces 2014, 140113152340002.
46. Katayama, M.; Lee, K.-Y.; Honda, S.; Hirao, T.; Oura, K. Ultra-Low-Threshold Field Electron Emission from Pillar Array of Aligned Carbon Nanotube Bundles. Jpn. J. Appl. Phys. 2004, 43, L774–L776.
47. Suh, J. S.; Jeong, K. S.; Lee, J. S.; Han, I. Study of the Field-Screening Effect of Highly Ordered Carbon Nanotube Arrays. Appl. Phys. Lett. 2002, 80, 2392.
48. Ren, H.; Yang, L.; Zhang, Y. Numerical Calculations on the Field Emission of Carbon Nanotubes. J. Phys. Conf. Ser. 2013, 418, 012007.
49. Tuinstra, F. Raman Spectrum of Graphite. J. Chem. Phys. 1970, 53, 1126.
50. Saito, R.; Hofmann, M.; Dresselhaus, G.; Jorio, A.; Dresselhaus, M. S. Raman Spectroscopy of Graphene and Carbon Nanotubes. Adv. Phys. 2011, 60, 413–550.
51. Ferrari, A. C. Raman Spectroscopy of Graphene and Graphite: Disorder, Electron–phonon Coupling, Doping and Nonadiabatic Effects. Solid State Commun. 2007, 143, 47–57.
52. Atthipalli, G.; Wang, H.; Gray, J. L. Catalyst-Assisted Vertical Growth of Carbon Nanotubes on Inconel Coated Commercial Copper Foil Substrates versus Sputtered Copper Films. Appl. Surf. Sci. 2013, 273, 515–519.
53. Lee, D. H.; Lee, J. A.; Lee, W. J.; Choi, D. S.; Lee, W. J.; Kim, S. O. Facile Fabrication and Field Emission of Metal-Particle-Decorated Vertical N-Doped Carbon Nanotube/Graphene Hybrid Films. J. Phys. Chem. C 2010, 114, 21184–21189.

54. Gadzuk, J.; Plummer, E. Field Emission Energy Distribution (FEED). Rev. Mod. Phys. 1973, 45, 487–548.

55. Tanaka, H.; Akita, S.; Pan, L.; Nakayama, Y. Barrier Effect on Field Emission from Stand-Alone Carbon Nanotube. Jpn. J. Appl. Phys. 2004, 43, 864–867.

56. Fujii, S.; Honda, S.; Machida, H.; Kawai, H.; Ishida, K.; Katayama, M.; Furuta, H.; Hirao, T.; Oura, K. Efficient Field Emission from an Individual Aligned Carbon Nanotube Bundle Enhanced by Edge Effect. Appl. Phys. Lett. 2007, 90, 153108.

57. Collins, P. G.; Zettl, A. Unique Characteristics of Cold Cathode Carbon-Nanotube-Matrix Field Emitters. Phys. Rev. B 1997, 55, 9391–9399.

CHAPTER VII

One Step Process for Infiltration of Fe_3O_4 into the CNT Array for Enhanced Field Emission

7.1 Introduction

As described in the previous chapters, carbon nanotubes (CNTs) due to their unique mechanical, electrical, thermal and optical properties [1-4] has emerged as one of the promising candidate for many nano-scale electronic devices [5-9]. Recently in order to improve /impart new optical, electric, electro chemical and magnetic properties of CNTs modification of the CNTs including both encapsulation of CNTs with metal particles inside [10-13] and attaching nanoparticles on the outer surface of the CNTs are reported [14-16]. Additionally, due to high specific surface area and the unique one-dimensional structure and of CNTs, various inorganic nanoparticles such as metals, metal oxides and semiconducting nanoparticles were attached on to the CNT's surface in order to improve the overall characteristics [17-20]. Many efforts have been devoted to decorate CNTs with diverse organic compound by the covalent attachment, polymer wrapping and surfactant treatment by non-covalent attachment [21].

7.2 Techniques used to decorate the CNTs with metals

Decoration of the CNTs with different metals such as Al and Cu , as explained in chapter 7, has certainly improved the field emission properties of the CNTs. Also, modification of the surface of the CNTs using metal alloys, metal oxides and polymers, can improve the

overall characteristics of CNTs. Numerous ways have been developed to fabricate CNT-based nanocomposites, including electron beam evaporation [22], chemical vapor deposition [23,24], hydrothermal process [25] , the sol-gel technique [26] and the conventional impregnation method[27]. In the above mentioned methods, we can find the introduction of transition metals, their oxide and sulphide particles, and inorganic materials like noble metals into the CNT based composite material. Among them, magnetic CNT composites made up of iron/iron oxide nanoparticle were suggested to be of great importance because of their potential uses in magnetic data storage, xerography, biosensors, microwave absorbing materials and in magnetic force microscopy as nanoprobes [28-32]. Some tedious and complicated technique such as wet chemistry method and high temperature treatment were used to decorate the CNTs with iron oxide nanoparticle [33,34]. But, CNT metal composite synthesis methods reported so far has some disadvantages associated with the synthesis methods, such as (1) use of complex synthesis technique/instrumentation, (2) destruction of CNT structure by strong acids which in turn deteriorate the performance of the CNTs, and (3) a non-uniform distribution of particles on the CNTs. But to our best knowledge, only very few literatures are there for field emission application of these type of CNT-iron oxide composite.

In this chapter we want to explain an easy, cost effective and scalable method to prepare magnetic CNTs. Since we used a magnet for the infiltration of iron nanoparticle into the CNT array, it doesn't require any complicated set-up or technique, making this more cost effective. Furthermore, field emission results prove that these composites can be used as excellent emitter source in X-ray and other vacuum microwave application as there was tremendous reduction in turn on and the threshold voltage when compared to earlier reports [35]. It is very clear that

this easily scalable and cost effective method of infiltrating Fe_3O_4 nanoparticles doesn't require any complicated/sophisticated set-up. Another major advantage of this method is that the physical structure of the 3D CNT forest remains unaltered. Furthermore, results of the field emission experiment proves that the tilting or inverting the CNT forest do not disturb the Fe_3O_3 nanoparticles after infiltration.

7.3 Experiment

7.3.1 Simple technique used to decorate CNTs with Fe_3O_4

We grew vertically aligned MWCNTs on Si and Inconel substrate in water assisted CVD system. CNTs grown on Si were around 1cm in height and those grown on Inconel were around 800 μn in height. Mono dispersed iron oxide (Fe_3O_4) nanoparticles were synthesized using the method described by Narayanan et al [36]. The particles were then dried. 2mg of these particles was spread across the surface of the CNTs using a spatula. Utmost care was taken for the uniform spreading of the nanoparticles on the CNT surface. The CNTs grown on both the substrates with the Fe_3O_4 particles was kept in a petri dish. Then a magnet with the magnetic field of 0.1T was brought beneath the petty dish and slowly moved across till most of the nanoparticles got infiltrated inside the CNT array . Through the control of the movement of the magnet below the CNT forest, the iron nanoparticles were uniformly distributed over the CNT surface and infiltrated into the centimeter long CNT forest. During this process, since the CNTs grown on Si

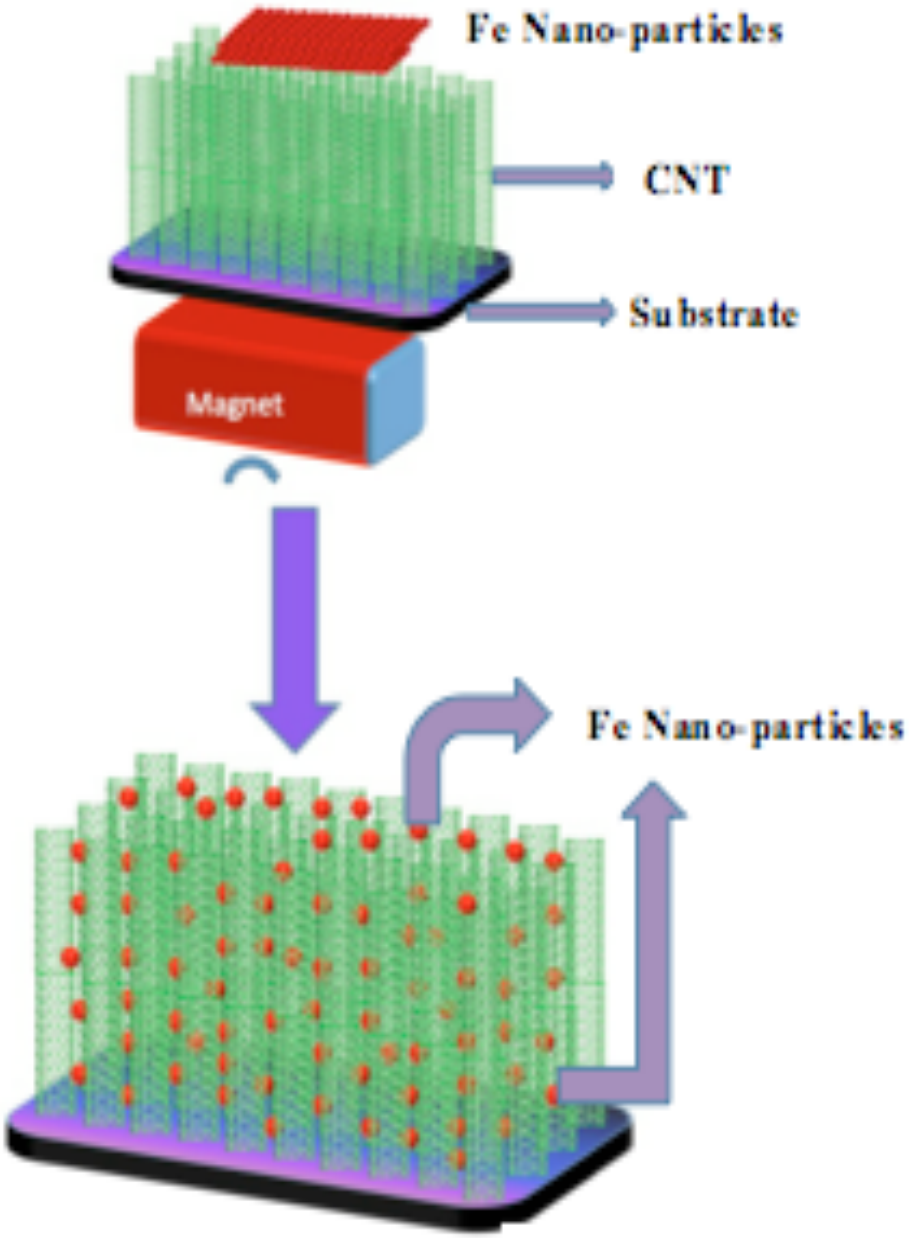

Figure 7.1 Schematic procedure for the infiltration of Fe_3O_4 particles inside the CNT forest

were around 1cm, we could clearly observe the movement of the Fe_3O_4 towards the magnet (i.e) into the CNT forest. On the other hand, since the CNTs grown on Inconel was only around 800 µn in height, we could not exactly observe the process of infiltration through them with naked eye.

The surface morphologies were characterized using scanning electron microscope (FEI Quanta 400 ESEM FEG), HRTEM (JEOL 2100 F TEM) and Raman spectroscopy (Kaiser Fiber-Optic RAMAN). The in-situ confocal microscopy of the process has been performed using Nikon Eclipse TE2000-U microscope equipped with the Eclipse C1 confocal system in order to understand the method of infiltration of nanoparticles into the CNT forest. For this, the iron oxide nanoparticles were mixed with colored dye in water and the process of infiltration is repeated.

7.3.2 Field Emission Measurement

After the infiltration of metal nano particles; the sample was transferred to a vacuum chamber with vacuum better than 10^{-6} Torr, for field emission measurement. ITO coated with green phosphorous was used as anode and the area of the sample was 1cm x 1cm. The distance between the cathode and the anode was adjusted using micrometer screw gauge arrangement and a suitable DC voltage was supplied using Keithley 2410 high voltage power supply.

7.3.3 Contact Resistance Measurement

The EIS measurements were performed using a two electrode setup with the CNT on the substrate as the working electrode, Lithium metal as the counter/reference electrode. In this, 1M LiPF6 in 1:1 v/v mixture of ethylene carbonate (EC) dimethyl carbonate (DMC) was used as the electrolyte and glass micro-fiber filter membrane was used as the separator. The EIS measurements were conducted over 70kHz to 10mHz by applying a constant dc bias with sinusoidal signal of 10 mV.

7.4 Results and Discussion

7.4.1 SEM Morphology after Infiltration

(i) Before Infiltration

Figure 7.1 shows the schematic procedure for the process of infiltration of Fe_3O_4 nano particles inside the CNT forest. Figure 7.2 (a & b) shows the SEM image of the CNTs grown on Si before the iron oxide (Fe_3O_4) infiltration in two different magnifications. From the morphology observed, it is very clear that the grown CNTs are vertically aligned.

(ii) Tilted View (to show both top and side of the CNTs)

In order to show both the top as well as the side of the 3D CNT forest, a 45˚tilted image is shown in Figure 7.2 (b). From this SEM image, we can clearly see the way in which the iron oxide nanoparticles are distributed uniformly across the top of the CNT array.

(iii) Cross Sectional View (To show the interior of the CNT forest after infiltration)

As explained in the experimental section, some of the iron oxide nanoparticles got infiltrated into the CNT array with the help of a magnet. In order to find out the exact path in which the nanoparticles are getting infiltrated into the CNT forest, we sliced a portion of the CNT forest to have the cross sectional view of the array.

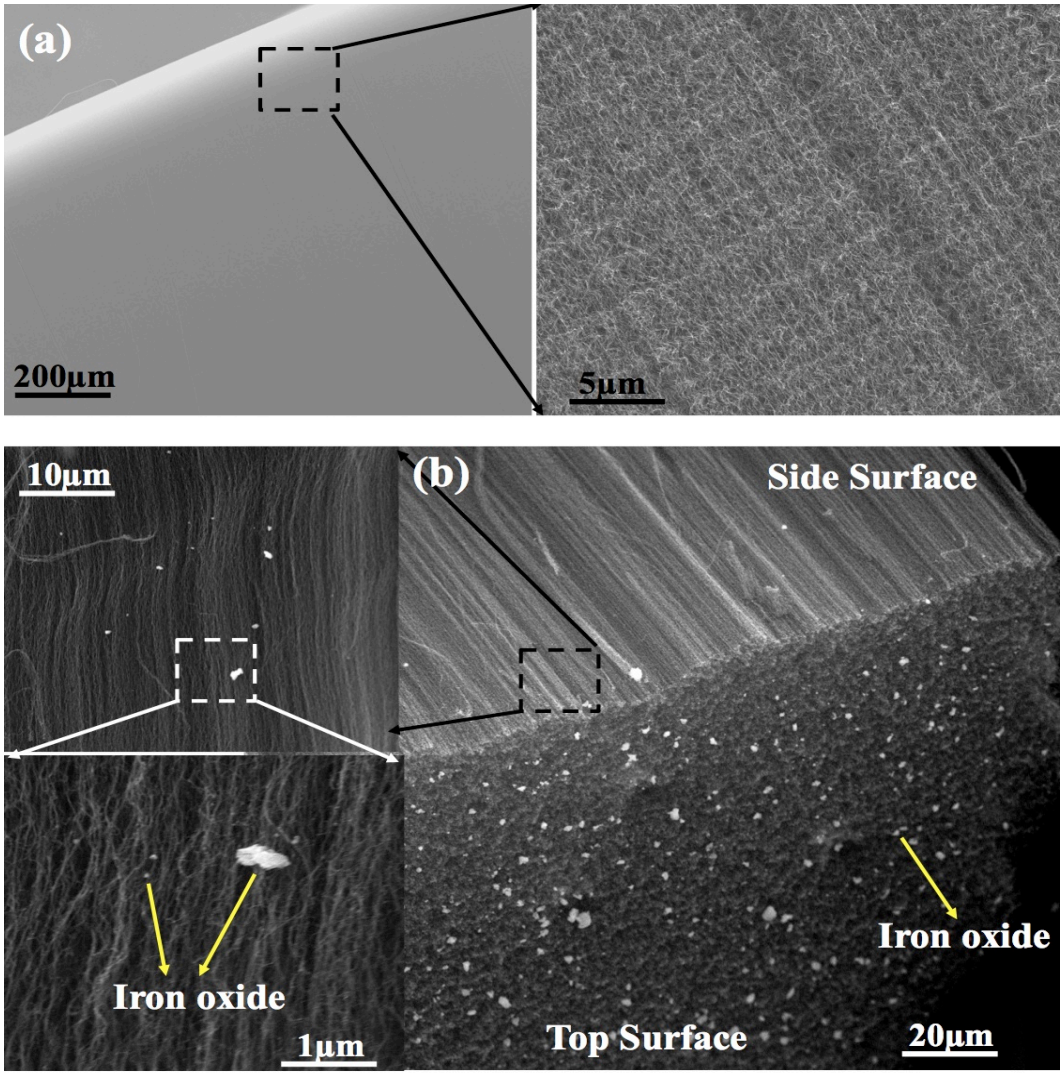

***Figure 7.2 (a)** SEM image of the CNTs grown on Si before the iron oxide (Fe_34_3) infiltration. (b) SEM image of top and side surface of the CNT forest at different magnification after the infiltration of (Fe_3O_4)*

The images at three different magnifications show the distribution of submicron size particle across the top surface. The higher magnification images of the subsurface shows infiltration of iron oxide of different size into the CNT array up to a certain depth. The combination of the SEM images in different magnification in tilted angle shows both

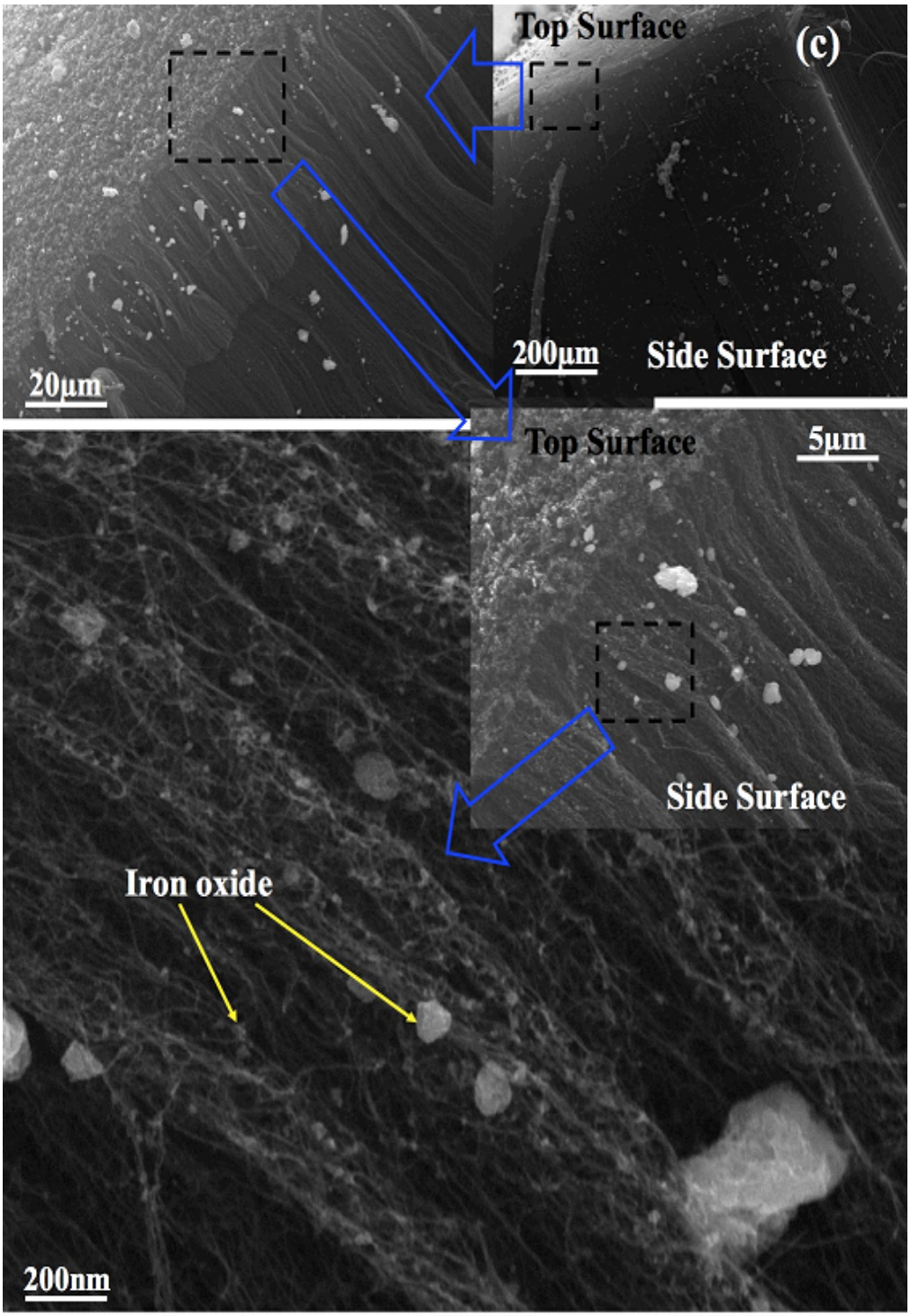

Figure 7.2 (c) SEM image of the sectional CNT (after being sliced to find out the amount of infiltration) at different magnification. The infiltration of Fe_3O_4particle through the CNT forest (into the array) is clearly observed. Also there is agglomeration of the particles as the amount of infiltration increases by the effect of the magnet.

the top and side view of the CNT forest infiltrated with iron oxide. It is very clear from the Figure 7.2 (c) that the size of the nanoparticle increases as the amount of nanoparticle into the CNT forest is increased. This is mainly because of the agglomeration of the infiltrated particle. Thus the particles collect to form a bigger particle (shown by white arrow in Figure 7.2 (c)).

Figure 7.2(d) shows the TEM observation of the MWCNTs in two different magnifications with iron particle trapped between them. The CNTs are found to have 4-6 graphitic layers. Higher magnification images shows that the particles are around 10-15 nm in size. The SAD of the particles confirm that these particles are in the FCC plane of Fe_3O_4.

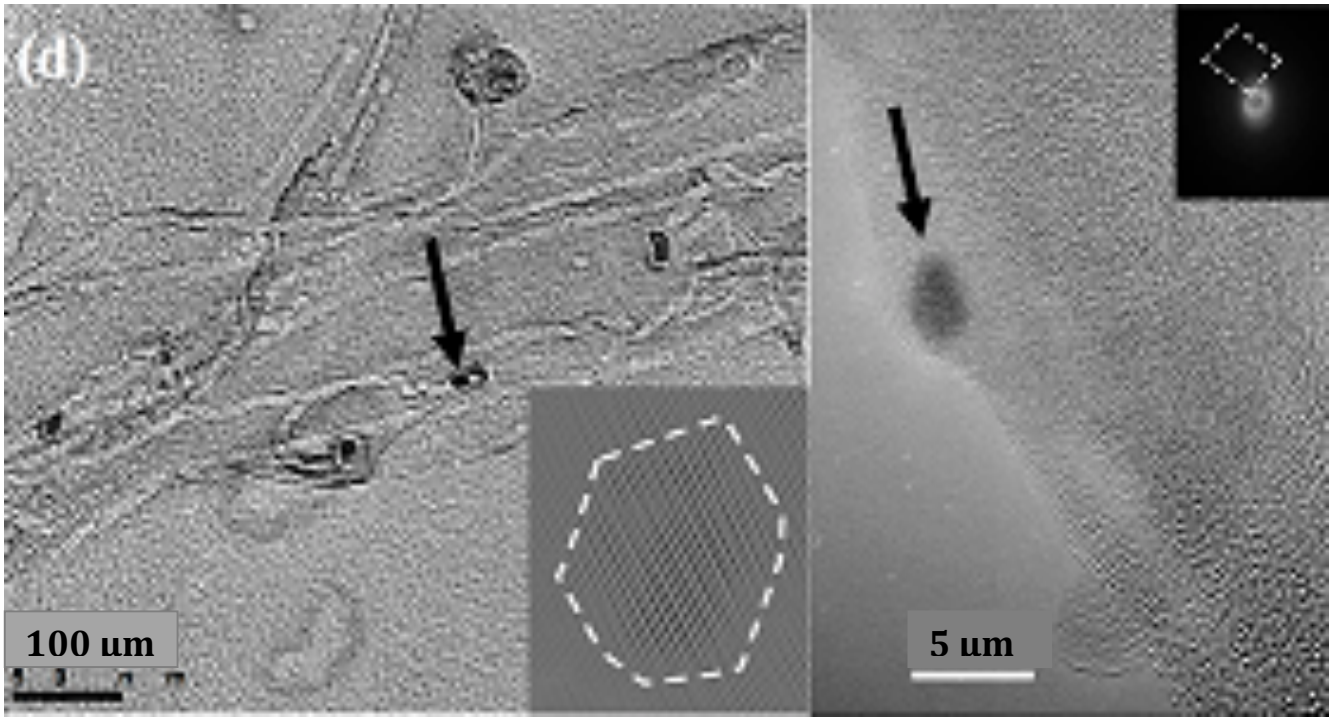

Figure 7.2 (d) TEM image showing the Fe_3O_4 between the CNTs

The quality of CNTs are further characterized using Raman spectroscopy (Figure 7.3) which clearly reveals the G and D band along with G' and D' bands.

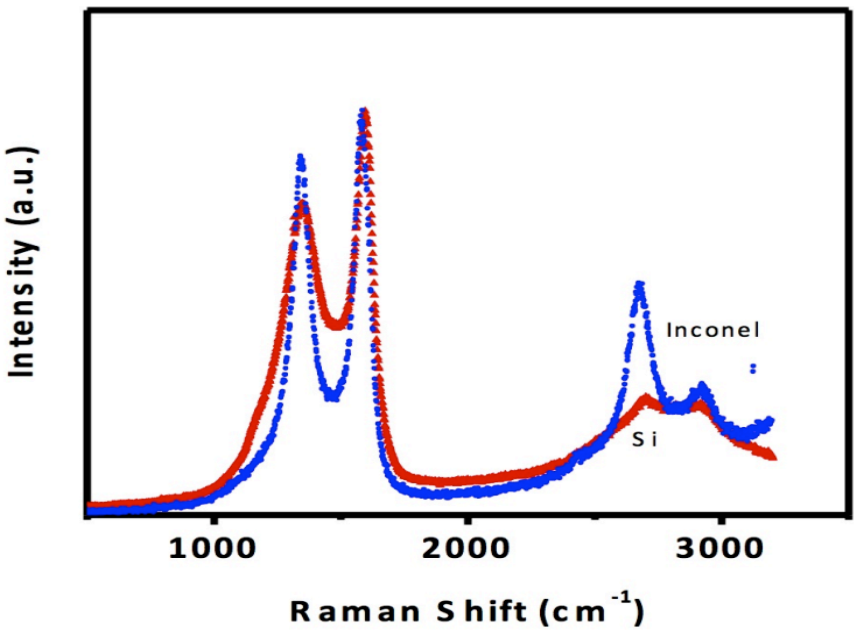

Figure 7.3 Raman spectra showing 3 distinct peaks [dis-order peak D, graphitic peak G and 2D peak for Si and Inconel after Fe_3O_4 infiltration

7.4.3 Field emission characteristics

Figure 7.4 (a & (b) shows the field emission characteristics of the CNTs grown on Si and Inconel both with and without iron nanoparticle infiltration. After the iron oxide infiltration, the turn on field for the sample grown on Si and Inconel was 0.18 V/µm and 0.2 V/µm respectively and the threshold field for the samples grown on Si and Inconel was 0.24 V/µm and 0.3 V/µm respectively. This value is very low when compared to the results we obtained in our earlier experiment without the iron infiltration (E_{to} was 0.8 V/µm for Si and 1.2 V/µm for Inconel and E_{th} was 2.6 V/µm and 2 V/µm for Si and Inconel respectively). This can be explained as

follows: First, the technique of infiltration of Fe nanoparticle, results in considerable reduction in the screening effect between the adjacent CNTs. Although the sharp tips and high aspect ratio are of great advantage for the CNTs to be used as good emitters, the screening effect from the neighboring CNTs compensates these advantages. So in order to use them in field emission devices, it is very important to reduce the screening.

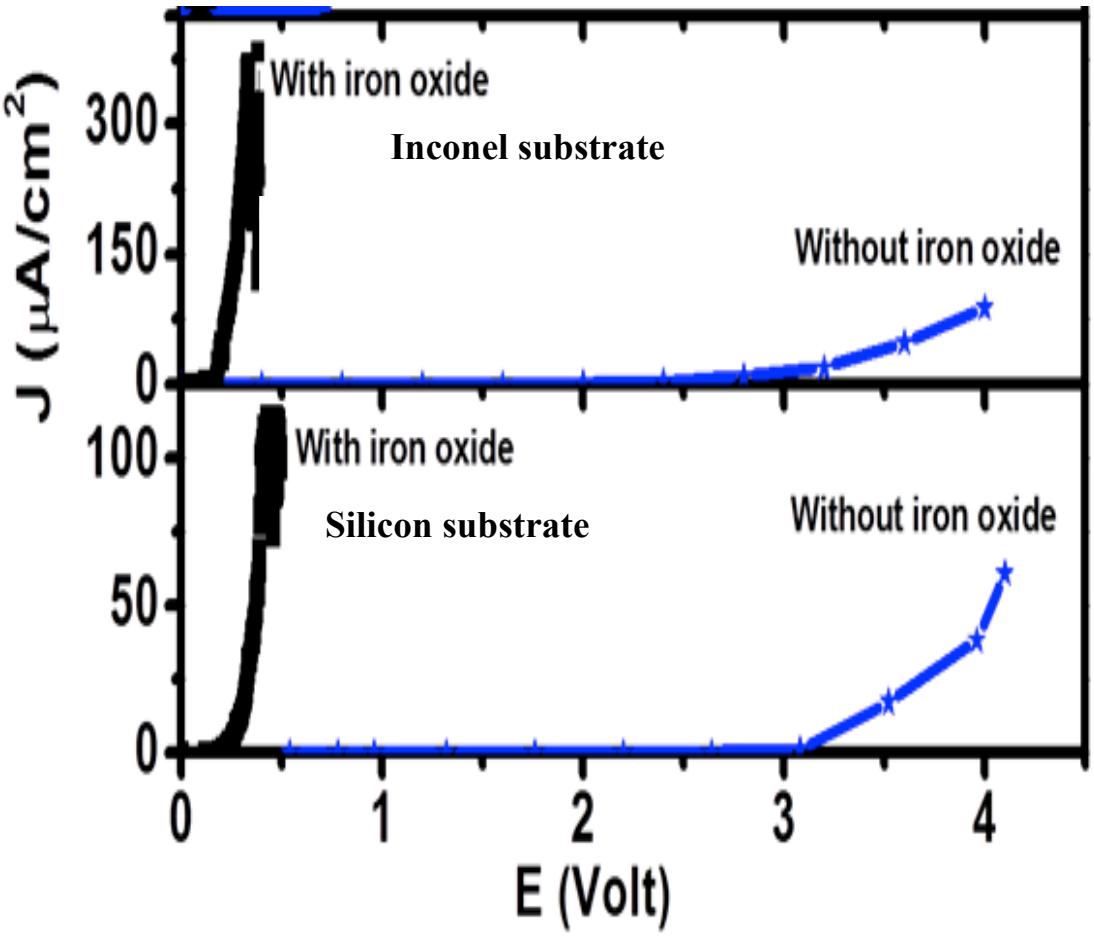

Figure 7.4 (a) & (b) J-E curve taken before and after Fe_3O_4 infiltration on Si and Inconel substrate respectively.

7.4.4 Effect of screening effect

In our experiment, the infiltrated Fe nanoparticle has certainly reduced the screening effect between the adjacent CNTs without any lithography based patterning because of the trapped iron nanoparticle inside the CNT forest. This is in accordance with the results obtained by Pandey et. al.[37]. They have suggested that the presence of $SrTiO_3$ in between the CNTs reduced the screening effect due to the high dielectric constant of $SrTiO_3$. Our CNT forest is now partially filled with Fe_3O_4 nanoparticle, which has a high dielectric constant (k=14 .2) as compared to those without any nanoparticle and filled with air (k=1).

7.4.5 Reduction of barrier 1 and 2

Secondly, as explained in the earlier chapters, it is well known that the electrons have to cross two barriers during the field emission; barrier 1 between the substrate and the CNT and barrier 2 between the CNT into the vacuum. The iron oxide nanoparticle (Fe_3O_4) has reduced these barriers because of its good electrical conductivity.

7.4.6 After Field Emission

Even after the field emission experiment, the iron nanoparticles were found to be inside the CNT forest, which was verified, by the SEM and the TEM images taken after the field emission experiment (Figure 7.5). This proves the fact that once the particles are infiltrated into the CNT forest, they are not disturbed by any physical changes (like tilting or inverting the CNT forest) even though there is no chemical process involved for the infiltration of these nanoparticle into the CNT forest.

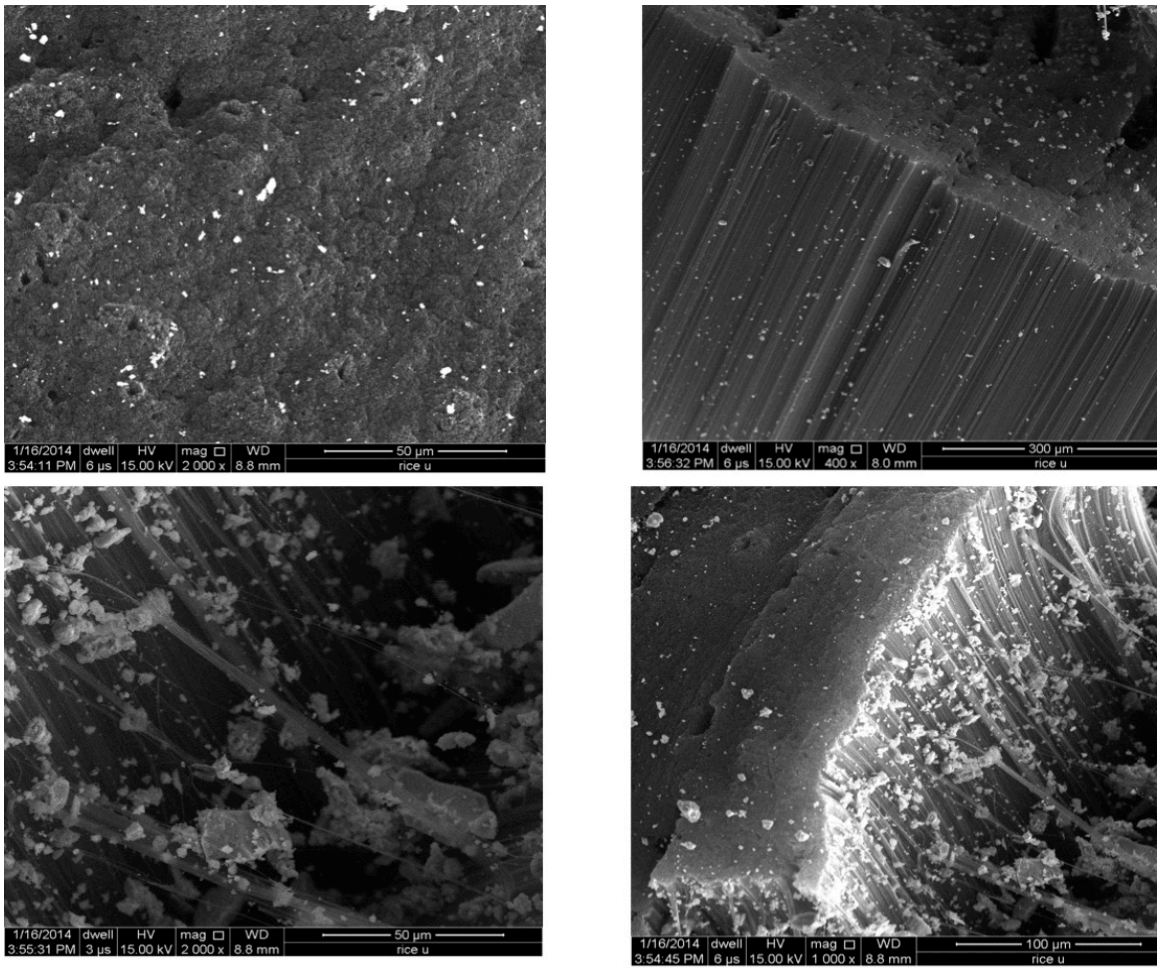

Figure 7.5 SEM image of the CNTs with Fe_3O_4 particles inside after the field emission

It is observed that the field emission properties of the CNTs with the iron nanoparticle qualitatively follow the conventional Fowler–Nordhein (F–N) theory. According to the F–N equation, the emission current density is J is given by

$$J = A(\beta E)^2 \exp\left(\frac{B\Phi^{\frac{3}{2}}}{\beta E}\right)$$

where J is the field emission current density of the cathodes, A and B are constants, E is the electric field applied between the cathode and the anode, β is the field enhancement factor, and Φ is the work function of the CNTs with iron oxide. The enhancement factor can be calculated from the slope of the F-N curve using the relation,

$$\beta = \frac{B\Phi^{\frac{3}{2}}d}{slope}$$

Where B =6.83 x 107 eV-3/2 Vcm^{-1} and d is the distance between the cathode and the anode. According to the above equation, it is clear that the current density depends on the work function and the field enhancement factor.

7.4.7 Enhancement factor increase by one order

Generally, we take the work function of CNTs as that of graphite (5eV). Since in our case the emission is from CNT/Fe_3O_4, as predicted by Zheng et. al. [38] , the work function is taken as 10.5 eV. Though the work function of CNT/Fe_3O_4 is higher than that of CNTs, substituting these values in the second equation for beta, gives us very high enhancement factor [35,39.40] which are listed in Table 7.1. From the table it is very clear that with iron oxide infiltration the enhancement factor for CNTs grown on Inconel substrate increases by one order and those on the Si grown CNTs increases by two order of magnitude. This can be attributed to the good electrical conductivity of Fe_3O_4 and reduction in the contact resistance between the CNTs and the substrate.

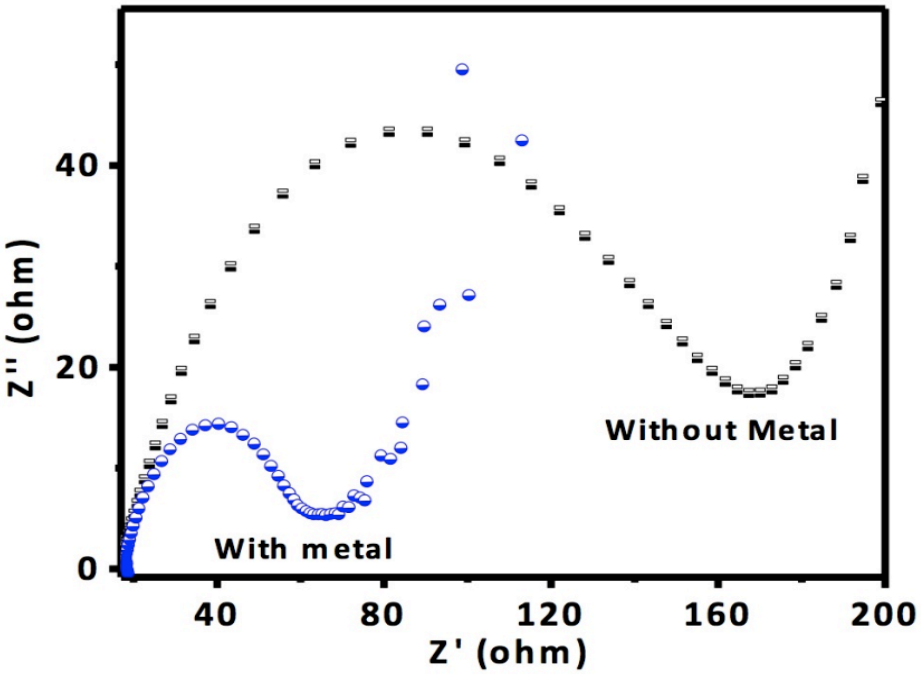

Figure 7.6 Nyquist plot of EIS spectra collected from the electrochemical lithium half cell of MWCNTs grown on Si before and after Fe_3O_4 infiltration.

7.4.8 Contact resistance measurement

Figure 7.6 shows the EIS plot of the contact resistance between the CNT and the substrate before and after the infiltration of Fe_3O_4 and the values are given in Table 7.2. Similar to the work of Chen et.al. [41] and Lim et. al. [42] the introduction of metal particles to decorate the CNTs increases the number of vacancies in the d orbital and reduce the contact resistance of each CNT. Now it is important to understand the method of penetration of these nanoparticles into the CNT forest.

Table 7.1

Material	E_{to} (V/µn)	E_{th} (V/µn)	Enhancement factor (β)
Si	0.8	2.6	4041
Inconel	1.2	2	1.5×10^4
Si/ Fe_3O_4	0.18	0.24	3×10^5
Inconel/ Fe_3O_4	0.2	0.3	1×10^5

Table 7.2

Material	Contact resistance (Ohms/cm^2) Before infiltration	After infiltration (Ohms/cm^2)
Si	258.85	147
Inconel	89.2	52

7.4.9 Confocal Microscopy

Figure 7.7 shows the confocal microscopy study at different time. We caped the iron oxide with florescent dye and observe in confocal microscope. The thin CNT bundle was kept near the iron oxide colloidal while the magnet is kept behind the forest. After five min we observed a splitting of CNT forest and the particles are getting inside the CNT array . Red color particles with dye were observed in CNT forest.

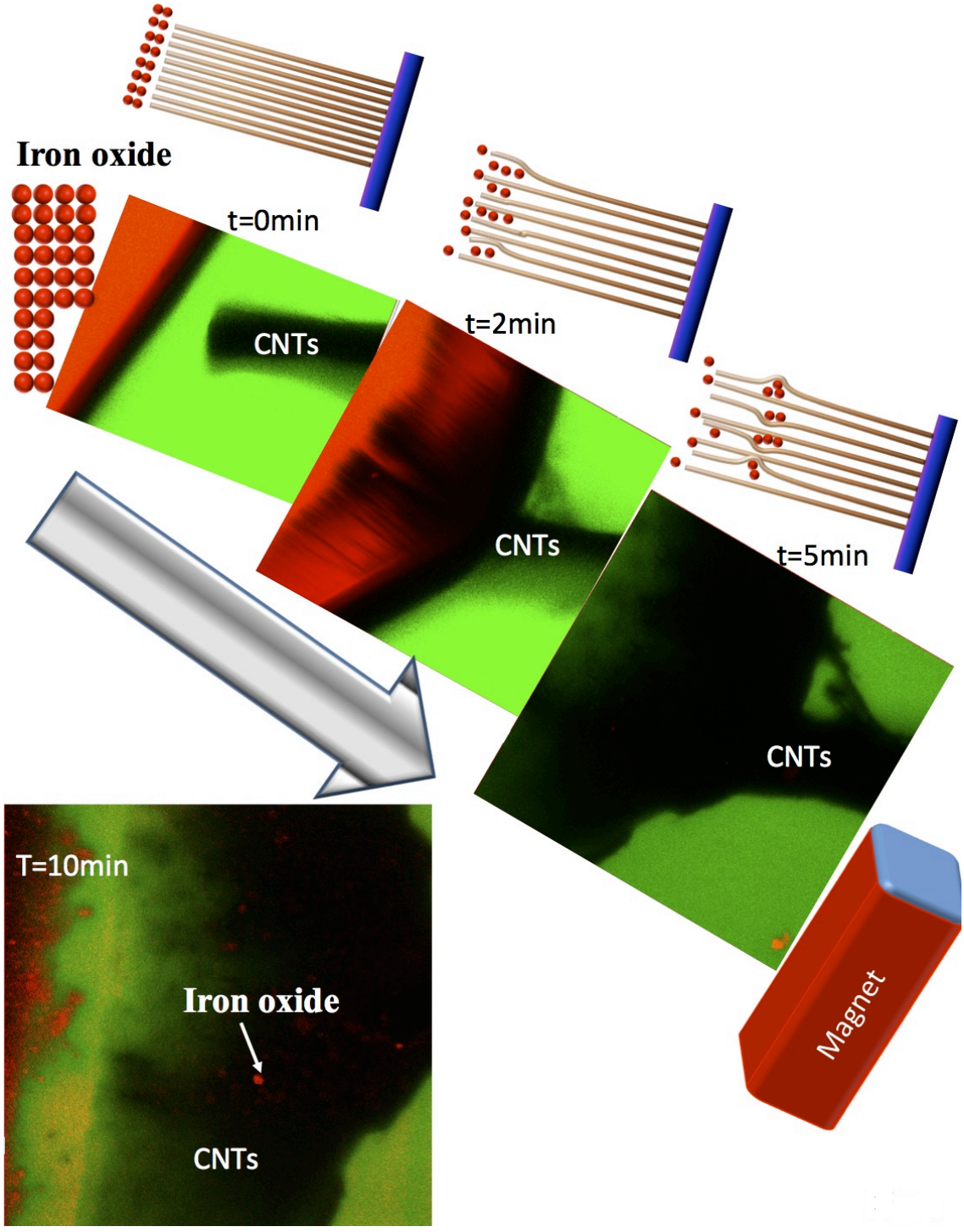

Figure 7.7 Confocal microscopy study at different times

A schematic of the process are shown along with the experimental observation. The highly dense forest getting filled with nanoparticles without destruction in the shape of the CNT forest can be explained with help of mechanical properties of CNTs. The force required to bend the CNT of extreme high elastic modulus decreases with an increase of height. As in our case the height of CNT forest are about 1cm, the stress required to bend such CNTs is less. In our case, the CNTs bend and make the particle enter into the array due to high elastic modulus and they recover back to original shape so that the particles are trapped inside the forest.

7.5 Conclusion

This work demonstrated that Fe_3O_4 nanoparticles can be infiltrated into the CNT forest using a magnet without destructing the physical structure of the 3D CNT forest. Drastic reduction of screening effect due to Fe_3O_4 nanoparticles resulted in ultra low turn on (0.1 V/μ) and threshold voltage (0.2 V/μ) of these nanostructures. There was two orders of magnitude increase in the enhancement factor making them a potential candidate for many micro electronic device applications. With certain refined parameters, we can focus on better emission current density from these nanostructures.

7.6 References

1. M. M. J. Treacy, T. W. Ebbesen, J. M. Gibson, Nature 1996, 381, 678.
2. E. W. Wong, Science 1997, 277, 1971.
3. T. W. Ebbesen, H. J. Lezec, H. Hiura, J. W. Bennett, H. F. Ghaemi, T. Thio, Nature 1996, 382, 54.
4. H. Dai, J. H. Hafner, A. G. Rinzler, D. T. Colbert, R. E. Smalley, Nature 1996, 384, 147.
5. H. Tanaka, S. Akita, L. Pan, Y. Nakayama, Jpn. J. Appl. Phys. 2004, 43, 864.
6. M. S. Fuhrer, Science 2000, 288, 494.
7. H. W. C. Postma, Science 2001, 293, 76.
8. P. G. Collins, Science 2001, 292, 706.
9. Dekker Encyclopedia of Nanoscience and Nanotechnology, M. Dekker, New York, 2004.
10. J. Bao, Q. Zhou, J. Hong, Z. Xu, Appl. Phys. Lett. 2002, 81, 4592.
11. B. K. Pradhan, T. Toba, T. Kyotani, A. Tomita, Chem. Mater. 1998, 10, 2510.
12. R. Kozhuharova, M. Ritschel, D. Elefant, A. Graff, A. Leonhardt, I. Mönch, T. Mühl, S. Groudeva-Zotova, C. M. Schneider, Appl. Surf. Sci. 2004, 238, 355.
13. W. Chen, X. Pan, M.-G. Willinger, D. S. Su, X. Bao, J. Am. Chem. Soc. 2006, 128, 3136.
14. J. Li, S. Tang, L. Lu, H. C. Zeng, J. Am. Chem. Soc. 2007, 129, 9401.
15. D. R. Kauffman, D. C. Sorescu, D. P. Schofield, B. L. Allen, K. D. Jordan, A. Star, Nano Lett. 2010, 10, 958.

16. K. Jiang, A. Eitan, L. S. Schadler, P. M. Ajayan, R. W. Siegel, N. Grobert, M. Mayne, M. Reyes-Reyes, H. Terrones, M. Terrones, Nano Lett. 2003, 3, 275.
17. J. Kong, M. G. Chapline, H. Dai, Adv. Mater. 2001, 13, 1384.
18. L. Fu, Z. Liu, Y. Liu, B. Han, P. Hu, L. Cao, D. Zhu, Adv. Mater. 2005, 17, 217.
19. H. S. Shin, Y. S. Jang, Y. Lee, Y. Jung, S. B. Kim, H. C. Choi, Adv. Mater. 2007, 19, 2873.
20. L. Jiang, L. Gao, Carbon 2003, 41, 2923.
21. B. He, W. Sun, M. Wang, Z. Shen, Mater. Chem. Phys. 2006, 95, 202.
22. Y. Zhang, N. W. Franklin, R. J. Chen, H. Dai, Chem. Phys. Lett. 2000, 331, 35.
23. R. Lv, F. Kang, D. Cai, C. Wang, J. Gu, K. Wang, D. Wu, J. Phys. Chem. Solids 2008, 69, 1213.
24. Y. Zhu, H. I. Elim, Y.-L. Foo, T. Yu, Y. Liu, W. Ji, J.-Y. Lee, Z. Shen, A. T. S. Wee, J. T. L. Thong, C. H. Sow, Adv. Mater. 2006, 18, 587.
25. B. Liu, J. Y. Lee, J. Phys. Chem. B 2005, 109, 23783.
26. B. Yoon, C. M. Wai, J. Am. Chem. Soc. 2005, 127, 17174.
27. H.-S. Kim, H. Lee, K.-S. Han, J.-H. Kim, M.-S. Song, M.-S. Park, J.-Y. Lee, J.-K. Kang, J. Phys. Chem. B 2005, 109, 8983.
28. S. Qu, J. Wang, J. Kong, P. Yang, G. Chen, Talanta 2007, 71, 1096.
29. Q. Liu, Z.-G. Chen, B. Liu, W. Ren, F. Li, H. Cong, H.-M. Cheng, Carbon 2008, 46, 1892.
30. L. Jiang, L. Gao, Chem. Mater. 2003, 15, 2848.
31. Z. Sun, Z. Liu, Y. Wang, B. Han, J. Du, J. Zhang, J. Mater. Chem. 2005, 15, 4497.
32. J. Wan, W. Cai, J. Feng, X. Meng, E. Liu, J. Mater. Chem. 2007, 17, 1188.

33. D. G. Larrude, P. Ayala, M. E. H. Maia da Costa, F. L. Freire, J. Nanomater. 2012, 2012,
34. H. He, C. Gao, J. Nanomater. 2011, 2011, 1.
35. S. Sridhar, L. Ge, C. S. Tiwary, A. C. Hart, S. Ozden, K. Kalaga, S. Lei, S. V. Sridhar, R. K. Sinha, H. Harsh, K. Kordas, P. M. Ajayan, R. Vajtai, ACS Appl. Mater. Interfaces 2014, 140113152340002.
36. T. N. Narayanan, A. P. Reena Mary, P. K. Anas Swalih, D. Sakthi Kumar, D. Makarov, M. Albrecht, J. Puthumana, A. Anas, M. R. Anantharaman, J. Nanosci. Nanotechnol. 2011, 11, 1958.
37. Pandey, A. Prasad, J. P. Moscatello, M. Engelhard, C. Wang, Y. K. Yap, ACS Nano 2013, 7, 117.
38. L. Zheng, L. Hu, F. Yang, T. Guo, J. Semicond. 2011, 32, 126001.
39. Y. M. Chen, C. A. Chen, Y. S. Huang, K. Y. Lee, K. K. Tiong, Nanotechnology 2010, 21, 035702.
40. X. Xiao, Y. Ye, L. Zheng, T. Guo, J. Semicond. 2012, 33, 053004.
41. Y. Chen, H. Jiang, D. Li, H. Song, Z. Li, X. Sun, G. Miao, H. Zhao, Nanoscale Res. Lett. 2011, 6, 537.
42. S. C. Lim, J. H. Jang, D. J. Bae, G. H. Han, S. Lee, I.-S. Yeo, Y. H. Lee, Appl. Phys. Lett. 2009, 95, 264103.

Applied Surface Science 256 (2010) 3563–3566

Contents lists available at ScienceDirect

Applied Surface Science

journal homepage: www.elsevier.com/locate/apsusc

Titanium buffer layer for improved field emission of CNT based cold cathode

S. Srividya [a,*], S. Gautam [b], P. Jha [b], P. Kumar [b], A. Kumar [b], U.S. Ojha [b], J.S.B.S. Rawat [b], S. Pal [b], P.K. Chaudhary [b], Harsh [b], R.K. Sinha [a]

[a] Department of Applied Physics, Delhi College of Engineering (Faculty of Technology, University of Delhi), Bawana Road, Delhi – 110042, India
[b] Solid State Physics Laboratory, Lucknow Road, Timarpur, Delhi – 110054, India

ARTICLE INFO

Article history:
Received 9 July 2009
Received in revised form 2 December 2009
Accepted 23 December 2009
Available online 4 January 2010

Keywords:
Carbon nanotube (CNT)
Chemical vapor deposition (CVD)
Photolithography
Field emission

ABSTRACT

Carbon nanotube (CNT) based cold cathodes are considered to be the most promising material for fabrication of next generation high-performance flat panel displays and vacuum microelectronic devices. Adhesion of CNTs with the substrate and the contact resistance between them are two of the important issues to be addressed in CNT based field emission (FE) devices. Here in this work, a buffer layer of titanium (Ti) is deposited prior to the catalyst deposition and the growth was carried out using chemical vapor deposition (CVD) technique. There was significant increase in emission current density from 10 mA/cm^2 to 30 mA/cm^2 at the field of 4 V/μm by the use of titanium buffer layer due to much less dense growth of CNTs of smaller diameter. Field emission results suggest that the adhesion of the CNTs to the substrate has improved. The titanium buffer layer has also lowered the contact resistance between the CNTs and the substrate because of which a stable emission of 30 mA for a longer duration was obtained.

1. Introduction

Carbon nanotubes (CNTs) have attracted significant attention since their discovery by Iijima in 1991 [1]. CNTs, because of its unique physical and chemical properties, have been considered as a potential material for various applications, such as electronic devices [2], flat panel displays [3], scanning probes [4], etc. Flat panel displays fabricated using CNTs as electron emitters have been recognized as one of the most promising display technologies for the future [5]. Fowler–Nordheim tunneling was published in 1928 [6,7]. Many materials and device structures have been developed to realize efficient field emitters [8] since then. Due to the high aspect ratio, low work function, high mechanical strength and high thermal conductivity, CNTs are considered to be a wonderful electron emitting sources in field emission displays. However, some critical issues such as screening effect, adhesion of CNTs with the substrate, reliability, high contact resistance and stability have to be addressed while using CNTs as electron emitters in field emission applications. The adhesion of CNTs with the substrate has to be increased and contact resistance between the CNTs and the substrate has to be lowered for improved device performance.

To synthesize CNTs more effectively, several techniques such as the arc discharge method, laser ablation, chemical vapor deposition (CVD) and plasma enhanced chemical vapor deposition (PECVD) have been developed so far [9,10]. In the CVD technique when using a Si substrate, the formation of metal–silicides as a result of the preheating, will poison the synthesis process. Buffer layers using Al, Ti or SiO_2 have been previously used in order to prevent the formation of metal–silicides [11]. It has been reported that the supporting layer can tune the shapes and curvatures of the catalyst particles [12]. Kyung et al., in their work, used Cr, W, and Ti as buffer layer during CNT growth and obtained a maximum current density of 0.78 mA/cm^2 at 7 V/μm [13]. Chuang et al., in their work reported that the carbon atoms for CNT growth were supplied from Ni catalyst particles at an early stage and from Ti interlayer at a later stage in the growth process [14]. Huang et al. obtained well-aligned CNT growth with the use of Ti buffer layer [15]. 1 mA/cm^2 current density was obtained at the field of 3.5 V/μm by Sato et al. [16]. In all these works, the current density obtained was not that good though there was improvement of adhesion of CNT with the substrate.

In this paper, we report the efforts made to increase the CNT tip density and improve the adhesion of CNTs with the substrate so as to make the CNT based cold cathodes suitable for high power microwave vacuum devices application, which require high current densities. To address the adhesion issue, substrate heating because of high contact resistance and shielding effect, we deposited titanium buffer layer on silicon substrate since it has been very recently reported that the field emission properties of electrophoretic deposition (EPD), carbon nanotubes (CNTs) film have been improved by depositing CNTs onto the titanium (Ti)-coated Si substrate [17]. The CNTs were grown using CVD

* Corresponding author. Tel.: +91 11 27871017.
E-mail address: vidya_shridar@yahoo.com (S. Srividya).

0169-4332/$ – see front matter © 2009 Elsevier B.V. All rights reserved.
doi:10.1016/j.apsusc.2009.12.155

technique [18]. Scanning Electron Microscopy (SEM) was employed to study the effect of titanium buffer layer towards the adhesion. The adhesion between CNTs and substrate was greatly improved because of the strong binding between titanium and the substrate. We presume that this will prevent the CNTs from pulling off from the substrate by the strong electro-static force at high electric field. We were able to achieve emission current density of 30 mA/cm^2 at a field of 4 V/μm. This suggests great promise for achieving higher current densities at practical electric fields.

2. Experimental procedure

N-type silicon ⟨1 0 0⟩ wafers with a low resistivity of 4–6 Ωcm were used as substrates. A 10 μm × 10 μm square openings with 10 μm interspace was formed on the silicon wafers by photolithography process. After the formation of an array, 30-nm-thick Ti was deposited by sputtering as a buffer layer and a thin layer of iron (Fe) was deposited subsequently as a catalyst. Photoresist was removed by a lift-off process. Then, the sample was loaded into the thermal-CVD furnace to grow carbon nanotubes. H_2, NH_3 and C_2H_2 were used as carrier and source gases. Growth temperature was kept around 850 °C and typical growth time was 10 min. SEM characterization was done using model JEOL JSM 840.

In the field-emission measurements, silicon substrate with CNTs was used as cathode and stainless steel plate as anode. The entire sample assembly was kept inside a vacuum chamber evacuated to vacuum better than 1×10^{-6} Torr. The cathode and anode were kept 600 μm apart, using micrometer screw gauge arrangement and a suitable DC voltage was applied across the cathode and anode using a high voltage power supply.

3. Results and discussion

Fig. 1(a) and (b) are the SEM images of the CNTs grown without and with the Ti buffer layer (30 nm in thickness) under the Fe catalyst layer respectively. From the morphology observed, it can be seen that individual CNT bundles grew almost vertically via a self-supporting mechanism, due to the extremely high density of the CNTs. The buffer layer has affected the CNT growth density. It can be seen that the density of CNTs grown with Ti buffer is less when compared with the CNTs grown without Ti buffer. Probably, when grown without Ti buffer, number of catalyst particle sites available for CNT growth will be more when compared with the sample grown with Ti buffer. This is because small portion of Fe particles will be reacting with Ti for improving the adhesion and so the number of Fe particles available for the growth of CNTs will be comparatively reduced resulting in the reduction of CNT tube density. SEM image shown in Fig. 1(a) clearly shows that the adhesion of CNTs with the substrate is not good when grown without the Ti buffer. On the other hand, the use of titanium buffer has improved the adhesion as seen in Fig. 1(b).

From the *J–E* curve (Fig. 2), we observe that there is an increase in the current density in the sample with the titanium buffer layer. Field-emission measurement data of the CNT array shows that the sample grown with the Ti buffer layer gave a better field emission result. The field emission current density increased from 10 mA/cm^2 to 30 mA/cm^2 at an electric field of 4 V/μm. This observed increase in the emission current density in case of the sample with Ti buffer layer could be attributed to much less dense growth of CNTs of smaller diameter. Both these factors are expected to improve the geometrical field enhancement factor by way of increased aspect ratio and reduced shielding effect of one emitter (CNT) over other. The increased geometrical field enhancement factor ultimately results in lowering of the threshold field and improved field emission current. This increase in current density

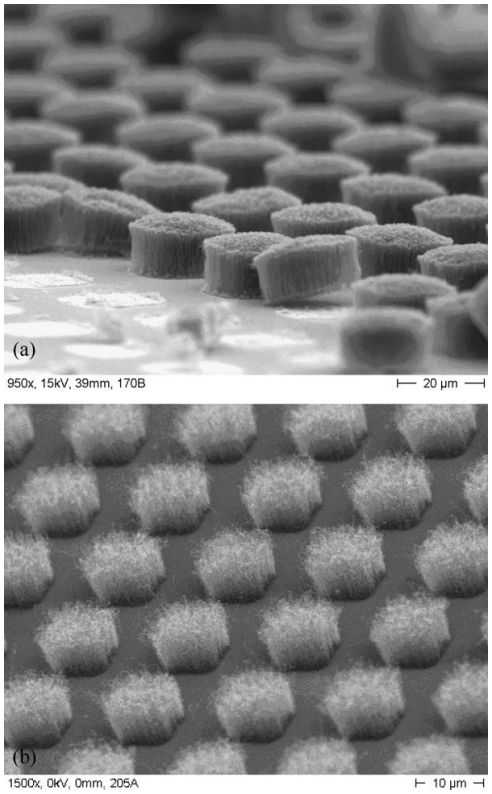

Fig. 1. (a) SEM images of CNTs grown without Ti buffer. (b) SEM images of CNTs grown with Ti buffer.

and field emission stability can also be attributed to the increase in the number of available emitters due to their strong adhesion with the substrate to support high field in addition to their difference in enhancement factor due to the change in the morphology of the CNT growth. The mechanism of Ti buffer layer in improving the adhesion can be explained as under:

For the sample without a thin Ti buffer layer, part of carbon nanotubes could be pulled off from the substrate due to poor adhesion during field emission experiment. This shows a mechanical destruction during the electrical breakdown. The paper of Okai et al. [19] suggests that a strong static electric force may be the main reason of the electrical breakdown in field-emission measurements.

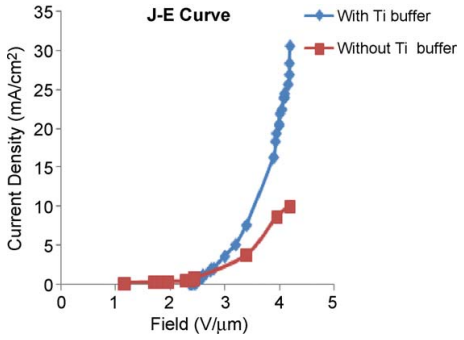

Fig. 2. *J–E* curves of CNTs with and without Ti buffer layer.

As the electric field between the anode and the cathode is increased, the dipole resulting from the concentration of electrons in the tips of carbon nanotubes will enhance the static electric force and pull the carbon nanotubes off from the substrate leading to an abrupt drop of emission current. This phenomenon is attributed to a poor adhesion between carbon nanotubes and the substrate. With a thin Ti buffer layer, there is no obvious electrical breakdown as the electric field is increased. This may be due to the better adhesion between catalytic nanoparticles and carbon nanotubes which could have resulted from the thin Ti buffer layer.

This could have been due to the following reasons; (i) the roots of carbon nanotubes bond strongly with the Ti layer underneath; (ii) the adhesion of the carbon nanotubes to the substrate is dramatically promoted because titanium has an excellent adhesion property to silicon and (iii) the titanium carbide could have formed which not only can reduce the effective work function, but also can protect the emitters from the attack of ionized molecules and thereby improving the field emission stability. Since in our lab it is not possible to perform scotch tape test to check adhesion, indirect way of exposure to higher field is adopted.

A rapid increase in the current is observed when the electric field is higher than 3 V/μm. When plotted in a Fowler–Nordheim representation (Fig. 3), two different regimes of emission are observed. The cathodes can reach currents of a few mA before showing degradation. When degradation of the cathode does occur, the field emission properties are not completely lost, but rather the voltage required to achieve a given current is merely increased. This suggests that either the emitting sites are not completely destroyed or they are replaced by other nanotubes in the film. The requirement for initial break-in of new cathodes and the hysteresis often observed in field emission data suggest a CNT reorganization within the film when an electric field is applied, giving the film a configuration more favorable for field emission. This reorganization is also interpreted as a cause of the robust behavior or strong adhesion of the cathodes.

In our earlier experiment [20], when the field was just raised above 5 V/μm, a fluctuation in vacuum reading was observed possibly due to substrate heating. It could happen if some sort of change in state had occurred either due to local evaporation [21], burning or melting of the CNTs or silicon [22] or both. The debris of CNTs was found all over the substrate. The destructive phenomenon in our earlier experiment can also be due to Joule heating. Bonard et al. [23] have reported that at high emission current density, a high contact resistance caused by the bad interface between the CNTs and the substrate will result in Joule heating and lead to local evaporation of CNTs. The sample with the titanium buffer layer might have reduced the contact resistance between CNTs and the substrate. This may in turn suppress the Joule heating. During FE measurements at high electric fields, vacuum remained moreover stable suggesting reduced substrate heating

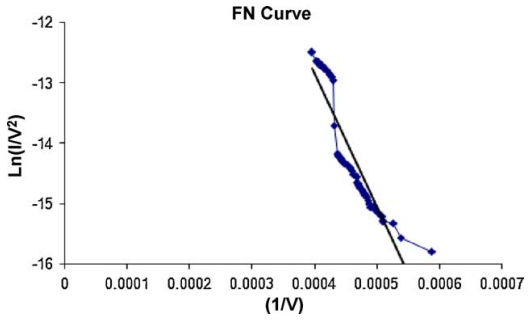

Fig. 3. *F–N* curve of CNTs grown with Ti buffer layer.

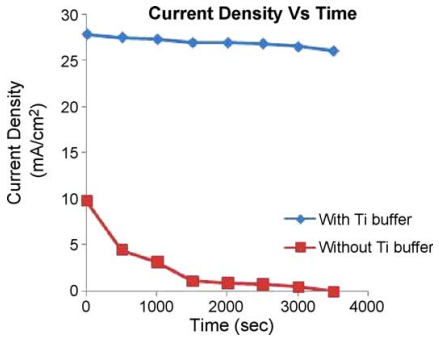

Fig. 4. Time trace of current density at a fixed field of 4 V/μm.

due to reduction in contact resistance. The emission current stability has also been examined and a typical time trace of the emission current density at a fixed field of 4 V/μm is shown in Fig. 4. It was found that there was stable emission for more than 50 min due to Ti buffer layer.

Efforts are being made to optimize the thickness of Ti buffer layer to get an emission current density of about 1 A/cm^2 at practical field. It was also observed that initially the emission current was a bit unstable which gets stabilized by conditioning the sample. The stability of the emission current was also found to depend upon the vacuum conditions during the measurement.

4. Conclusion

Using titanium buffer layer during CNT growth, the density of carbon nanotubes can be efficiently modified to promote the electrical characteristics of field emission. The field emission current density increased from 10 mA/cm^2 to 30 mA/cm^2 at electric field of 4 V/μm with the help of the buffer layer. Also better adhesion of CNTs with the substrate was achieved which in turn suppressed the mechanical destruction and prevented the emitters from the electrical breakdown. So, stable emission of electron was realized for a longer duration without vacuum degradation. With some refinement in the growth parameters, we can certainly increase the current density of the emitter to a considerable extent.

Acknowledgements

The authors wish to acknowledge the Silicon Group and Characterization Group of Solid State Physics Laboratory for carrying out photolithography SEM analysis respectively.

References

[1] S. Iijima, Nature (Lond.) 354 (1991) 56.
[2] R. Martel, et al. Appl. Phys. Lett. 73 (1998) 2447.
[3] H. Dai, N. Franklin, J. Han, Appl. Phys. Lett. 73 (1998) 1508.
[4] H. Dai, J.H. Hafner, A.G. Rinzler, D.T. Colbert, R.E. Smalley, Nature (Lond.) 388 (1997) 756.
[5] K. Shibayama, M. Hiraki, Y. Saito, A. Hosong, Jpn. J. Appl. Phys., Part 1 42 (2003) 3698.
[6] R.H. Fowler, L. Nordheim, Proc. R. Soc. Lond., Ser. A 119 (1928) 173.
[7] T.E. Stern, B.S. Grossling, R.H. Fowler, Proc. R. Soc. Lond., Ser. A 124 (1929) 699.
[8] D. Temple, Mater. Sci. Eng., R. 24 (1999) 185.
[9] Y. Huh, J.Y. Lee, C.J. Lee, Jpn. J. Appl. Phys. 42 (2003) 7154.
[10] A.V. Melechko, V.I. Merkulov, T.E. McKnight, M.A. Guillorn, K.L. Klein, D.H. Lowndes, M.L. Simpson, J. Appl. Phys. 97 (2005) 041301.
[11] T. de los, F. Arcos, M.G. Vonau, V. Garnier, H.G. Thommen, P. Boyen, M. Oelhafen, D. Düggelin, R. Mathys, Guggenheim, Appl. Phys. Lett. 80 (2002) 2383–2385.
[12] Y. Wang, B. Li, P.S. Ho, Z. Yao, L. Shi, Appl. Phys. Lett 89 (2006) 183113.
[13] K.H. Park, J.H. Yim, S. Lee, K.H. Koh, Thin Solid Films 501 (2006) 233–237.
[14] Chuang, et al. Surf. Coat. Technol. 202 (2008) 2121–2125.

[15] Huang, et al. IVNC 2004 (2004) 34–35.
[16] H. Sato, et al. IVNC 2004 (2004) 210–211.
[17] Y. Qin, M. Hu, Appl. Surf. Sci. 255 (17) (2009) 7618S–7622S.
[18] P. Chaturvedi, S. Pal, Lamba, A.B. Dhaulakhandi, D.S. Rawal, M. Bal, Harsh, S.K. Agrawal, IWPSD Chennai (2003) 974.
[19] M. Okai, T. Fujieda, K. Hidaka, T. Muneyoshi, T. Yaguchi, Jpn. J. Appl. Phys., Part 1 44 (2005) 2051.
[20] P. Verma, S. Gautham, P. Kumar, P. Chaturvedi, J.S. Rawat, s. Pal, R. Chaubey, H.P. Harsh, P.K. Vyas, Bhatnagar, J. Vac. Sci. Technol. B 25 (2007) 1584.
[21] A.T. Sowers, B.L. Ward, S.L. English, R.J. Nemanish, J. Appl. Phys. 86 (1999) 3973.
[22] J.C. She, et al. Appl. Phys. Lett. 83 (2003) 2671.
[23] J.-M. Bonard, C. Klinke, Phys. Rev. B 67 (2003) 115406.

ACS APPLIED MATERIALS & INTERFACES

Research Article

www.acsami.org

Enhanced Field Emission Properties from CNT Arrays Synthesized on Inconel Superalloy

S. Sridhar,[†,‡] L. Ge,[‡] C. S. Tiwary,[‡,⊗] A. C. Hart,[‡] S. Ozden,[‡] K. Kalaga,[‡] S. Lei,[‡] S. V. Sridhar,[§] R. K. Sinha,[†] H. Harsh,[⊥] K. Kordas,[∥] P. M. Ajayan,[‡] and R. Vajtai*[,‡]

[†]Department of Applied Physics, Delhi Technological University (Formerly Delhi College of Engineering), Bawana Road, Delhi 110042, India

[‡]Department of Material Science and NanoEngineering, Rice University, Houston, Texas 77005, United States

[§]Department of Chemical and Biomolecular Engineering, Rice University, Houston, Texas 77005, United States

[⊥]Department of Physics, Jamia Millia Islamia, New Delhi 110025, India

[∥]Microelectronics and Materials Physics Laboratories, Department of Electrical Engineering, University of Oulu, P.O. Box 4500, FI-90014 Oulu, Finland

[⊗]Materials Engineering, Indian Institute of Science, Bangalore, Karnataka 560012, India

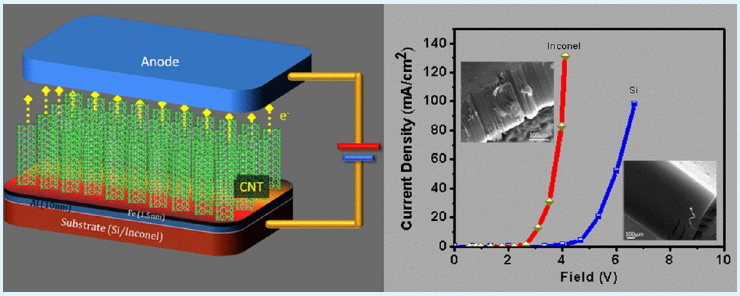

ABSTRACT: One of the most promising materials for fabricating cold cathodes for next generation high-performance flat panel devices is carbon nanotubes (CNTs). For this purpose, CNTs grown on metallic substrates are used to minimize contact resistance. In this report, we compare properties and field emission performance of CNTs grown via water assisted chemical vapor deposition using Inconel vs silicon (Si) substrates. Carbon nanotube forests grown on Inconel substrates are superior to the ones grown on silicon; low turn-on fields (~1.5 V/μm), high current operation (~100 mA/cm^2) and very high local field amplification factors (up to ~7300) were demonstrated, and these parameters are most beneficial for use in vacuum microelectronic applications.

KEYWORDS: *carbon nanotube, water assisted CVD, adhesion, field emission, ohmic contact*

INTRODUCTION

Since the reports made by Heer et al.[1] and Rinzer et al.,[2] on the field emission from films and individual multiwalled carbon nanotubes (MWCNTs), respectively, various experimental studies on the field emission of MWCNTs grown using various techniques on different substrates have been pursued.[3−15] Reliability and reproducibility are the biggest aspects needing improvement when using CNTs in field emission devices; electrical breakdown and current degradation are the two major limiting factors of the reliability of CNT based field emitters. The electrical breakdown is a sudden discharge caused by an avalanche of charged particles above a certain threshold field. The process is associated by the evaporation of electrode materials and/or surface adsorbed impurities as a consequence of electron bombardment of the anode, resistive heating of the sharp cathode or simple desorption of surface impurities so that a low pressure vapor forms in the proximity of the electrodes.[16] Above the threshold field, the vapor undergoes ionization and sparking, similar to that in ordinary low pressure gases, takes place.[17] On the other hand, the emission current degradation is a slow process that occurs below the threshold field. Heating by the emission current and subsequent evaporation of the electrode materials results in a gradual loss, structural collapse and deterioration of the cathode. Apart from thermal and electrical stability of the electrode materials, high quality robust electrical contacts that are interfacing the emitter back side are also vital for multiple reasons. First, the contact must be uniform along the entire interface to allow optimal, uniform

Received: November 8, 2013
Accepted: January 3, 2014
Published: January 13, 2014

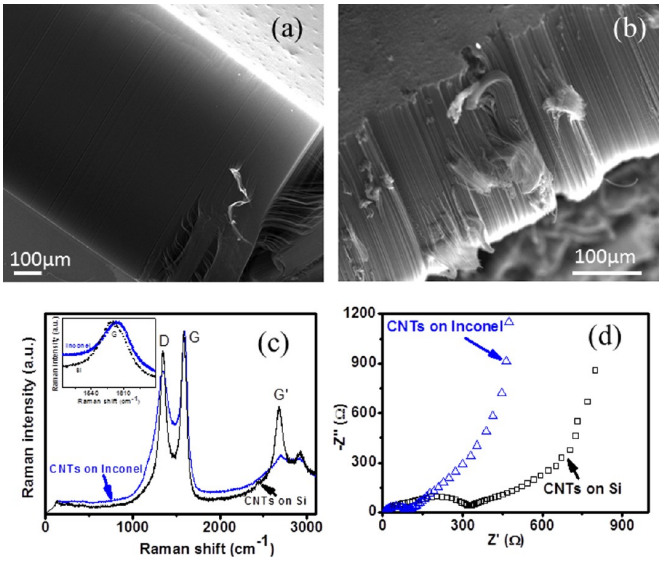

Figure 1. SEM images of CNT films grown on (a) Si and (b) Inconel substrates showing that the CNTs on Si are longer when compared with those on Inconel. (c) Raman spectra of films synthesized on the two substrates (the inset shows the shifted peak position of the G band) and (d) Nyquist plots of the films (on the substrates) measured by electrical impedance spectroscopy using electrochemical lithium half-cell of MWCNTs grown on silicon and Inconel as anodes.

current densities throughout the joint area. This is especially important for carbon nanotube forests, to ensure each nanotube is in direct electrical contact with the substrate with similar contact resistance all around at the interface eliminating the formation of hot spots. Second, good ohmic contacts at the CNT−substrate interface introduce only minor series resistances in the emitter circuit thus resulting in higher emission currents (when voltage regulated) or lower interfacial losses (when current regulated). Third, mechanical strength, or good adhesion, between the nanotube/catalyst and the substrate interface is also an important criterion to minimize problems related to delamination of the emitter material from the back side contact.[18−21]

The above list of requirements suggests two kinds of technical approaches that may offer feasible and reasonably simple solutions to meet the stringent thermal, mechanical and electrical boundary conditions. One solution is a solder transfer of CNT films to electrically conductive surfaces, which has been proven to be a robust and versatile method to obtain joints with excellent structural, thermal and electrical integrity.[22−27] The other, more feasible approach is the direct growth of CNTs on conductive surfaces. As demonstrated previously, growing CNTs on metal substrates or on alloys containing one of the common catalyst metals can result in CNT films of high footprint density, which is electrically advantageous.[28−30] For instance, Talapatra et al.[31] estimated an average total contact resistance of aligned CNTs on Inconel to be about 500 Ω, whereas measurements carried out on similar structures by Halonen et al.[32] showed the contact resistance is as low as ∼10 Ω (for a pattern footprint area of ∼0.4 cm^2). Although relatively low turn-on fields are observed for such devices, the maximum emission current densities reported were typically not higher than 10 mA/cm^2.[32−36] For CNTs to be used in field emission devices, it is not only essential to develop techniques to grow CNTs on conducting substrates but also to get good current density besides reducing the turn on and threshold voltages.

In this paper, we report the growth of CNTs on Inconel and Si substrates in water assisted CVD and compare their field emission behavior. CNTs grown on Inconel exhibited excellent field emission properties: the maximum current densities from the produced emitters were around 100 mA/cm^2. Although CNTs on Si substrates also yielded high initial current densities (>100 mA/cm^2), early arcing and rapid failure of the devices indicate their limited use in high current density applications. The results presented here may be adopted for CNT based cold cathodes suitable for high power microwave vacuum devices and also for long-lifetime low-power applications.

EXPERIMENTAL SECTION

Vertically aligned MWCNTs were synthesized using a water assisted CVD process on Si and Inconel 718 substrates coated previously with 10 nm Al buffer and 1.5 nm Fe catalyst layers using e-beam evaporation (as shown in Figure 1, inset). For CNT growth, the substrate is inserted into a quartz tube inside a furnace and initially purged with argon, then heated up to 775 °C under Ar/H_2 (15% H_2/balance argon). Once the growth temperature, Ar/H_2 is bubbled through water and the carbon source, ethylene, is flown into the reactor. The CNTs are grown for 30 min and, finally, the furnace is cooled under Ar.

Scanning electron microscopy (SEM, FEI Quanta 400 ESEM FEG) and transmission electron microscopy (JEOL 2100 F TEM) were used for sample characterization. Raman spectroscopy was performed using a Renishaw inVia Raman Microscope (laser wavelength of 514 nm). For the field-emission measurements, the silicon (Si) and Inconel substrates with CNTs were used as the cathode and ITO coated glass plate as the anode. The cathode and anode mounting stands are machine ground to ensure that they are perfectly parallel. The whole sample assembly was kept inside a vacuum chamber evacuated to at least 2×10^{-6} Torr, and the distance between the cathode and the

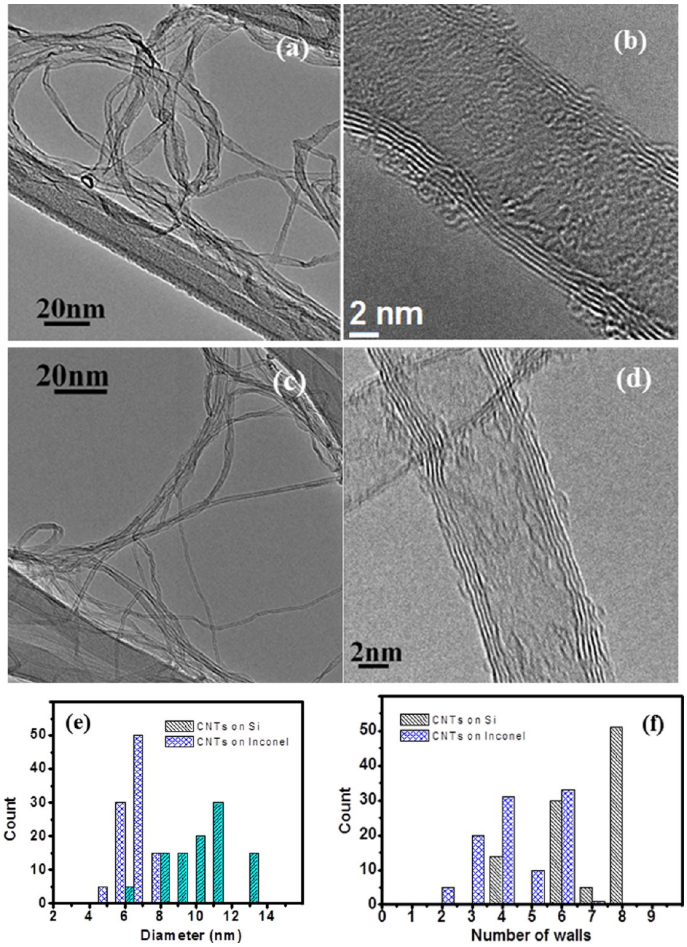

Figure 2. Transmission electron micrographs of CNTs grown (a), (b) on Si and (c), (d) on Inconel substrates. Panels (e) and (f) display the nanotube diameter and wall number distribution plots, respectively.

anode was maintained at 200 μm through a spring loaded micrometer gauge. The CNT sample is mounted on the cathode stand and I–V measurements are done using a Keithley 2410 instrument.

Electrical impedance spectroscopy (EIS) measurements were performed using a two electrode setup with the CNTs on the substrate as the working electrode and lithium metal as the counter/reference electrode. In this, 1 M $LiPF_6$ in 1:1 v/v mixture of ethylene carbonate (EC) and dimethyl carbonate (DMC) is used as the electrolyte and a glass microfiber filter membrane as the separator. The EIS measurements were conducted over 70 kHz to 10 mHz by applying a 10 mV dc bias.

RESULTS AND DISCUSSION

Figure 1a,b displays SEM images of the CNTs grown on Si and Inconel, respectively. The CNTs are vertically aligned via a self-supporting mechanism; according to scanning and transmission electron microscopy analyses, the CNTs grown on Inconel are more tangled and have smaller diameters compared to those grown on Si (Figure 2). Because the same amount of iron is deposited on both substrates, the catalyst interaction with the surface is the only plausible explanation for the differences. One main reason is the different surface roughness of the two substrates. The smooth polished single crystal of Si, in contrast with the rolled foil of the polycrystalline metal alloy of Inconel, ensures that the nanotubes grow parallel with each other. On the other hand, the different chemical qualities and thus surface energy of the two substrates influence the wetting properties of the catalyst metals which affect the catalyst island morphology, size and surface density when heating the samples to the growth temperature resulting in differences in the nanotube diameter distributions for the two substrates. Furthermore, the Inconel substrate itself can also act as an additional catalyst resulting in thinner and denser CNTs. It can be seen that the CNTs on Si are longer when compared with those grown on Inconel most likely due to the partial tangling of the nanotubes and more efficient diffusion of the Al/Fe catalyst into the polycrystalline metal than the single crystal Si surface.

The Raman spectra collected from both samples are plotted together after being normalized to the G band intensity

maximum. Raman analysis in Figure 1c shows the typically observed 3 main distinct bands, the D band (disorder) around 1350 cm^{-1}, the G band (graphitic peak) around 1580 cm^{-1} and the G′ band (long-range order) around 2700 cm^{-1} for the CNTs on both types of substrates. There is a minor shift in the D band and G band positions for the CNTs grown on the two substrates due to their different diameter distribution and the number of walls (Figure 2e,f). The D peak arises due to the formation of sp^3 and dangling sp^2 bonds on the CNT side walls as well as from the deposition of amorphous carbon; the G peak arises from graphitic sp^2 carbon in the nanotubes; the G′ peak is the indicator of long-range order present within the CNTs. For these CNTs, we obtained the intensity ratio I_D/I_G of 0.78 and 0.91 for Inconel and Si, respectively, and the values are very close to the values reported earlier for CNTs synthesized on Inconel.[37]

Electric impedance spectroscopy measurements performed for CNTs grown on both Si and Inconel substrates suggest the structures are sufficiently conductive for emitter applications (Figure 1d). It can be seen from the Nyquist plots that the contact resistance between the CNT and Si is ∼320 Ω/cm^2 whereas for the CNT-Inconel contact it is ∼90 Ω/cm^2. The semicircles in the impedance spectra indicate the presence of a capacitive component most likely caused by the nanotube films of large specific surface area.

From the TEM analysis (Figure 2a−d), it is clear that the number of walls and also the average diameter of CNTs grown on Si are higher than those synthesized on Inconel. TEM analysis also reveals the presence of more amorphous carbon on the surface of the CNTs in the case of Si as compared to those grown on Inconel substrates.

Initially, the CNTs grown on both substrates demonstrated excellent field emission properties. From the J−E curves displayed in Figure 3, we observe that the initial current density of the CNT array grown on Si is higher than that for the corresponding sample obtained on Inconel (131 mA/cm^2 vs 99 mA/cm^2). Initially, the turn-on field (which is the field required to give a current density of 10 μA/cm^2) for the sample grown on Si (2.2 V/μm) is less than that for the nanotubes grown on Inconel (3.4 V/μm). However, the turn-on field for the latter samples decreased considerably from 3.4 to ∼1.5 V/μm after arcing. The threshold field, i.e., the field required to reach a current density of 10 mA/cm^2, also shows a similar tendency. For the CNT films grown on Si, it gradually increases; meanwhile a significant decrease of the corresponding threshold value is observed for the samples synthesized on the metal alloy substrate (from ∼5.0 to 2.8 V/μm). The increase in the turn on and threshold fields as well as the early device failure for the films grown on Si might be because of the structural damage of the emitters[38] as also indicated by the voids and fused CNTs visible in SEM images (Figure 4).

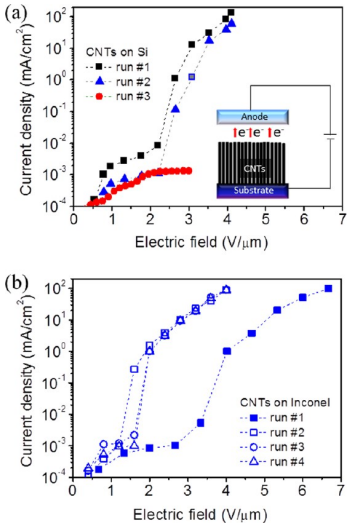

Figure 3. Plots of emission current density as a function of applied electric field in repeated experiments for CNTs grown on (a) Si and (b) Inconel.

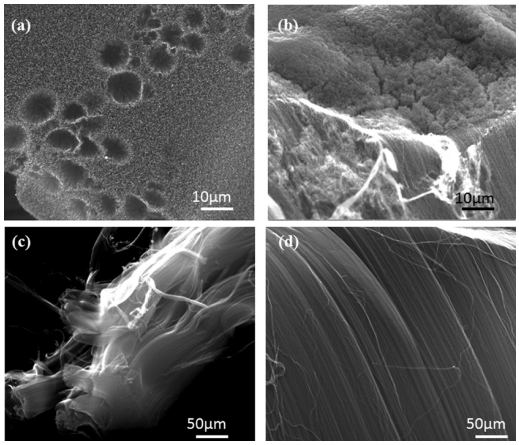

Figure 4. SEM images of the samples after field emission. CNT films (a) on Si, top view, (b) on Inconel, top view, (c) on Si side view and (d) on Inconel, top view. Microscopic voids in the used films on Si show the structural instability in contrast with the continuous surface of the films grown on Inconel.

The causes of CNT degradation on the Si substrate can be associated with a number of different mechanisms: (1) Poor adhesion of CNTs to the substrate and consequent peeling, (2) high and/or inhomogeneous contact resistance between the CNTs and the substrate resulting in large local current densities and excessive joule heating and (3) at high electric fields, resistive heating and related stress due to thermal expansion coefficient mismatch at the CNT−substrate junction causing mechanical failure. According to Okai et al.,[18] the strong repulsive electrostatic forces may also be a reason for the electrical breakdown during field emission. As reported in our earlier work,[39,40] when the electric field between the anode and the cathode is increased, the dipole resulting from the concentration of electrons in the tips of carbon nanotubes will enhance the static electric force and pull the carbon nanotubes off from the substrate, leading to an abrupt drop of emission current. As noticed by Wang et al.,[38] the electrostatic force created by the flow of emission current acting in the tip of nanotube can induce a split or even burning of the emitters. On the other hand, there was no obvious electrical breakdown in

the case of the sample grown on Inconel while the emission threshold fields were improving with use. The superior field emission properties and reliability of the nanotube films grown on Inconel as compared to those on Si are inevitable and can be explained by the good electrical and thermal interface between the nanotubes and the metallic substrate. The excellent electrical contact ensures uniform current distribution in the entire cross-section of the emitter, thus eliminating the formation of hot spots and also avoiding the evolution of excess Joule heat in local microscopic volumes at the nanotube−substrate interface as well as at the tips of the nanotubes. The improved overall field emission performance of the Inconel-supported films may be due to localized cleaning caused by mild arcing at the tips of the nanotubes. In addition, a uniform fusing of the CNT−catalyst−Inconel interface caused by the current might have also taken place by which the electrical and mechanical properties of the interfacial contact are improved.

Another important aspect is the field enhancement factor (β) that describes how much the emitter tips amplify the macroscopic electric field around the sharp and highly curved apexes. As predicted by Mc. Clain et al.,[41] as the diameter of the CNTs decreases (in our case, the CNTs grown on Inconel), the emission field decreases with a corresponding increase in field amplification. The total emission current depends on the field enhancement factor and, accordingly, on the diameter of the CNTs, the smaller the diameter the higher the emission current. From the slope of the linearized Fowler−Nordheim plot (i.e., by plotting $\ln(J/U^2)$ versus $1/U$ (Figure 5), where J is the current density and U is the voltage drop on the emitter, β can be determined. The slope is $m = (Bd\phi^{3/2})/\beta$, where B is a constant with the value of 6.83×10^9 V eV$^{-3/2}$ m^{-1}, ϕ is the work function of the emitter material (~5 eV for CNTs) and d is the distance between the cathode and the anode (200 μm in our case).

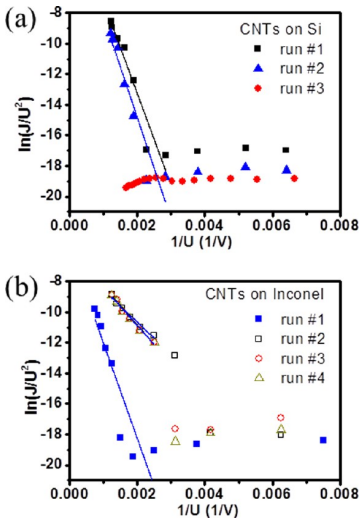

Figure 5. Fowler−Nordheim curves of the samples grown on (a) Si and (b) Inconel substrate (from the data in Figure 3). The corresponding field enhancement factors are determined from the linear fitting slopes in the high field regime.

The enhancement factors for both types of emitter structures are very similar having values of ~2500. In the case of the Si-supported CNT films, this value remained unchanged as long as the emitters were functional. Interestingly, for the nanotube films synthesized on Inconel, this initial field amplification value is abruptly increased to ~7300 when repeating the measurement on the same device and then it kept the increased value in the subsequent tests. Such a substantial increase in the field amplification is a consequence of surface cleaning by the mild arcing in the course of the first emission experiment but also sharpening of the nanotube tips might have taken place as suggested by Talapatra and co-workers.[31] Although the initial values for β are rather close to the ones reported for nanotube films in the literature (i.e., typically between 500 and 3000),[1,5,31,42,43] the improved enhancement factors are considerably higher than those.

CONCLUSIONS

In conclusion, vertically aligned CNTs on Inconel substrates grown via water assisted chemical vapor deposition have shown excellent field emission properties clearly outperforming similar films synthesized on Si substrates. The field emitter devices synthesized on the metallic substrate have low turn-on fields (~1.5 V/μm), enable high current operation (~100 mA/cm^2) and show very high local field amplification with factors up to ~7300. These properties, along with their increased reliability, make the demonstrated structures as a potential candidate for future flat panel displays based on CNT-electron emitters.

AUTHOR INFORMATION

Corresponding Author

*R. Vajtai. E-mail: Robert.Vajtai@rice.edu.

Notes

The authors declare no competing financial interest.

ACKNOWLEDGMENTS

C. S. Tiwary thanks IISc (Indian Institute of Science), Bangalore for their support. A. Hart, R. Vajtai and P.M. Ajayan acknowledge financial support from U.S. Army Research Laboratory/Army Research Office (No. W911NF).

REFERENCES

(1) Heer, W. A.; Chatelain, A.; Ugarte, D. *Science* **1995**, *270*, 1179−1180.
(2) Rinzler, A. G.; Hafner, J. H.; Nikolaev, P.; Lou, L.; Kim, S. G.; Tomanek, D. *Science* **1995**, *269*, 1550−1553.
(3) Saito, Y.; Hamaguchi, K.; Hata, K.; Uchida, K.; Tasaka, Y.; Ikazaki, F.; Yumura, M.; Kasuya, A.; Nishina, Y. *Nature* **1997**, *389*, 554−555.
(4) Wang, Q. H.; Corrigan, T. D.; Dai, J. Y.; Chang, R. P. H.; Krauss, A. R. *Appl. Phys. Lett.* **1997**, *70*, 3308−3310.
(5) Bonard, J. M.; Maier, F.; Stockli, T.; Chatelain, A.; Heer, W. A.; Salvetat, J. P.; Forro, L. *Ultramicroscopy* **1998**, *73*, 7−15.
(6) Teo, K. B. K.; Chhowalla, M.; Amaratunga, G. A. J.; Milne, W. I.; Pirio, G.; Legagneux, P.; Wyczisk, F.; Pribat, D.; Hasko, D. G. *Appl. Phys. Lett.* **2002**, *80*, 2011−2013.
(7) Chen, Y.; Sun, Z.; Chen, J.; Xu, N. S.; Tay, B. K. *Diamond Relat. Mater.* **2006**, *15*, 1462−1466.
(8) Siegal, M. P.; Miller, P. A.; Provencio, P. P.; Tallant, D. R. *Diamond Relat. Mater.* **2007**, *16*, 1793−1798.
(9) Pandey, A.; Prasad, A.; Moscatello, J. P.; Engelhard, M.; Wang, C.; Yap, Y. K. *ACS Nano* **2013**, *7*, 117−125.
(10) Su, J.; Guo, D. Z.; Xing, Y. J.; Zhang, G. M. *Phys. Status Solidi A* **2013**, *210*, 349−355.

(11) Ren, H.; Yang, L.; Zhang, Y. *J. Phys.: Conf. Ser.* **2013**, *418*, 012007.
(12) Bhattacharya, S.; De, D.; Ghosh, S.; Ghatak, K. P. *J. Comput. Theor. Nanosci.* **2013**, *10*, 1−5.
(13) Atthipalli, G.; Epur, R.; Kumta, P. N.; Gray, J. L. *J. Vac. Sci. Technol., B: Nanotechnol. Microelectron.: Mater., Process., Meas., Phenom.* **2011**, *29*, 04D102.
(14) Sun, P. C.; Deng, J. H.; Cheng, G. A; Zheng, R. T.; Ping, Z. X. *J. Nanosci. Nanotech.* **2012**, *12*, 6510−6515.
(15) Berhanu, S.; Gröning, O.; Chen, Z.; Merikhi, J.; Kaiser, M.; Rupesinghe, N. L.; Bachmann, P. K. *Phys. Status Solidi A* **2012**, *209*, 2114−2125.
(16) Wijker, W. J. *Appl. Sci. Res., Sect. B* **1961**, *9*, 1−20.
(17) Almy, J. E. *Phys. Rev. (Series I)* **1907**, *24*, 50−59.
(18) Okai, M.; Fujieda, T.; Hidaka, K.; Muneyoshi, T.; Yaguchi, T. *Jpn. J. Appl. Phys.* **2005**, *44*, 2051−2055.
(19) Bonard, J. M.; Klinke, C. *Phys. Rev. B* **2003**, *67*, 115406−115415.
(20) Nessim, G.; Seita, M.; O'Brien, K.; Hart, A.; Bonaparte, R.; Mitchell, R.; Thompson, C. *Nano Lett.* **2009**, *9*, 3398−3405.
(21) Kim, B.; Chung, H.; Chu, K.; Yoon, H.; Lee, C.; Kim, W. *Synth. Met.* **2010**, *160*, 584−587.
(22) Fu, Y.; Nabiollahi, N.; Wang, T.; Wang, S.; Hu, Z.; Carlberg, B.; Zhang, Y.; Wang, X.; Liu, J. *Nanotechnology* **2012**, *23*, 045304.
(23) Kordás, K.; Tóth, G.; Moilanen, P.; Kumpumäki, M.; Vähäkangas, J.; Uusimäki, A.; Vajtai, R.; Ajayan, P. M. *Appl. Phys. Lett.* **2007**, *90*, 1231051−3.
(24) Fu, Y. F.; Qin, Y. H.; Wang, T.; Chen, S.; Liu, J. H. *Adv. Mater.* **2010**, *22*, 5039−5042.
(25) Kumar, A.; Pushparaj, V. L.; Kar, S.; Nalamasu, O.; Ajayan, P. M.; Baskaran, R. *Appl. Phys. Lett.* **2006**, *89*, 163120 1−3.
(26) Tóth, G.; Mäklin, J.; Halonen, N.; Palosaari, J.; Juuti, J.; Jantunen, H.; Kordás, K.; Sawyer, W. G.; Vajtai, R.; Ajayan, P. M. *Adv. Mater.* **2009**, *2*, 211−215.
(27) Mittal, J.; Lin, K. L. *J. Nanosci. Nanotech.* **2013**, *13*, 5590−5596.
(28) Masarapu, C.; Wei, B. *Langmuir* **2007**, *23*, 9046−9049.
(29) Baddour, C.; Fadlallah, F.; Nasuhoglu, D.; Mitra, R.; Vandsburger, L.; Meunier, J. *Carbon* **2008**, *47*, 313−318.
(30) Benito, S.; Lefferts, L. *Carbon* **2010**, *48*, 2862−2872.
(31) Talapatra, S.; Kar, S.; Pal, S.; Vajtai, R.; Ci, L.; Victor, P.; Shaijumon, M.; Kaur, S.; Nalamasu, O.; Ajayan, P. M. *Nat. Nanotechnol.* **2006**, *1*, 112−116.
(32) Halonen, N.; Mäklin, J.; Rautio, A. R.; Kukkola, J.; Uusimäki, A.; Toth, G.; Reddy, L. M.; Vajtai, R.; Ajayan, P. M.; Kordas, K. *Chem. Phys. Lett.* **2013**, *583*, 87−91.
(33) Sung, W.; Kim, W.; Lee, H.; Kim, Y. *Vacuum* **2008**, *82*, 551−555.
(34) Lahiri, I.; Seelaboyina, R.; Hwang, J.; Banerjee, R.; Choi, W. *Carbon* **2001**, *48*, 1531−1538.
(35) Mahanandia, P.; Arya, V.; Bhotla, P.; Subramanyam, S.; Schneider, J.; Nanda, K. *Appl. Phys. Lett.* **2009**, *95*, 083108.
(36) Yi, W.; Yang, Q. *Diam. Relat. Mater.* **2010**, *19*, 870−874.
(37) Atthipalli, G.; Wang, H.; Gray, J. L. *Appl. Surf. Sci.* **2013**, *273*, 515−519.
(38) Wang, Z. L.; Gao, R. P.; Heer, W. A.; Poncharal, P. *Appl. Phys. Lett.* **2002**, *80*, 856−858.
(39) Verma, P.; Gautham, S.; Kumar, P.; Chaturvedi, P.; Rawat, J. S.; Pal, S.; Chaubey, R.; Harsh, H. P.; Vyas, P. K.; Bhatnagar. *J. Vac. Sci. Technol., B: Microelectron. Nanometer Struct.–Process., Meas., Phenom.* **2007**, *25*, 1584−1587.
(40) Srividya, S.; Gautam, S.; Jha, P.; Kumar, P.; Kumar, A.; Ojha, U. S.; Rawat, J. S. B. S.; Pal, S.; Chaudhary, P. K.; Harsh, R.; Sinha, K. *Appl. Surf. Sci.* **2010**, *256*, 3563−3566.
(41) McClain, D.; Wu, J.; Taven, N.; Jiao, J.; McCarter, C.; Richards, C.; Richards, R.; Bahr, D. *J. Phys. Chem. C* **2007**, *111* (20), 7514−7520.
(42) Guillorn, M. A.; Melechko, A. V.; Merkulov, V. I.; Hensley, D. K.; Simpson, M. L.; Lowndes, D. H. *Appl. Phys. Lett.* **2002**, *81*, 3660−3662.
(43) Saito, Y.; Uemura, S. *Carbon* **2000**, *38*, 169−182.

Field Emission with Ultralow Turn On Voltage from Metal Decorated Carbon Nanotubes

Srividya Sridhar,[†] Chandrasekhar Tiwary,[‡,#] Soumya Vinod,[‡] Jose Jaime Taha-Tijerina,[‡] Srividvatha Sridhar,[§] Kaushik Kalaga,[‡] Benjamin Sirota,[∥] Amelia H. C. Hart,[‡] Sehmus Ozden,[‡] Ravindra Kumar Sinha,[†] Harsh,[⊥] Robert Vajtai,[‡] Wongbong Choi,[∥] Krisztián Kordás,[▽] and Pulickel M. Ajayan[‡,*]

[†]Department of Applied Physics, Delhi Technological University (Formerly Delhi College of Engineering), Bawana Road, Delhi 110042, India, [‡]Department of Materials Science and NanoEngineering, Rice University, Houston, Texas 77005, United States, [§]Department of Chemical and Biomolecular Engineering, Rice University, Houston, Texas 77005, United States, [⊥]Department of Physics, Jamia Millia Islamia, New Delhi 110025, India, [∥]Department of Material Science and Engineering, University of North Texas, Denton, Texas 76203, United States, [#]Materials Engineering, Indian Institute of Science, Bangalore, Karnataka 560012, India, and [▽]Microelectronics and Materials Physics Laboratories, Department of Electrical Engineering, University of Oulu, P.O. Box 4500, FI-90014 Oulu, Finland

ABSTRACT A simple and scalable method of decorating 3D-carbon nanotube (CNT) forest with metal particles has been developed. The results observed in aluminum (Al) decorated CNTs and copper (Cu) decorated CNTs on silicon (Si) and Inconel are compared with undecorated samples. A significant improvement in the field emission characteristics of the cold cathode was observed with ultralow turn on voltage ($E_{to} \sim 0.1$ V/μm) due to decoration of CNTs with metal nanoparticles. Contact resistance between the CNTs and the substrate has also been reduced to a large extent, allowing us to get stable emission for longer duration without any current degradation, thereby providing a possibility of their use in vacuum microelectronic devices.

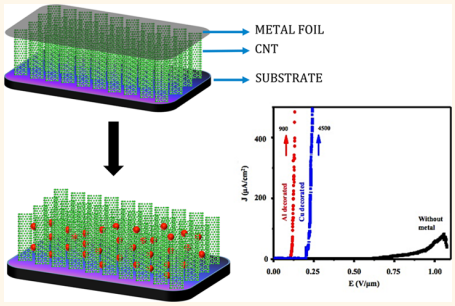

KEYWORDS: field emission · metal decoration · screening effect · work function · edge effect

Because of the high aspect ratio, high mechanical strength and high thermal conductivity, CNTs are considered to be an ideal electron emitting sources in field emission displays.[1−8] Aligned and well-separated CNT cathode morphology is important for many potential applications where a high electric-field is needed, such as in field emission devices. The growth in these cases is usually achieved by chemical vapor deposition (CVD). However, the highly dense growth of CNTs by thermal CVD method may compromise the field emission properties, due to a field-screening effect caused by the proximity of neighboring tubes. Also some critical issues such as adhesion of CNTs with the substrate, reliability, and stability have to be addressed while using CNTs as electron emitters in field emission applications. To improve the field emission performance from CNT emitters, different methods such as doping of CNTs with nitrogen,[9,10] surface coatings with low work function materials such as LaB_6 or Ha for low turn on field[11,12] and decorations with ZnO and Ru[13−15] have been investigated. Previous studies have also shown that tuning the structure of the CNTs such as the radius,[16] geometry,[17,18] structural change by oxygen plasma treatment[19] and improving their density[20] could improve the field emission property. Also by decorating the CNT walls with organic functional groups[21−23] or by inorganic semiconductor[24−31] the field emission properties of CNTs could be enhanced. Chi *et al.*[32] reported a threshold field of 0.9 V/ μm at 1 mA/cm^2, which correlated to a turn on voltage of 0.6 V/μm at 10 μA/cm^2 by growing CNTs on a mesh electrode. Also, Zuo *et al.*[33] demonstrated low turn on field of 0.63 V/μm at 10 μA/cm^2 by decorating the surface of the CNT with titanium nanoparticles. Pandey *et al.*[34] arrived at a threshold field of 0.8 V/μm in strontium titanate coated CNTs. On the other hand, Liu *et al.*[15] decorated CNTs with Ru nanoparticle and the turn on field reduced from 2.5 to 1.3 V/μm after Ru decoration. In the recent report of Zannin

* Address correspondence to ajayan@rice.edu.

Received for review February 15, 2014 and accepted July 15, 2014.

Published online 10.1021/nn500921s

et al.[35] hybrid diamond-like carbon and CNT composite structures showed threshold field of 2 V/μm. Thus, to the best of our knowledge, such low turn on field of 0.1 V/μm achieved in this work has not been reported so far.

Electrophoretic deposition (EPD) technique is a common method used for decorating the CNTs with the desired metal particle to improve the field emission properties of the cold cathode.

Fan *et al.*[36] used CNT/Ni composite and Chen *et al.*[37] fabricated CNT/Cu composite to enhance the field emission properties of the CNTs. But during the fabrication, the CNTs in the composites would be easily covered by the deposited nanoparticles in the chemical process resulting in the decrease of effective field emitters in the CNT cathode. Another important issue of CNTs getting bundled together is also common in this process. Once they are bundled, without the use of aggressive treatment like ultrasonication or chemical functionalization, it is extremely difficult to achieve a stable dispersion or homogeneous mixture. These measures are known to damage the walls of the CNTs and degrade their electrical properties to a larger extent. Moreover, this process cannot alter the distance between the CNTs. Although it is important to lower the turn on and threshold voltage for better field emission results, reducing the screening effect is crucial for CNTs to be used in field emission application. It is well-known that if the separation between the tubes, *d*, is much less than the tube height, *h*, in an array, the electrostatic shielding between the CNTs can drastically affect the field emission performance of the cold cathode. Numerical simulations show that if the distance between the CNTs is equal to or more than twice the height of the CNTs, then the screening effect can be considerably reduced which in turn could improve the field emission property of the cathode.[38−40] Electrostatic shielding becomes a significant hurdle for future device applications because of the exponential dependence of the emission current on the electric field in accordance with the Fowler-Nordheim theory. Work has also been done on thermally evaporated nanoparticles on nanotubes.[41−43] The results in these work indicate that the morphology of the metal particle or the film on the CNTs is dependent on the intrinsic properties of the metal themselves than on the process parameters. On the other hand, the work of Muratore *et al.*[44] reported the effect of particle growth temperature and time on the decorated metal nanoparticles' density and morphology. However, the sputtered metal nanoparticles were attached to the surface of the CNTs without penetrating in between the CNTs to change the inter tubular spacing of those.

The current paper proposes a simple and scalable procedure for decorating the vertically aligned CNTs forest with metal nanoparticles for improved field emission properties. This process enabled the CNTs to bundle toward a metal particle forming a pattern due to which the CNT bundles are separated by almost 3 times the height of the bundle reducing the screening effect considerably. Further, by the deposition of metal nanoparticles on the surface of the nanotubes, emitting centers are obtained that ensure highly conductive paths for the electrons from the nanotubes toward the vacuum helping bypass the amorphous carbon impurities, known as one of the major hurdles in CNT based emitters.

RESULTS AND DISCUSSION

Figure 1a shows the scanning electron microscope (SEM) images of the multiwalled carbon nanotubes (MWCNTs) grown on Si with Al decoration on them. Before the metal decoration, the CNTs were vertically aligned *via* self-supporting mechanism as described in our previous work,[45] due to extremely high density of CNTs. Interestingly, after metal evaporation, the morphology of the CNTs changed completely. Groups of CNTs became linked together by their tips while attaching to the Al particles forming microscopic patterns in the nanotube forest. Accordingly, the CNTs are no longer individual strands for field emission; instead they are individual bundles. Choi *et al.*[20] also observed similar morphology by H_2 plasma treatment. The surface morphology of vertically aligned MWCNTs changed from flat surface to sharp conical stacks of CNTs due to the post plasma treatment. They claimed that there was improvement in the field emission properties of the CNTs due to the formation of such stacks.

Figure S1a,b (Supporting Information) shows the distribution histogram of the number of CNTs with their height and the number of CNT bundles with the interbundle distance, respectively. From the histogram, it is very clear that most of the CNT bundles are of around 2 μm in their height with inter bundle distances varying mostly between 3 and 5 μm. It is to be noted that bundled CNTs have the advantage of realizing the ideal ratio of inter tube distance to the height for achieving maximum field emission by reducing charge screening effects in adjacent CNTs in the forest.[46] According to Suh *et al.*[47] the field emission would be optimum when the tube height is similar to the intertube distance, while the results of Ren *et al.*[48] suggest 3-fold intertube distance in reference to CNT height to achieve maximum emitter efficiency. In our case, since most of the CNT bundles are separated by almost 3 times the height of the bundle and the bundle are emitting as a whole, the screening effect is reduced considerably and the emitter efficiency has increased substantially. Figure 1b corresponds to the SEM images of Al decorated CNTs grown on Inconel. SEM images clearly show that the CNTs on Inconel are also no longer a uniform film after the metal deposition, however the surface texture of the forests are not the same as for the

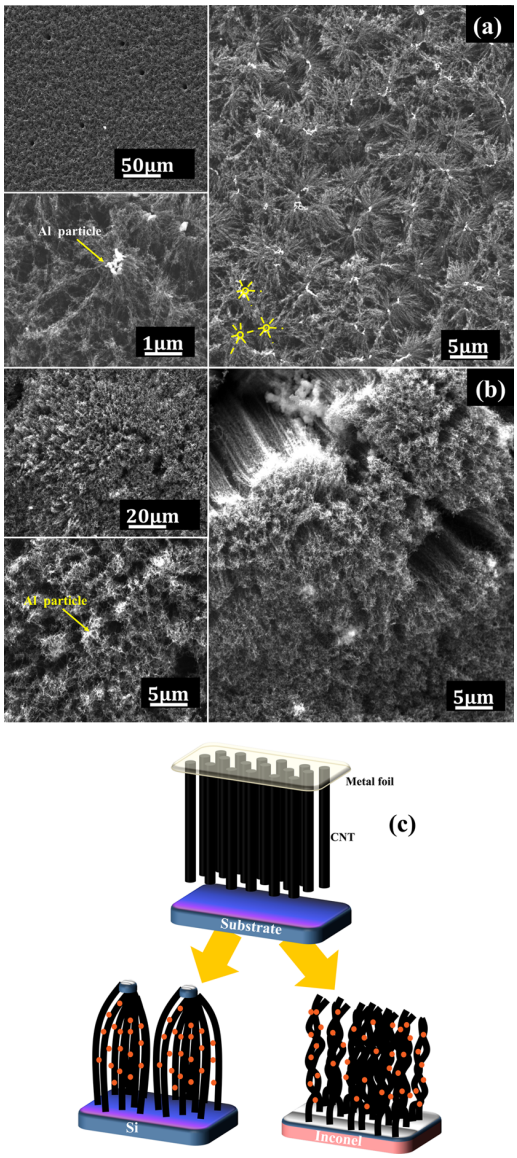

Figure 1. (a) SEM image of CNTs grown on Si with Al decoration in different magnification. SEM image shows the way in which the CNTs got attached to Al particle forming a beautiful pattern. (b) SEM image of the CNTs grown on Inconel with Al decoration on them in different magnification. (c) The schematic procedure for the fabrication of metal decorated CNTs.

other CNTs grown on the other substrate material. The nanotubes in this case formed bundles which reduced the screening effect. A schematic of the morphology of CNTs grown on Si and Inconel substrate is shown in Figure 1c. Although the mechanisms responsible for the differing surface textures after evaporating the metals on the different films are not clear, a number of different reasons associated with the wetting behavior of the CNT forests with the molten metal (and/or with the condensing metal from the vapor phase) might explain our observations. Figure 2a shows the transmission electron microscope images (TEM) and high resolution transmission electron microscope images (HRTEM) of Al decorated CNTs grown on Si substrate. The low magnification image resembles a similar morphology as seen in SEM. The TEM observation of the CNTs revealed the formation of MWCNTs consisting of 4−6 graphite layers. It is clear that individual CNTs form bundles with adjacent nanotubes and share a metal tip. Selected area diffraction (SAD) of the particle confirms these particles to be FCC plane (111) of Al. The high magnification image at the point of joint in a bundle confirms the presence of metal particles and several CNTs tangled together. The high magnification image also reveals the nanoparticles embedded in the amorphous carbon layer are in reasonably close contact with the nanotubes, while the other side of the particles is unraveled. The increase in wall diameter due to bundle formation is further verified with Raman measurements. The Al deposition on Inconel shows very similar

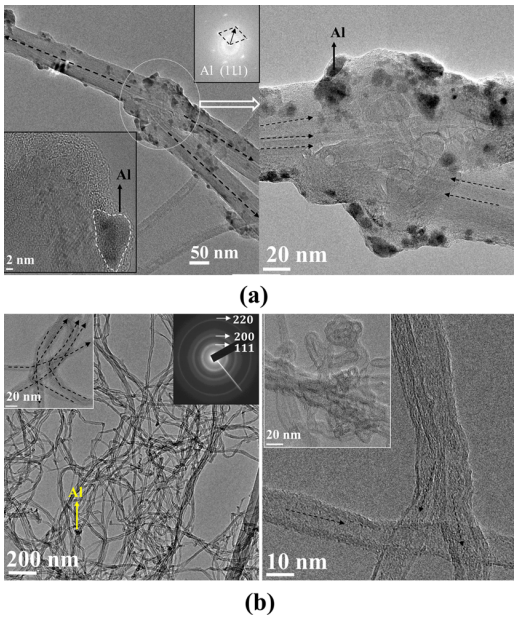

Figure 2. (a) TEM and HRTEM micrograph of the CNTs grown on Si substrate with Al decoration on them. It shows how the CNTs are joined together at the tip, and the high magnification confirms the presence of metal particle. (b) TEM and HRTEM micrograph of the CNTs grown on Inconel.

morphology as shown in Figure 2b. The large area SAD shows the presence of Al planes. The high magnification image shows an increase in diameter with a narrow distribution because of CNTs joining together to form a bundle. The size of the metal nanoparticles was found to be 5−10 nm in diameter.

Raman spectra of the pristine CVD grown CNTs with and without metal deposition are shown in Figure 3a. Raman spectroscopy is the inelastic scattering of light usually associated with absorption or emission of phonons and is rich in information about the structure and chemical bonding of CNTs. Defects and sp^3 hybridized carbon atom give rise to D-band (1340 cm^{-1}) and height of this band is inversely related to the quality of the nanotube (*i.e.*, presence of disorder in the graphitic material). The G-band (~1580 cm^{-1}) is associated with the sp^2 hybridized carbon atom in the nanotube wall and is a good measure of the graphitization of the sample. The G′ or 2D peak (around 2600 cm^{-1}) arises due to two phonon second order scattering process and indicates long-range order in a sample. The ratio of the intensities of the defect or the disorder induced D-band to the symmetry allowed graphitic band or the G-band I_d/I_g characterizes the defect density or degree of disorder in sp^2 hybridized carbon material.[49] The ratio I_{2d}/I_g can be used for identifying the number of walls in the given MWCNT.[50] It is also to be noted that increase in the number of layer leads to a significant decrease in the peak intensity of the 2D peak and this peak becomes hardly distinguishable if the number of layer exceeds 5.[51]

The intensity ratios I_d/I_g and I_{2d}/I_g are given in Table.1. From the results, it is clear that the intensity ratio I_d/I_g of CNTs grown on Si substrate without any metal decoration and with Al decoration was 0.78 and these values are very close to the values reported by Athipalli *et al.*[52] For the CNTs grown on Si substrate with Cu decoration on them this ratio became 0.51. The lower the value of this ratio, lesser the defect, which in turn means lesser amorphous carbon, and greater the degree of graphitic crystallinity. Also, the 2D peak for Al decorated CNTs grown on Inconel was hardly distinguishable and hence the ratio I_{2d}/I_g became zero. As predicted by the work of Ferrari[51] the number of walls must have exceeded five and hence this peak became hardly distinguishable. This was also consistent with TEM, where it is clear that the CNTs join together thereby increasing the number of walls. From the above predictions, it is clear that the CNTs grown on Si with Cu decoration on them have higher graphitic crystallinity with lesser defect. The occurrence of sharp 2D peak on this sample indicates a good long-range order in those samples.

In order to characterize the phase deposited on the CNT forest, the samples are analyzed by X-ray diffraction. Figure 3b shows the representative image of the Al deposition and Cu deposition on Si. In the diffraction pattern we observe reflections at $2\theta = 38°$ and 44° which can be assigned to the (111) and (200) planes of FCC phase of Al. The reflection at $2\theta = 43°$ corresponds to the FCC plane (111) of Cu. These diffraction patterns confirm the presence of metallic particles of Al and Cu and absence of their crystalline oxides. The broadened reflections from the metals clearly reveals the small crystallite size of the metallic particles (~5 nm) supporting observations done with TEM.

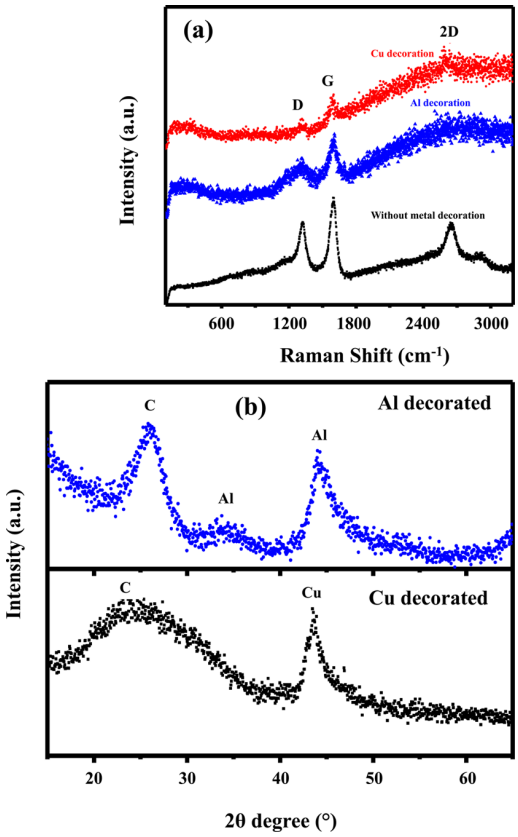

Figure 3. (a) Raman spectra showing 3 distinct peaks [disorder peak D, graphitic peak G and long-range order peak G′ for Si without metal decoration, with Al decoration and Cu decoration]. (b) XRD pattern on Si with Al decoration and XRD pattern on Si with Cu decoration. Al, Cu and C peak clearly prove that there is no oxide formation.

TABLE 1. Values of I_d/I_g and I_{2d}/I_g Ratio for Different Types of CNTs

type of CNTs	I_d/I_g	I_{2d}/I_g
Si substrate	0.78	0.71
Inconel substrate	0.65	0.41
Si substrate/Al decoration	0.78	0.80
Inconel substrate/Al decoration	0.67	0.00
Si substrate/Cu decoration	0.51	0.58
Inconel substrate/Cu decoration	0.66	0.77

The field emission characteristics of the CNTs grown on Si with and without any metal decorations are shown in Figure 4a. The turn on field E_{to}, which is the field required to obtain a current density of 1 μA/cm^2 and the threshold field E_{th}, which is the field required to obtain a current density of 100 μA/cm^2 are summarized in Table 2. The data clearly reveals that Si grown CNTs with Al decoration on them gave the lowest E_{to} and E_{th}, 0.13 and 0.14 V/μm, respectively. One explanation for our low E_{to} and E_{th} for Si grown CNTs with Al decoration on them is due to the lower work function of Al as predicted by Lee *et al.*[53] Similar field emission characteristics were observed for CNTs grown on Inconel

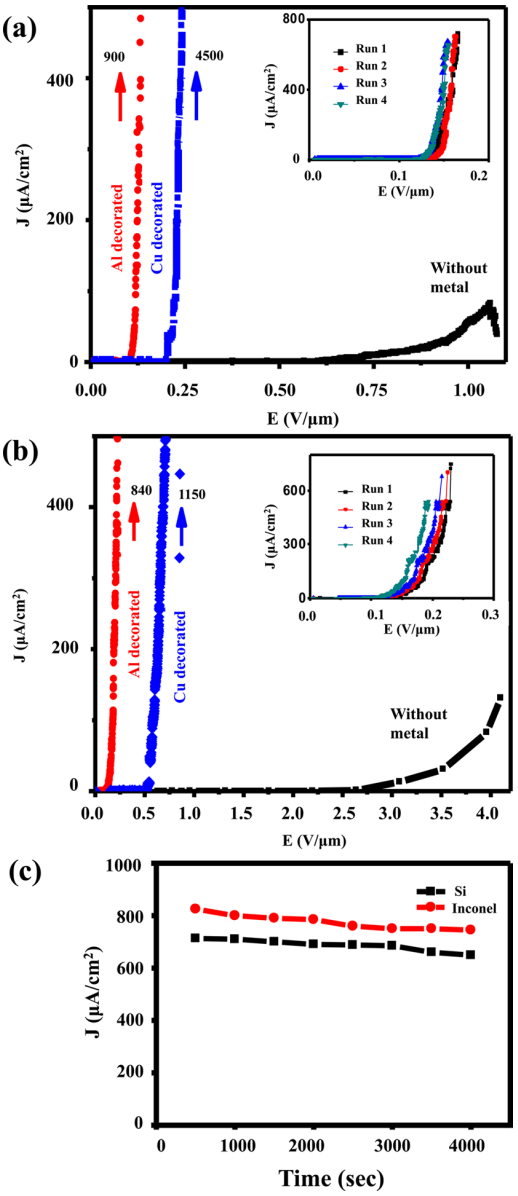

Figure 4. (a) Field emission characteristics of the CNTs grown on Si with and without any metal decorations. It is very clear that the turn on field E_{to} and the threshold field E_{th} are significantly reduced after the metal decoration. Inset in the *J*–*E* plot shows emission stability. (b) Field emission characteristics of the CNTs grown on Inconel showing the same phenomena. Inset in the *J*–*E* plot shows emission stability. (c) Time trace of current density at the fixed field of 0.15 V/μm for Si grown CNTs and 0.25 V/μm for Inconel grown CNTs, both decorated with Al nanoparticles.

with and without any metal decorations on them. (Figure 4b) The *J*–*E* plot was repeatedly measured and it showed good reproducibility. No current saturation was observed over E_{th}.

It is well-known that during field emission, the electrons have to cross two barriers.[54] Barrier 1 is the barrier between the substrate and the CNT and barrier 2 is the barrier between the CNT and the vacuum. Since the Inconel and Al coated Si substrates on which CNTs are

TABLE 2. Values of E_{to} and E_{th} for Different Type of Substrates with and without Metal Decoration

type of CNTs	E_{to} (V/μm)	E_{th} (V/μm)
Si substrate	0.78	2.6
Inconel substrate	1.2	2
Si substrate/Al decoration	0.13	0.14
Inconel substrate/Al decoration	0.14	0.18
Si substrate/Cu decoration	0.19	0.22
Inconel substrate/Cu decoration	0.53	0.58

directly grown have good electrical conductivity, barrier 1 is expected to be reduced substantially enhancing the overall field emission properties of our structures. The measured low contact resistance values for the CNT–substrate interfaces are in agreement with our assumptions as seen in Figure S3 (Supporting Information). Barrier 2 on the other hand has also improved. According to Tanaka *et al.*[55] the presence of amorphous carbon can increase the work function and the E_{th} to a larger extent. One of the explanations for the low E_{th} values for metal decorated CNTs can be due to the reduced amount of amorphous carbon.[45] Although the mechanism that would reduce the amorphous carbon content obtained after Cu decoration is not clear, a plausible explanation might be a partial dissolution of carbon by Cu at the process temperatures applied in the course of evaporation. Another, probably more important, effect that helps electron emission is the promoted electron passage from the nanotubes toward the vacuum through the metal nanoparticles, which may reasonably explain why we observe significant reduction of E_{th} for both metals. The metal nanoparticles form highly conductive electrical paths for the electrons through the amorphous carbon layer (Figure 2a) covering the nanotubes thus ensuring emission centers with clean surface toward the vacuum.

Furthermore, according to Fuji *et al.*[56] the electric field of the bundle is significantly higher at the edge than at the center when compared to the electric field of the flat film which is constant all over the emitter surface. In our samples, due to the metal decoration, the emitter surface is no longer a flat film; instead they are transformed into individual bundles since some of the Al particles went in between the CNTs, thereby increasing the number of edges. The CNTs at the periphery of the bundle formed due to metal decoration acted as a major emission sites. Thus, the excellent field emission property of our emitters can also be attributed to the edge effect.

In addition to the improved field emission $I-V$ characteristics, better emission uniformity is observed from the emission pattern of Al decorated CNTs grown on both Si and Inconel, as shown in the inset of Figure 4. This is because of the increase in the number of available emitters and reduced screening effect. Figure 4c shows the time trace of current density at the fixed field of 0.15 V/μm for Si grown CNTs and 0.25 V/μm for Inconel grown CNTs, both decorated with Al nanoparticles. It was found that there was stable emission for more than an hour due to metal decoration on the CNTs.

CONCLUSIONS

In conclusion, vertically aligned CNTs grown on Al coated Si and Inconel substrates were decorated with Al and Cu particles using a simple and scalable process. The synthesized hybrid structures showed enhanced field emission properties with ultralow turn on and threshold voltages of 0.13 and 0.14 V/μm respectively measured for the Al decorated CNTs grown on Al coated Si. Contact resistance also got reduced substantially in the metal decorated structures which resulted in stable emission for a longer duration without any current degradation. The excellent field emission properties of the metal decorated CNTs can be attributed to the edge effect, reduced screening effect, lower contact resistance, which may pave the road for future devices that require substantially lower bias than the currently existing ones.

METHODS

First the CNTs were grown on Al coated silicon (Si) and Inconel as described elsewhere.[45,57] The grown CNTs were kept inside the CVD chamber with aluminum (Al) sheet of thickness 150 μm over them and the temperature of the system was gradually increased to 700 °C for 10 min and cooled gradually. Since the melting point of Al is 660 °C, it got melted and the CNTs were decorated with Al particles. As the sheet was kept over the array of CNTs, some of the Al particles penetrate in between the CNTs in the array. This process of annealing was done in the presence of Argon (Ar) at a low flow rate. The schematic procedure for the fabrication of metal decorated CNTs is shown in Figure 1c. The same procedure was repeated for the deposition of Cu particles using Cu sheet to obtain Cu decorated CNTs.

The surface morphologies were characterized using scanning electron microscopy (SEM, FEI Quanta 400 ESEM FEG) and high resolution transmission electron microscopy (HRTEM JEOL v2100 F TEM). The content of Al and Cu particles is identified using X-ray diffraction (Rigaku D/Max Ultima II Powder XRD with a Cu Kα source) and Raman spectroscopy (Renishaw in *via* Raman microscope). The area of the sample used was 1 cm^2. After the deposition with metal particles; the sample was transferred to a vacuum chamber with vacuum better than 2×10^{-6} Torr, for field emission measurement. The silicon (Si) and Inconel substrates with CNTs were used as the cathode and indium tin oxide (ITO) coated glass plate as the anode. The cathode and anode mounting stands were machine ground to ensure that they are perfectly parallel. The distance between the cathode and the anode (100 μm) was adjusted using micrometer screw gauge arrangement and a suitable DC voltage (up to 400 V) was supplied using Keithley 2410 high voltage power supply. The electron impedance spectroscopy (EIS) measurements were performed using a two electrode setup with the CNT on the substrate as the working electrode and lithium metal as the

counter/reference electrode. In this, 1 M LiPF6 in 1:1 v/v mixture of ethylene carbonate (EC) and dimethyl carbonate (DMC) are used as the electrolyte and glass microfiber filter membrane as the separator. The EIS measurements were conducted over 70 kHz to 10 mHz by applying a constant dc bias with sinusoidal signal of 10 mV.

Conflict of Interest: The authors declare no competing financial interest.

Acknowledgment. The work done at Rice University has been supported by U.S. Department of Defense: U.S. Air Force Office of Scientific Research for the Project MURI: "Synthesis and Characterization of 3-D Carbon Nanotube Solid Networks" Award No. FA9550-12-1-0035. C.S.T. would like to thank Indian Institute of Science, Bangalore for their support. J.T.-T. acknowledges the support from CONACYT (213780).

Supporting Information Available: A histogram of distance distribution between the CNT bundles and the height of the bundle is included. This is followed by F–N plot for Al decorated CNTs and Cu decorated CNTs grown on both Si and Inconel substrates. Nyquist plots of EIS spectra collected from electrochemical lithium half cell of raw MWCNTs grown without any metal decoration and with Al decoration on CNTs (grown on Si and Inconel substrates) are shown. Information about SEM, TEM and HRTEM characterization of CNTs grown on Silicon and Inconel with Copper decoration on them is available in this section. Images after field emission on metal decorated CNTs are also available. This material is available free of charge *via* the Internet at http://pubs.acs.org.

REFERENCES AND NOTES

1. Planeix, J. M.; Coustel, N.; Coq, B.; Brotons, V.; Kumbhar, P. S.; Dutartre, R.; Geneste, P.; Bernier, P.; Ajayan, P. M. Application of Carbon Nanotubes as Supports in Heterogeneous Catalysis. *J. Am. Chem. Soc.* **1994**, *116*, 7935–7936.
2. Fu, Y.; Zhang, L.; Chen, G. Preparation of a Carbon Nanotube-Copper Nanoparticle Hybrid by Chemical Reduction for Use in the Electrochemical Sensing of Carbohydrates. *Carbon* **2012**, *50*, 2563–2570.
3. Liu, Z.; Lin, X.; Lee, J. Y.; Zhang, W.; Han, M.; Gan, L. M. Preparation and Characterization of Platinum-Based Electrocatalysts on Multiwalled Carbon Nanotubes for Proton Exchange Membrane Fuel Cells. *Langmuir* **2002**, *18*, 4054–4060.
4. Sun, Y.; Wang, H. H. High-Performance, Flexible Hydrogen Sensors That Use Carbon Nanotubes Decorated with Palladium Nanoparticles. *Adv. Mater.* **2007**, *19*, 2818–2823.
5. Li, W.; Liang, C.; Zhou, W.; Qiu, J.; Zhou; Sun, G.; Xin, Q. Preparation and Characterization of Multiwalled Carbon Nanotube-Supported Platinum for Cathode Catalysts of Direct Methanol Fuel Cells. *J. Phys. Chem. B* **2003**, *107*, 6292–6299.
6. Reddy, A.; Ramaprabhu, S. Hydrogen Storage Properties of Nanocrystalline Pt Dispersed Multi-Walled Carbon Nanotubes. *Int. J. Hydrogen Energy* **2007**, *32*, 3998–4004.
7. Kong, J.; Chapline, M. G.; Dai, H. Functionalized Carbon Nanotubes for Molecular Hydrogen Sensors. *Adv. Mater.* **2001**, *13*, 1384–1386.
8. Teo, K. B. K.; Chhowalla, M.; Amaratunga, G. A. J.; Milne, W. I.; Pirio, G.; Legagneux, P.; Wyczisk, F.; Pribat, D.; Hasko, D. G. Field Emission from Dense, Sparse, and Patterned Arrays of Carbon Nanofibers. *Appl. Phys. Lett.* **2002**, *80*, 2011.
9. Stephan, O.; Ajayan, P. M.; Colliex, C.; Redlich, P.; Lambert, J. M.; Bernier, P.; Lefin, P. Doping Graphitic and Carbon Nanotube Structures with Boron and Nitrogen. *Science* **1994**, *266*, 1683–1685.
10. Golberg, D.; Bando, Y.; Bourgeois, L.; Kurashima, K.; Sato, T. Large-Scale Synthesis and HRTEM Analysis of Single-Walled B- and N-Doped Carbon Nanotube Bundles. *Carbon* **2000**, *38*, 2017–2027.
11. Zhang, J.; Yang, C.; Wang, Y.; Feng, T.; Yu, W.; Jiang, J.; Wang, X.; Liu, X. Improvement of the Field Emission of Carbon Nanotubes by Hafnium Coating and Annealing. *Nanotechnology* **2006**, *17*, 257–260.
12. Wei, W.; Jiang, K.; Wei, Y.; Liu, P.; Liu, K.; Zhang, L.; Li, Q.; Fan, S. LaB[sub 6] Tip-Modified Multiwalled Carbon Nanotube as High Quality Field Emission Electron Source. *Appl. Phys. Lett.* **2006**, *89*, 203112.
13. Min, Y.-S.; Bae, E. J.; Park, J. B.; Kim, U. J.; Park, W.; Song, J.; Hwang, C. S.; Park, N. ZnO Nanoparticle Growth on Single-Walled Carbon Nanotubes by Atomic Layer Deposition and a Consequent Lifetime Elongation of Nanotube Field Emission. *Appl. Phys. Lett.* **2007**, *90*, 263104.
14. Green, J. M.; Dong, L.; Gutu, T.; Jiao, J.; Conley, J. F.; Ono, Y. ZnO-Nanoparticle-Coated Carbon Nanotubes Demonstrating Enhanced Electron Field-Emission Properties. *J. Appl. Phys.* **2006**, *99*, 094308.
15. Liu, C.; Kim, K. S.; Baek, J.; Cho, Y.; Han, S.; Kim, S.-W.; Min, N.-K.; Choi, Y.; Kim, J.-U.; Lee, C. J. Improved Field Emission Properties of Double-Walled Carbon Nanotubes Decorated with Ru Nanoparticles. *Carbon* **2009**, *47*, 1158–1164.
16. Jonge, N. de; Allioux, M.; Doytcheva, M.; Kaiser, M.; Teo, K. B. K.; Lacerda, R. G.; Milne, W. I. Characterization of the Field Emission Properties of Individual Thin Carbon Nanotubes. *Appl. Phys. Lett.* **2004**, *85*, 1607.
17. Han, S.; Ihm, J. First-Principles Study of Field Emission of Carbon Nanotubes. *Phys. Rev. B: Condens. Matter Mater. Phys.* **2002**, *66*, 241402.
18. Kim, H.-S.; Lee, H.; Han, K.-S.; Kim, J.-H.; Song, M.-S.; Park, M.-S.; Lee, J.-Y.; Kang, J.-K. Hydrogen Storage in Ni Nanoparticle-Dispersed Multiwalled Carbon Nanotubes. *J. Phys. Chem. B* **2005**, *109*, 8983–8986.
19. Kim, J.-Y.; Jeong, T.; Baik, C.-W.; Park, S. H.; Han, I.; Kim, G.-H.; Yu, S. Field-Emission Performance and Structural Change Mechanism of Multiwalled Carbon Nanotubes by Oxygen Plasma Treatment. *Thin Solid Films* **2013**, *547*, 202–206.
20. Choi, H.; Ji Shin, Y.; Il Cha, S.; Ho Kang, I.; Bahng, W. Enhanced Field-Emission Capacity by Density Control of a CNT Cathode Using Post-Plasma Treatment. *Solid State Commun.* **2013**, *171*, 50–54.
21. Xiao, L.; Liu, P.; Liu, L.; Jiang, K.; Feng, X.; Wei, Y.; Qian, L.; Fan, S.; Zhang, T. Barium-Functionalized Multiwalled Carbon Nanotube Yarns as Low-Work-Function Thermionic Cathodes. *Appl. Phys. Lett.* **2008**, *92*, 153108.
22. Lyth, S. M.; Hatton, R. A.; Silva, S. R. P. Efficient Field Emission from Li-Salt Functionalized Multiwall Carbon Nanotubes on Flexible Substrates. *Appl. Phys. Lett.* **2007**, *90*, 013120.
23. Jin, F.; Liu, Y.; Day, C. M.; Little, S. A. Enhanced Electron Emission from Functionalized Carbon Nanotubes with a Barium Strontium Oxide Coating Produced by Magnetron Sputtering. *Carbon* **2007**, *45*, 587–593.
24. Feng, M.; Sun, R.; Zhan, H.; Chen, Y. Decoration of Carbon Nanotubes with CdS Nanoparticles by Polythiophene Interlinking for Optical Limiting Enhancement. *Carbon* **2010**, *48*, 1177–1185.
25. Wang, W.; Serp, P.; Kalck, P.; Silva, C. G.; Faria, J. L. Preparation and Characterization of Nanostructured MWCNT-TiO_2 Composite Materials for Photocatalytic Water Treatment Applications. *Mater. Res. Bull.* **2008**, *43*, 958–967.
26. Haremza, J. M.; Hahn, M. A.; Krauss, T. D.; Chen, S.; Calcines, J. Attachment of Single CdSe Nanocrystals to Individual Single-Walled Carbon Nanotubes. *Nano Lett.* **2002**, *2*, 1253–1258.
27. Huang, C.-S.; Yeh, C.-Y.; Chang, Y.-H.; Hsieh, Y.-M.; Ku, C.-Y.; Lai, Q.-T. Field Emission Properties of CNT–ZnO Composite Materials. *Diamond Relat. Mater.* **2009**, *18*, 452–456.
28. Yang, M.; Liang, T.; Peng, Y.; Chen, Q. Synthesis and Characterization of a Nanocomplex of ZnO Nanoparticles Attached to Carbon Nanotubes. *Acta Phys.-Chim. Sin.* **2007**, *23*, 145–151.
29. An, G.; Na, N.; Zhang, X.; Miao, Z.; Miao, S.; Ding, K.; Liu, Z. SnO_2 /carbon Nanotube Nanocomposites Synthesized in Supercritical Fluids: Highly Efficient Materials for Use as a Chemical Sensor and as the Anode of a Lithium-Ion Battery. *Nanotechnology* **2007**, *18*, 435707.

30. Zhai, L.; Wei, Z.; Yang, Z.; Ni, X. Polymerization Initiated by ZnS Nanocrystals Anchored on Carbon Nanotubes. *Mater. Lett.* **2010**, *64*, 531–533.
31. Cho, N.; Roy Choudhury, K.; Thapa, R. B.; Sahoo, Y.; Ohulchanskyy, T.; Cartwright, A. N.; Lee, K.-S.; Prasad, P. N. Efficient Photodetection at IR Wavelengths by Incorporation of PbSe−Carbon-Nanotube Conjugates in a Polymeric Nanocomposite. *Adv. Mater.* **2007**, *19*, 232–236.
32. Li, C.; Ding, S.; Lei, W.; Zhang, X.; Wang, B. Enhanced Field Emission from Vertically Aligned Carbon Nanotubes on Metal Mesh Electrode. *Appl. Surf. Sci.* **2013**, *285*, 505–508.
33. Zuo, Y.; Ren, Y.; Wang, Z.; Han, X.; Xi, L. Enhanced Field Emission and Hysteresis Characteristics of Aligned Carbon Nanotubes with Ti Decoration. *Org. Electron.* **2013**, *14*, 2306–2314.
34. Pandey, A.; Prasad, A.; Moscatello, J. P.; Engelhard, M.; Wang, C.; Yap, Y. K. Very Stable Electron Field Emission from Strontium Titanate Coated Carbon Nanotube Matrices with Low Emission Thresholds. *ACS Nano* **2013**, *7*, 117–125.
35. Zanin, H.; May, P. W.; Hamanaka, M. H. M. O.; Corat, E. J. Field Emission from Hybrid Diamond-like Carbon and Carbon Nanotube Composite Structures. *ACS Appl. Mater. Interfaces* **2013**, *5*, 12238–12243.
36. Fan, Y. C.; Liu, Y. M.; Chen, Y. C.; Sung, Y.; Ger, M. D. Carbon Nanotube Field Emission Cathodes Fabricated with Chemical Displacement Plating. *Appl. Surf. Sci.* **2009**, *255*, 7753–7758.
37. Chen, Y.; Jiang, H.; Li, D.; Song, H.; Li, Z.; Sun, X.; Miao, G.; Zhao, H. Improved Field Emission Performance of Carbon Nanotube by Introducing Copper Metallic Particles. *Nanoscale Res. Lett.* **2011**, *6*, 537.
38. Nilsson, L.; Groening, O.; Emmenegger, C.; Kuettel, O.; Schaller, E.; Schlapbach, L.; Kind, H.; Bonard, J.-M.; Kern, K. Scanning Field Emission from Patterned Carbon Nanotube Films. *Appl. Phys. Lett.* **2000**, *76*, 2071.
39. Bonard, J.-M.; Dean, K.; Coll, B.; Klinke, C. Field Emission of Individual Carbon Nanotubes in the Scanning Electron Microscope. *Phys. Rev. Lett.* **2002**, 89.
40. Bonard, J.-M.; Weiss, N.; Kind, H.; Stöckli, T.; Forró, L.; Kern, K.; Châtelain, A. Tuning the Field Emission Properties of Patterned Carbon Nanotube Films. *Adv. Mater.* **2001**, *13*, 184–188.
41. Bittencourt, C.; Ke, X.; Van Tendeloo, G.; Thiess, S.; Drube, W.; Ghijsen, J.; Ewels, C. P. Study of the Interaction between Copper and Carbon Nanotubes. *Chem. Phys. Lett.* **2012**, *535*, 80–83.
42. Gingery, D.; Bühlmann, P. Formation of Gold Nanoparticles on Multiwalled Carbon Nanotubes by Thermal Evaporation. *Carbon* **2008**, *46*, 1966–1972.
43. Charlier, J.-C.; Arnaud, L.; Avilov, I. V.; Delgado, M.; Demoisson, F.; Espinosa, E. H.; Ewels, C. P.; Felten, A.; Guillot, J.; Ionescu, R.; *et al.* Carbon Nanotubes Randomly Decorated with Gold Clusters: From Nano ^{2} Hybrid Atomic Structures to Gas Sensing Prototypes. *Nanotechnology* **2009**, *20*, 375501.
44. Muratore, C.; Reed, A. N.; Bultman, J. E.; Ganguli, S.; Cola, B. A.; Voevodin, A. A. Nanoparticle Decoration of Carbon Nanotubes by Sputtering. *Carbon* **2013**, *57*, 274–281.
45. Sridhar, S.; Ge, L.; Tiwary, C. S.; Hart, A. C.; Ozden, S.; Kalaga, K.; Lei, S.; Sridhar, S. V.; Sinha, R. K.; Harsh, H.; *et al.* Enhanced Field Emission Properties from CNT Arrays Synthesized on Inconel Superalloy. *ACS Appl. Mater. Interfaces* **2014**, 1986–1991.
46. Katayama, M.; Lee, K.-Y.; Honda, S.; Hirao, T.; Oura, K. Ultra-Low-Threshold Field Electron Emission from Pillar Array of Aligned Carbon Nanotube Bundles. *Jpn. J. Appl. Phys.* **2004**, *43*, L774–L776.
47. Suh, J. S.; Jeong, K. S.; Lee, J. S.; Han, I. Study of the Field-Screening Effect of Highly Ordered Carbon Nanotube Arrays. *Appl. Phys. Lett.* **2002**, *80*, 2392.
48. Ren, H.; Yang, L.; Zhang, Y. Numerical Calculations on the Field Emission of Carbon Nanotubes. *J. Phys.: Conf. Ser.* **2013**, *418*, 012007.
49. Tuinstra, F. Raman Spectrum of Graphite. *J. Chem. Phys.* **1970**, *53*, 1126.
50. Saito, R.; Hofmann, M.; Dresselhaus, G.; Jorio, A.; Dresselhaus, M. S. Raman Spectroscopy of Graphene and Carbon Nanotubes. *Adv. Phys.* **2011**, *60*, 413–550.
51. Ferrari, A. C. Raman Spectroscopy of Graphene and Graphite: Disorder, Electron−Phonon Coupling, Doping and Nonadiabatic Effects. *Solid State Commun.* **2007**, *143*, 47–57.
52. Atthipalli, G.; Wang, H.; Gray, J. L. Catalyst-Assisted Vertical Growth of Carbon Nanotubes on Inconel Coated Commercial Copper Foil Substrates *versus* Sputtered Copper Films. *Appl. Surf. Sci.* **2013**, *273*, 515–519.
53. Lee, D. H.; Lee, J. A.; Lee, W. J.; Choi, D. S.; Lee, W. J.; Kim, S. O. Facile Fabrication and Field Emission of Metal-Particle-Decorated Vertical N-Doped Carbon Nanotube/Graphene Hybrid Films. *J. Phys. Chem. C* **2010**, *114*, 21184–21189.
54. Gadzuk, J.; Plummer, E. Field Emission Energy Distribution (FEED). *Rev. Mod. Phys.* **1973**, *45*, 487–548.
55. Tanaka, H.; Akita, S.; Pan, L.; Nakayama, Y. Barrier Effect on Field Emission from Stand-Alone Carbon Nanotube. *Jpn. J. Appl. Phys.* **2004**, *43*, 864–867.
56. Fujii, S.; Honda, S.; Machida, H.; Kawai, H.; Ishida, K.; Katayama, M.; Furuta, H.; Hirao, T.; Oura, K. Efficient Field Emission from an Individual Aligned Carbon Nanotube Bundle Enhanced by Edge Effect. *Appl. Phys. Lett.* **2007**, *90*, 153108.
57. Collins, P. G.; Zettl, A. Unique Characteristics of Cold Cathode Carbon-Nanotube-Matrix Field Emitters. *Phys. Rev. B: Condens. Matter Mater. Phys.* **1997**, *55*, 9391–9399.

List of Publications

Journals:

1. " Ultra-Low Turn-On Voltage from Metal Decorated Carbon Nanotubes" ***S. Sridhar****, C. S. Tiwary, S. Vinod , J. J. Taha-Tijerina, S. V. Sridhar, K. Kalaga, S. Ben, A .Hart, S. Ozden, R.K. Sinha, H. Harsh, R. Vajtai, W. B. Choi and P.M. Ajayan,* ***ACS Nano****, 2014* ***(Impact Factor 2012: 12.062)***
2. "Enhanced Field Emission Properties from CNT Arrays Synthesized on Inconel Superalloy" ***S. Sridhar****, L. Ge, C. S. Tiwary, A. C. Hart, S. Ozden, K. Kalaga, S. Lei, S. V. Sridhar, R. K. Sinha, H. Harsh, K. Kordas, P. M. Ajayan, and R. Vajtai.* ***ACS Applied Materials and Interface****, 2014* ***(Impact Factor 2012: 5.008)***
3. "Titanium Buffer layer for improved field emission of CNT based cold cathode" ***S. Srividya,*** *S. Gautam, P.Jha, P.Kumar, A. Kumar, US Ojha, JSBS Rawat, S.Pal, P.K. Choudhary, Harsh and R.K.Sinha,* ***Applied Surface Science****, 2010* ***(Impact Factor 2012: 2.112)***
4. "One step process for infiltration of Fe_3O_4 into the CNT array for enhanced field emission" (*Advance Materials - Under Process*)

National and International Conferences Attended:

1. **S. Srividya**, P. Verma, S. Gautham, P. Jha, P. Kumar, P. Choudary, J.S. Rawat, S. Pal, Harsh and R. K. Sinha, "Effect of Titanium Buffer Layer for improved field emission of CNT based cold cathode", International Conference on Nanoscience and Technology (ICONSAT 2008), February 27^{th} -29^{th} 2008
2. **S. Srividya**, S. Gautham, P. Jha, S. Pal, U. S. Ohja, J.S.B.S. Rawat, P. K. Choudary, Harsh, R. K. Sinha and P. K. Basu, "CNT Density Control by Titatnium Capping for improved Field Emission" National Conference on Electron Microscope Society of India (EMSI 2007), November 26^{th} – 28^{th} 200

GROWTH AND CHARACTERIZATION OF CARBON NANOTUBES FOR IMPROVED FIELD EMISSION

A thesis submitted to the
Faculty of Technology, University of Delhi
for the award of the degree of

DOCTOR OF PHILOSOPHY
in
APPLIED PHYSICS

by

Srividya Sridhar

Under the guidance of

(PROF. R. K. SINHA)
Department of Applied Physics
Delhi College of Engineering
(Now Delhi Technological University)
Delhi

Dr. HARSH
Scientist G (Retd.)
Solid State Physics Laboratory
New Delhi

Delhi College of Engineering
(Now, Delhi Technological University)
Faculty of Technology
University of Delhi
Delhi-110042, India

CHAPTER VIII

Conclusion and future work

8.1 Summary

We began by developing a deeper understanding of the basic terms involved in Field Emission and Carbon nanotubes in Chapter 1. In chapter 2, we focused on improving the field emission properties of CNTs with the help of Ti buffer layer. We deposited titanium buffer layer on silicon substrate to address the adhesion issue, substrate heating because of high contact resistance and shielding effect. Some critical issues such as screening effect, adhesion of CNTs with the substrate, reliability, high contact resistance and stability have to be addressed while using CNTs as electron emitters in field emission applications. The adhesion of CNTs with the substrate has to be increased and contact resistance between the CNTs and the substrate has to be lowered for improved device performance. CNT synthesis in a CVD process involves the dissociation of hydrocarbon molecules catalyzed by the transition metal, which is then followed by the dissolution and saturation of carbon atoms in the metal nanoparticles. Finally, the precipitation of carbon from the saturated metal particle leads to the formation of tubular carbon solids in a graphite structure. Since most of the CNT growth involves the use of transition metal catalyst, it is worth emphasizing that the preparation and pre-conditioning of transition metal catalysts can have a significant role on the growth of carbon nanostructures since it is a catalyst-assisted process. When using a Si substrate, the formation of metal silicides as a result of the preheating, will poison the synthesis process. For that reason prior to the catalyst deposition

different buffer layers are usually deposited on top of the substrates. As field emission electron sources, for better field emission performance and stable electron emission, CNTs must have excellent electrical conductivity to the electrode and good adhesion with the substrate. Efforts were made to increase the CNT tip density and improve the adhesion of CNTs with the substrate so as to make the CNT based cold cathodes suitable for high power microwave vacuum devices application, which require high current densities. The adhesion between CNTs and substrate was greatly improved because of the strong binding between titanium and the substrate. This prevented the CNTs from pulling off from the substrate by the strong electro-static force at high electric field. Emission current density of 30 mA/cm^2 at a field of 4 V/μm was achieved.

In chapter 3 and 4, efforts were turned towards the effect of the buffer layer thickness on the field emission properties of the CNTs and density control of the grown CNTs. Field emission experiment were performed for the sample with 10nm and 20nm thick Ti buffer layer and the emission current density of the sample with 20nm thick titanium found to be 200 times more than those with 10nm thick titanium buffer layer because of better adhesion. It is well known that the density of CNTs plays a crucial role in determining the field emission properties. Unfortunately, the density of carbon nanotubes synthesized through CVD technique is much higher than 10^7 cm^{-2}. So in our work, a barrier layer of Ti is first sputtered on the substrate to improve the adhesion of CNTs. On top of the barrier layer, a layer of Fe (which catalyses the growth of CNTs) is sputtered. Over this, sputtering of a thin capping layer of Ti of varying thickness is carried out in order to suppress the screening effect. By varying the thicknesses of the capping layer, the density of carbon nanotubes was controlled effectively without serious damages to their crystallinity.

In chapter 5, research was done to grow CNTs on Inconel super alloy to enhance the field emission properties. Apart from thermal and electrical stability of the electrode materials, high quality robust electrical contacts that are interfacing the emitter back side are also vital for multiple reasons. Firstly, the contact must be uniform along the entire interface to allow optimal, uniform current densities throughout the joint area. This is especially important for carbon nanotube forests, to ensure each nanotube is in direct electrical contact with the substrate with similar contact resistance all around at the interface eliminating the formation of hot spots. Secondly, good ohmic contacts at the CNT-substrate interface introduce only minor series resistances in the emitter circuit thus resulting in higher emission currents or lower interfacial losses (when current regulated). Thirdly, mechanical strength, or good adhesion, between the nanotube/catalyst and the substrate interface is also an important criterion in order to minimize problems related to delamination of the emitter material from the back side contact. For this, we grew CNTs on Inconel and Si substrates in water assisted CVD and compare their field emission behavior. CNTs grown on Inconel exhibited excellent field emission properties: The maximum current densities from the produced emitters were around 100 mA/cm^2.

In chapter 6, focus turned towards reducing the turn on and threshold voltages as they are very important properties for the CNTs to be used in the fabrication of next generation high-performance flat panel displays and vacuum microelectronic devices. For this a simple and scalable procedure was developed for decorating the vertically aligned CNTs forest with metal nanoparticles for improved field emission properties. This process enabled the CNTs to bundle towards a metal particle forming a pattern due to which the CNT bundles are separated by almost 3 times the height of the bundle reducing the screening effect considerably. Further, by

the deposition of metal nanoparticles on the surface of the nanotubes, emitting centers are obtained that ensure highly conductive paths for the electrons from the nanotubes towards the vacuum helping to by-pass the amorphous carbon impurities, known as one of the major hurdles in CNT based emitters. Thus, to the best of our knowledge, such low turn on field of 0.1 V/μm achieved in this work has not been reported so far.

In chapter 7, a very novel, easy, cost effective and scalable method to prepare magnetic CNTs was developed. Decoration of the CNTs with different metals such as Al and Cu has certainly improved the field emission properties of the CNTs. The process was tedious and high temperature treatment were used to decorate the CNTs. We used a magnet for the infiltration of iron nanoparticle into the CNT array. So it doesn't require any complicated set-up or technique making this more cost effective. Furthermore, field emission results prove that these composites can be used as excellent emitter source in X-ray and other vacuum microwave application as there was tremendous reduction in the turn on and the threshold voltage when compared to earlier reports. Although this method produce some encouraging results, it is an easily scalable and cost effective method of infiltrating Fe_3O_4 nanoparticles doesn't require any complicated/sophisticated set-up. Another major advantage of this method is that the physical structure of the 3D CNT forest remains unaltered. Furthermore, results of the field emission experiment proves that the tilting or inverting the CNT forest do not disturb the Fe_3O_3 nanoparticles after infiltration.

8.2 Future Work

CNTs have many novel properties that make them potential candidate in many applications including vacuum micro-electronic devices, field emission displays, energy storage etc. In order to avail the full potential of these structures, it is imperative that the future experimental work to be focused on the following issues.

8.2.1 TEM study of cross sectional view of CNTs

From the TEM image, we can find out the mode of growth, particularly in tip growth mode if the catalyst particles are present on tip of the CNTs. Apart from finding the innermost wall of the MWCNTs to be filled with catalyst material in some cases, knowing the diameter of the CNTs and number of walls on the MWCNTs can also be found out from TEM results. Since the sample preparation involves sonication, chances of the catalyst to peel off from the root or the tip of the CNTs are more. In order to avoid this, we can use the SEIKO DUAL BEAM FIB, where we need to anchor the cross sectional portion of the CNTs to the copper grid. This will facilitate the identification of the exact location of the catalyst particle in the sample.

8.2.2 CNT density calculation

We may need to calculate the CNT density in many of the experiment (For example the experiment described in Chapter 4 while using Ti capping layer). Generally, CNT density will be calculated using TEM and SEM data. This may not give us the exact value but more often, an over estimation. To avoid this, we can calculate the density using the weight of the sample

post growth, average CNT height, CNT mass per unit length which in turn could be calculated from the number of walls and the CNT diameter measured using TEM.

8.2.3 Flowery pattern obtained in Al decoration on Si substrate

As explained in Chapter 6, we observed a flowery pattern while decorating the CNTs grown on Si substrate with Al. This could be due to the wetting nature of Al on different substances. This needs further thorough investigation to make them use in various applications.

8.2.4 Effect of Inconel super alloy

As described in Chapter 5, we found that while using Inconel substrate, it acted as an additional catalyst along with Fe. We were able to get higher current density due to the higher enhancement factor. This in turn could have resulted from minor arcing which led to localized cleaning and there was stable emission. For future investigation, we can try using Inconel as a barrier material as it contains high surface energy elements like Cr, Ni and Fe.

8.2.5 Duration of water vapor

During our growth experiments in water assisted CVD system, we turn on the supply of water vapor for 30 seconds after the introduction of carbon source (Ethylene). It is well known that the catalyst material start nucleating after the reduction or deoxidization. So we use hydrogen for the reduction of the catalyst. It would be very useful to study the effect of the

duration of the water vapor and the result of hydrogen on the catalyst material by simulation and modeling so as to increase their application in various field.

Although detailed study has been done to enhance the field emission properties of CNTs, the results presented in this thesis can serve as base for future research.